UNIVERSITÉ DE GENÈVE
Département de physique théorique

FACULTÉ DES SCIENCES
Professeur M. Büttiker

Electron-electron and electron-phonon interactions in ballistic mesoscopic conductors

THÈSE

présentée à la Faculté des sciences de l'Université de Genève
pour obtenir le grade de Docteur ès sciences, mention physique

par

Georg Friedrich David SEELIG
de
Bâle (BS) et Allemagne

Thèse No 3424

GENÈVE
Atelier de reproduction de la Section de physique
2003

Contents

CHAPITRE 1

Introduction et résumé

Cette thèse est consacrée à l'étude de quelques effets dus aux interactions entre électrons et aux interactions entre électrons et phonons dans les conducteurs mésoscopiques balistiques. Le domaine mésoscopique désigne des échelles intermédiaires entre les mondes microscopique et macroscopique. Pour définir plus précisément ce que nous entendons par un conducteur mésoscopique balistique, il est utile de commencer par introduire quelques échelles de longueur caractérisant de tels systèmes. Le libre parcours moyen l_e désigne la distance typique qu'un électron peut parcourir avant de subir une collision élastique qui change la direction de son impulsion. La longueur de cohérence de phase l_ϕ est la distance sur laquelle un électron perd la mémoire de sa phase, c'est-à-dire, sur laquelle la phase a diffusé d'environ 2π. Dans un conducteur mésoscopique cette longueur de cohérence est comparable aux dimensions du conducteur lui-même. Si, en outre, le libre parcours moyen est supérieur à la longueur de cohérence ($l_e > l_\phi$), le conducteur est balistique, tandis que le régime diffusif est défini par la relation inverse $l_\phi \gg l_e$. Une introduction à la physique mésoscopique peut être trouvée dans les livres d'Imry [1] ou de Datta [2].

Les très longs libres parcours moyens nécessaires pour le transport balistique peuvent être réalisés expérimentalement dans un gaz bidimensionnel d'électrons. Dans une hétérostructure semiconductrice AlGaAs/GaAs les électrons de conduction, fournis par des donneurs de l'AlGaAs, sont confinés à l'interface entre les deux matériaux. Les électrons sont donc libres de se déplacer uniquement dans un plan. La densité d'électrons dans un tel gaz est typiquement de l'ordre de 10^{11} cm^{-2} et le libre parcours moyen l_e est de quelques micromètres.

A l'aide de différentes téchniques expérimentales il est possible de confiner le gaz d'électrons dans une région du plan. De cette manière des conducteurs d'une grande variété de propriétés et de formes peuvent être créés. Par exemple

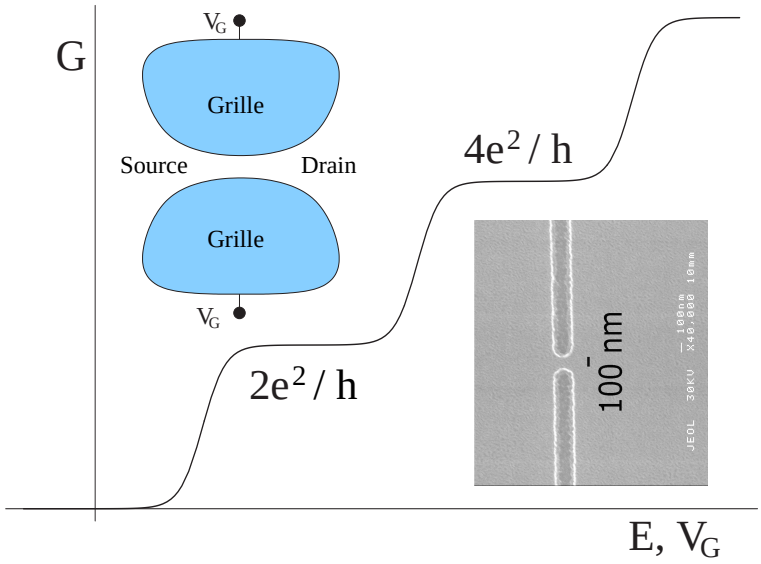

Fig. 1.1: Conductance d'un contact ponctuel en fonction de l'énergie des électrons où du potentiel de grille V_G. A gauche le contact ponctuel est esquissé et les grilles métalliques, la source et le drain d' électrons sont indiqués. La lithographie en bas à droite montre le contact ponctuel avant que le grilles ne soient déposées (A. Hansen).

on peut citer les contacts ponctuels (quantum point contacts), les points quantiques (quantum dots) ou les anneaux mésoscopiques (voir Réfs. [1, 2, 3]). Un contact ponctuel est une constriction séparant deux parties d'un gaz bidimensionnel (voir Fig. [1.1]). La largeur de l'ouverture, de l'ordre de quelques centaines de nanomètres, peut être ajustée à l'aide d'un potentiel de grille. Une mesure de la conductance du contact ponctuel est réalisée en induisant une différence de potentiel entre les deux moitiés du gaz bidimensionnel, nommées alors la source et le drain. Le confinement latéral dans le contact ponctuel donne lieu à la quantification de la partie transverse de la fonction d'onde et de l'énergie associée (on peut supposer que l'équation de Schrödinger est séparable). L'énergie totale d'un électron s'écrit alors

$$E = E_n + \frac{\hbar^2 k_x^2}{2m} \tag{1.1}$$

où E_n ($n = 0, 1, 2..$) est la contribution transverse (quantifiée) à l'énergie, k_x est le vecteur d'onde dans la direction du contact ponctuel et m est la masse effective d'un électron. Les états électroniques sont indicés par les deux nombres quantiques n et k_x. Tous les états de même n appartiennent à la même bande de conduction – on parle également du $n$ième canal. Le $n$ième canal participe au transport à travers le contact ponctuel si $E_n < E_F$ où E_F est l'énergie de Fermi, c'est-à-dire le potentiel chimique du conducteur. Une telle nomenclature ne s'applique d'ailleurs pas seulement au cas d'un contact ponctuel mais à tous les conducteurs effectivement unidimensionnels. Une conséquence de la quantification de l'énergie transverse dans le cas d'un contact ponctuel est le phénomène

intéressant de la quantification de la conductance (voir Fig. [1.1]). Lorsque la constriction s'élargit, la conductance augmente de $2e^2/h$ chaque fois qu'un nouveau canal de conduction est ouvert. La quantification de la conductance était observée expérimentalement pour la première fois en 1988 [4]. Une explication théorique a bientôt suivi [5, 6].

A température nulle et dans la limite de la réponse linéaire la conductance d'un conducteur cohérent avec deux contacts est donnée par la formule de Landauer

$$G = \frac{2e^2}{h} \sum_n T_n(E_F). \tag{1.2}$$

La somme porte sur les canaux de transport et le facteur deux permet de prendre en compte le spin des électrons. $T_n(E_F)$ est la probabilité de transmission par le potentiel effectif dans la direction du courant pour un électron appartenant au $n$ième canal de transport. La formule de Landauer a été généralisée par Büttiker pour le cas d'un conducteur avec plusieurs contacts [7]. On parle alors de la formule Landauer-Büttiker. Pour un contact ponctuel la transmission varie rapidement en fonction de l'énergie. Elle est nulle, si l'énergie totale de l'électron est petite comparée au maximum du potentiel de la barrière et elle tend vers un, si l'énergie électronique dépasse ce maximum. Cette dépendance en énergie de la transmission explique la quantification de la conductance. A l'aide d'un modèle simple la quantification est discutée en détail dans la Réf. [6]. On montrera par la suite que les interactions entre les électrons de conduction et les modes de vibration du réseau cristallin, les phonons, peuvent entraîner des déviations du modèle simple de la quantification de la conductance qu'on vient de décrire.

Comme le contact ponctuel, un point quantique (quantum dot) est une structure relativement simple avec des propriétés physiques très riches. Un point quantique désigne un puits de potentiel dans un gaz électronique qui confine des électrons dans un domaine. Des grilles métalliques sont utilisées pour contrôler avec précision la taille du puits et le nombre d'électrons. Ce dernier peut ainsi varier entre quelques unités et quelques milliers. On calculera la charge moyenne et la capacitance d'un point quantique connecté à un réservoir et couplé capacitivement à une grille métallique. On s'intéressera en particulier au cas où le point quantique est couplé au réservoir par un contact ponctuel avec deux canaux de transport (par exemple électrons avec spin). Les probabilités de transmission pour les deux canaux peuvent être différentes.

Les anneaux mésoscopiques balistiques (voir Fig. [1.2]) sont les structures les plus complexes qu'on rencontrera dans cet étude. Ils sont d'un intérêt particulier, parce qu'une mesure de la conductance d'un anneau constitue un test direct de la cohérence de phase des électrons de conduction. Lorsque la longueur de cohérence est plus grande ou de l'ordre du rayon de l'anneau, la conductance contient une partie cohérente due aux interférences entre les ondes traversant les deux bras. La conductance présente une structure périodique en fonction d'un flux magnétique traversant l'anneau. Cette dépendance en fonction du flux est une manifestation

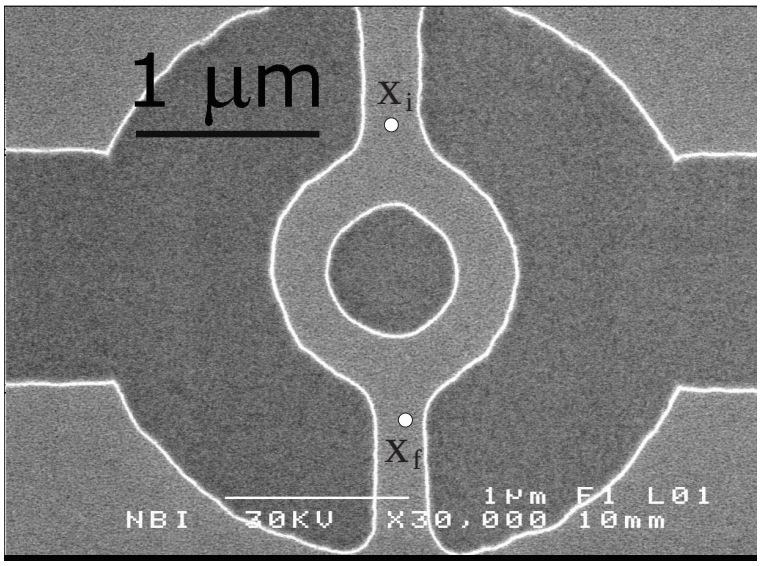

Fig. 1.2: Un anneau mésoscopique (A. Hansen).

de l'effet Aharonov-Bohm [8]. La conductance et les courants permanents d'un anneau balistique ont été élaborés par Büttiker et ses collaborateurs [9, 10, 11].

Au lieu de calculer exactement la probabilité de transmission d'un anneau avec des branches effectivement unidimensionnelles comme cela a été fait dans la Réf. [11] nous nous contentons ici de présenter un argument simple, suffisant toutefois pour comprendre l'origine de la dépendance en flux magnétique de la conductance. Pour la probabilité de transmission on écrit

$$T \propto |\Psi_A(x_f; x_i) + \Psi_B(x_f; x_i)|^2 \tag{1.3}$$

où $\Psi_\alpha(x_f; x_i)$ est l'amplitude de probabilité de propager au point x_f par la branche α (voir Fig. [1.2]). Lorsque la longueur de cohérence est supérieure à la longueur des bras on doit calculer la somme cohérente au lieu de la somme incohérente $|\Psi_A|^2 + |\Psi_B|^2$.

En présence d'un potentiel vecteur $\mathbf{A}$ (Le champ magnétique est $\mathbf{B} = \nabla \times \mathbf{A}$) l'amplitude de transmission $\Psi_\alpha(x_f; x_i)$ acquiert une phase

$$\Psi_\alpha(x_f; x_i) \to \Psi_\alpha(x_f; x_i) \mathrm{e}^{i\Theta_\alpha}, \;\; \Theta_\alpha = \frac{e}{\hbar c} \int_\alpha d\mathbf{x} \cdot \mathbf{A}(\mathbf{x}) \tag{1.4}$$

où l'intégrale est évaluée le long du chemin suivi par l'électron. On trouve alors pour la transmission

$$T \propto |\Psi_A + \Psi_B \mathrm{e}^{-i2\pi\Phi/\Phi_0}|^2 \tag{1.5}$$

où le quantum de flux est $\Phi_0 = hc/e$ et Φ est le flux magnétique traversant l'anneau. Ce modèle simple nous permet de comprendre l'origine de la dépendance en flux magnétique de la transmission d'un anneau mésoscopique. Puisque la

conductance d'un système cohérent est entièrement déterminée par la probabilité de transmission (voir Eq. [2]), les oscillations cohérentes de la transmission en fonction du flux magnétique sont observables par une mesure de la conductance.

La situation rencontrée dans une expérience de physique mésoscopique est un peu différente de la situation décrite par Aharonov et Bohm [19]. Dans l'effet Aharonov-Bohm, le champ magnétique est nul là où passe la particule et non-nul dans la région délimitée par les deux chemins, tandis que le potentiel vecteur a une valeur finie aussi dans les régions explorées par l'électron. Dans une expérience le champ magnétique n'est pas restreint au centre de l'anneau, mais il est non-nul aussi dans les bras. La similarité avec l'effet discuté originellement par Aharonov et Bohm devient plus explicite en faisant l'approximation que la largeur des bras est négligeable, comparée au rayon de l'anneau.

1.1 La décohérence dans un anneau

La décohérence supprime les effets d'interférence, inévitables à l'échelle microscopique. Elle est responsable de la transition vers le monde macroscopique caractérisé par l'absence de cohérence quantique. Comme on l'a vu, les systèmes mésoscopiques se situent à la frontière entre les domaines microscopique et macroscopique. Il n'est donc pas surprenant que la décohérence joue un rôle central en physique mésoscopique.

Ces dernières années ont vu l'émergence d'une nouvelle direction de recherche, qui relie la physique mésoscopique à la théorie de l'information quantique. Parmi les buts principaux de la recherche dans ce domaine on peut mentionner la création des unités de base (les "qubits" ou bit quantique) d'un ordinateur quantique, ou le contrôle des interactions entre ces unités. Des nombreuses applications supplémentaires ont été envisagées. Puisque la cohérence de phase est indispensable à ces développements, il est peu surprenant qu'ils aient suscité un regain d'intérêt dans les problèmes liés à la décohérence. Bien que par la suite nous n'abordions plus directement les questions motivées par la théorie de l'information, les résultats que nous présentions peuvent aider à élucider l'effet des interactions entre électrons pour de telles applications.

Les interactions entre les électrons fournissent le mécanisme principal responsable de la décohérence dans les conducteurs mésoscopiques désordonnés [12]. A très basse température et pour des systèmes mésoscopiques de dimensions réduites – des conducteurs bi-dimensionnels, voire unidimensionnels – ce sont les processus de diffusion électron-électron pour de petits transferts d'énergie qui jouent un rôle primordial. Ce dernier mécanisme, dit de Nyquist, correspond à l'interaction d'un électron avec les fluctuations électromagnétiques dues au mouvement thermique des autres électrons. Cette théorie canonique de la décohérence dans les systèmes désordonnés est en bon accord avec les observations expérimentales dans un grand régime de température. Par contre, elle n'explique pas la saturation du taux de décohérence observée lorsque la température tend vers

zero. L'origine de cette saturation n'est pas comprise aujourd'hui et reste une des questions parmi les plus débattues en physique mésoscopique. La décohérence à température nulle est un problème en soi qui sort du cadre de ce travail. Une introduction à ces problèmes et des références peuvent être trouvées dans l'article de revue écrit par Lin et Bird [13].

Il existe aujourd'hui un grand nombre de résultats expérimentaux sur la décohérence dans les conducteurs balistiques [13, 14, 15, 16, 17]. Le taux de décohérence Γ_ϕ a été déterminé pour des points quantiques chaotiques [14, 15] et pour des anneaux mésoscopiques [16, 17]. A très basse température le taux de décohérence est constant et indépendant de la température comme dans le cas des conducteurs désordonnés. Jusqu'à présent cette saturation a été observée uniquement pour les points quantiques, probablement car la température minimale atteinte dans les mesures sur les anneaux était encore trop élevée. Lorsque la température augmente, le taux de décohérence croit linéairement en température : $\Gamma_\phi \propto T$. A l'exemple des anneaux mésoscopiques on montrera par la suite que cette dépendance linéaire en température est due aux interactions entre électrons pour un faible transfert d'énergie.

Dans ce travail on examinera la décohérence dans un interféromètre balistique. Notre système idéalisé consiste en un anneau Aharonov-Bohm avec quatre contacts, chaque bras de l'anneau étant couplé capacitivement avec une grille métallique (voir Fig. [2.1]). On suppose qu'il n'y a pas de rétro-diffusion dans l'interféromètre et que, par conséquent, il n'y a pas d'orbite électronique fermée.

Un conducteur mésoscopique connecte un ou plusieurs réservoirs d'électrons. Dans les réservoirs les interactions entre les électrons sont fortement écrantées et de peu d'effet. A l'intérieur du conducteur l'écrantage est moins effectif et les interactions jouent un rôle plus grand. L'échange de charges entre les réservoirs et le conducteur est responsable de fluctuations du potentiel effectif dans le conducteur. On supposera que la charge totale contenue dans le système constitué de l'anneau et des grilles est toujours nul. Néanmoins il est possible de créer des dipôles électriques en chargeant une partie du système (un bras de l'anneau) relativement à une autre partie (la grille voisine). Les fluctuations de la charge dans les bras de l'anneau donnent lieu à des fluctuations de potentiel et les électrons qui traversent l'interféromètre sont diffusés inélastiquement par ces fluctuations. Le but de cette étude est de démontrer que le contraste des oscillations Aharonov-Bohm de la conductance (voir la discussion à la fin du chapitre précédant) est diminué par les interactions électron-électron effectives dans les bras de l'intérferomètre. On obtiendra le taux de suppression Γ_ϕ en fonction de la température et de la force des interactions. En particulier on montrera que $\Gamma_\phi \propto T$ en accord avec les expériences [16, 17].

1.2 Le bloquage de Coulomb et le modèle Kondo

Dans le deuxième chapitre on s'intéressera également aux effets des interactions entre les électrons dans un conducteur mésoscopique balistique. Toutefois, une toute autre limite sera examinée. Pour le traitement de la décohérence dans les anneaux mésoscopiques on a pu supposer que les interactions sont relativement faibles. Une telle hypothèse est justifiée pour des conducteurs ouverts qui peuvent facilement échanger des charges avec les réservoirs. Ici, on va considérer un point quantique qui est couplé à un réservoir, par un contact ponctuel. On s'intéressera en particulier à la limite où la conductance G du contact ponctuel est plus petite que $2e^2/h$. Le point quantique n'est donc que faiblement couplé au réservoir. Dans cette limite les interactions sont importantes et doivent être traitées d'une manière plus rigoureuse qu'on ne l'a fait dans la discussion sur la décohérence.

Si C est la capacitance totale du point quantique, l'énergie nécessaire pour y ajouter un électron est $E_C = e^2/2C$. Pour des températures T nettement inférieures à l'énergie de charge E_C ($T \ll E_C$), l'échange de charges entre point quantique et réservoir est supprimé et on parle du bloquage de Coulomb[18, 19, 20]. Si on couple le point quantique capacitivement (avec une capacitance C_{gd}) à une grille macroscopique, l'énergie électrostatique

$$E_Q(V_G) = -QV_G + Q^2/2C \tag{1.6}$$

du système devient une fonction de la différence de potentiel V_G appliquée entre la grille et le point quantique. Le premier terme dans l'expression pour l'énergie est dû à l'attraction entre la charge Q du point quantique et et la charge $-Q$ de la grille alors que le terme positif représente les interactions répulsives entre les électrons dans le point quantique. A une constante près, l'énergie électrostatique, donnée dans l'équation précédente, peut aussi être écrite comme

$$E_Q(N) = E_C(n - N)^2 \tag{1.7}$$

où n est le nombre d'électrons sur le point quantique et $N = CV_G/e$ est un paramètre sans dimension proportionnel à la différence de potentiel V_G. Un Hamiltonien effectif pour les interactions est obtenu en remplaçant la charge classique en dans l'expression pour l'énergie électrostatique par l'opérateur de charge $e\hat{n}$. Ce modèle capacitif pour l'interaction dans le point quantique est une bonne approximation pour des point quantiques chaotiques [21, 22].

Si N est proche de la valeur $N = n+1/2$ les deux états de charge avec n et $n+1$ électrons dans le point quantique ont la même énergie et le nombre d'électrons fluctue. Par contre, loin de ces points de symétrie le nombre d'électrons est bien défini. Un électron est ajouté à la charge du point quantique chaque fois que N passe par un point $N = n + 1/2$. Il s'ensuit que la charge du point quantique en fonction de la différence de potentiel se présente comme un escalier avec des marches de hauteur e.

Il est intéressant d'examiner la dépendance de la charge moyenne $e\langle\hat{n}\rangle$ dans le point quantique non seulement en fonction du potentiel V_G mais aussi de la conductance du contact ponctuel (voir Réfs. [22, 23, 24, 25]). On peut distinguer deux cas limites bien différents : si le point quantique est couplé fortement au réservoir – pour cela il suffit qu'un seul canal de transport soit complètement ouvert ($T = 1$) – il n'y a aucune trace du bloquage de Coulomb et la charge moyenne croît linéairement avec la différence de potentiel [23]. Dans la limite opposée où le point quantique est presque entièrement isolé de son environment on observe la quantification de la charge et donc l'escalier de Coulomb. Dans la discussion suivante nous nous concentrerons sur le cas d'un seul canal de transport dans le contact ponctuel. En traitant la barrière de potentiel entre point quantique et réservoir d'une manière perturbative – le paramètre petit de la théorie de perturbation étant $R = 1 - T \ll 1$ dans la limite de fort couplage et $T \ll 1$ si on part d'un point quantique isolé – il est possible de calculer la charge moyenne dans la proximité des deux cas limites $T = 0$ et $T = 1$ qu'on vient de décrire. Cependant, il s'est avéré [23, 24] qu'une simple théorie de perturbation n'est pas toujours suffisante puisque des divergences logarithmiques sont rencontrées à tous les ordres de la perturbation au moins si on se situe en proximité à un point de symétrie $N = n + 1/2$.

Il a été établi qu'il existe une relation entre le modèle Kondo, qui décrit l'interaction des électrons de conduction dans un métal avec une impureté magnétique, et la physique du bloquage de Coulomb que nous venons de décrire [23, 24]. Le Hamiltonien du modèle Kondo standard est un Hamiltonien de Heisenberg de la forme

$$H_K = J\mathbf{s}_c(0) \cdot \mathbf{S}_I \tag{1.8}$$

où $\mathbf{s}_c(0)$ est le spin d'un électron de conduction mesuré au niveau de l'impureté et $\mathbf{S}_I$ est le spin de l'impureté (on suppose que l'impureté a un spin 1/2). Le Hamiltonien de Kondo décrit des processus de retournement de spin, c'est-à-dire des processus de diffusion qui renversent la direction du spin de l'électron et la direction du spin de l'impureté.

On peut appliquer le Hamiltonien pour le bloquage de Coulomb sur le Hamiltonien du modèle de Kondo dans les deux limites de faible transparence du contact ponctuel [23] et pour un contact ponctuel près de la transparence maximale $G = 2e^2/h$ [24]. Dans le premier cas on peut comprendre cette relation à l'aide de l'analogie suivante : admettons que la différence de potentiel V_G entre grille et point quantique soit telle qu'on se trouve dans le voisinage du point $n = 1/2$, de sorte que les deux états, avec zero et un électron sur le puits, aient des énergies comparables et tous les autres états de charge aient une énergie plus grande que E_C. On identifie alors l'état de charge avec le spin d'une impureté fictive, qui prend la valeur "up" si la charge est un, et "down" si la charge est zero. Simultanément on introduit un deuxième spin fictif qui est associé à la position de l'électron. Pour ce deuxième spin un électron dans le point quantique correspond à spin "up" et un électron dans le réservoir correspond à spin "down". Il est important de noter que les deux spins qu'on a introduits sont des quantités auxi-

liaires et n'ont aucune relation avec le spin physique de l'électron. Le transfert d'une charge du réservoir au point quantique ou du point quantique au réservoir est alors accompagné d'une inversion simultanée des deux spins auxiliaires et ressemble au processus de diffusion entre spins dans le problème de Kondo.

Cette correspondance a permis à Matveev [23] de calculer la charge moyenne sur le point quantique près des points de symétrie $N = n + 1/2$, où une simple théorie de perturbation n'est pas suffisante.

Le lien avec le modèle Kondo permet également d'évaluer la charge moyenne dans la limite de faible réflexion au contact ponctuel [24]. Contrairement à la limite de faible transmission qu'on vient de discuter, l'application est purement mathématique et ne s'explique pas par une simple analogie physique. En partant du Hamiltonien pour le point quantique et le contact ponctuel, on aboutit au Hamiltonien de Kondo dans la limite Emery-Kivelson. Dans cette limite il existe une solution exacte pour le modèle de Kondo. Il est donc à nouveau possible de trouver une expression pour la charge sur le point quantique en fonction de la différence de potentiel à proximité des points de symétrie.

Par la suite nous allons démontrer comment ces correspondances peuvent être généralisées au cas à deux canaux de transmission avec une probabilité de transmission différente dans le contact ponctuel (voir aussi [25]). Expérimentalement une telle situation est réalisée en champ magnétique. Par l'effet Zeeman le champs magnétique induit une différence entre les coefficients de transmission pour les électrons avec spin up et spin down ($T_\uparrow \neq T_\downarrow$ ou $R_\uparrow \neq R_\downarrow$). On verra que l'anisotropie entre les coefficients de réflexion pour les deux canaux est reflétée dans une anisotropie entre les couplages dans le modèle Kondo. De cette observation on pourra déduire quelques résultats intéressants.

Finalement, on peut ajouter que dans cet étude nous négligeons les effets dus à la taille finie du point quantique. Nous supposons que le point quantique est suffisamment grand pour que la distance moyenne Δ entre deux niveaux d'énergie soit petite comparée à la température et à l'énergie de charge E_C. Les différentes échelles d'énergie respectent alors la hiérarchie $E_C \gg T \gg \Delta$.

1.3 Interaction électron-phonon dans un contact ponctuel

Dans la dernière partie de cette thèse nous examinerons les déviations, dues à la diffusion entre électrons et phonons, au résultat obtenu pour la conductance d'un contact ponctuel dans le modèle des électrons sans interactions. Dans cette approximation la conductance suit la dépendance en énergie de la transmission à travers la barrière de potentiel créée par le confinement du contact ponctuel (voir la discussion dans le premier chapitre de cette introduction). L'écart le plus frappant et le mieux étudié entre le résultat théorique pour les électrons libres et les mesures expérimentales est ce qu'on appelle "l'anomalie 0.7". Il s'agit d'une

épaule dans la courbe de conductance vers $0.7(2e^2/h)$. Bien que cette structure fût déjà visible dans les toutes premières expériences sur la quantification de la conductance [4], la première étude détaillée de cet effet date seulement de 1995 [26]. Depuis, plusieurs expériences ont démontré que dans un champ magnétique appliqué dans le plan de l'échantillon il existe une transition continue entre l'anomalie à $0.7(2e^2/h)$ et le plateau de conductance à $0.5(2e^2/h)$ pour les électrons sans spin [26, 27, 28]. Cette observation semble suggérer qu'un effet de spin est à l'origine de l'anomalie à 0.7 [26].

Nous allons nous concentrer sur une autre propriété de la structure, notamment sa forte dépendance en température. Les expériences [26, 28, 29] ont montré que l'épaule est faible aux plus basses températures et qu'elle devient plus importante lorsque la température augmente. Une étude détaillée [29] a indiqué que la correction à la conductance obéit une loi d'Arrhenius

$$\delta G \propto \mathrm{e}^{-T_A/T} \tag{1.9}$$

avec une température d'activation T_A de l'ordre du Kelvin. Une telle dépendance en fonction de la température implique qu'un mécanisme de rétrodiffusion entre en action à une température $T \approx T_A$ et conduit à une suppression partielle de la conductance.

Admettons que les électrons dans le contact ponctuel puissent échanger de l'énergie avec le réseau cristallin. A basse température l'effet de l'interaction électron-phonon sur le transport est fortement supprimé. En effet, pour réfléchir un électron au niveau de Fermi le vecteur d'onde du phonon doit être de l'ordre de $q = 2k_F$ dans la direction du contact ponctuel. L'énergie minimale d'un tel phonon est donc

$$T_A = 2\hbar k_F = \sqrt{E_s E_F} \tag{1.10}$$

où s est la vitesse du son, E_F l'énergie de Fermi des électrons dans le fil, $E_S = 8ms^2$ et m la masse d'un électron. Pour un fil mésoscopique dans l'Arséniure de Gallium on peut estimer que l'énergie de Fermi est d'environ 100 K, $E_s \approx 0.03$ K et donc $T_A \approx 5$ K. Dans le voisinage de la première marche de la conductance la densité d'électrons est très basse. Si on estime que l'énergie de Fermi au centre du contact ponctuel est d'environ 2 K, on obtient $T_A \approx 0.8$ K, ce qui est en accord avec les températures d'activation mesurées dans l'expérience.

Nous présenterons des résultats pour la correction à la conductance dans la limite semi-classique, c'est-à-dire lorsque la conductance du contact ponctuel est près de $G = 2e^2/h$. Nous verrons que la dépendance de nos résultats en fonction de la température et de la tension appliqué entre source et drain, est en bon accord avec les résultats expérimentaux.

1.4 Bibliographie

[1] Y. Imry, *Introduction to mesoscopic physics*, Oxford University Press, 1997.

[2] S. Datta, *Electronic transport in mesoscopic systems*, Cambridge University Press, 1997.

[3] L. L. Sohn, L. P. Kouwenhoven, and G. Schön (Eds.), *Mesoscopic electron transport*, NATO ASI Series E : Vol. 345, Kluwer Academic Publishers.

[4] B. J. van Wees, H. van Houten, C. W. J. Beenakker, J. G. Williamson, L. P. Kouwenhoven, D. van der Marel, and C. T. Foxon, Phys. Rev. Lett. **60**, 848 (1988) ; D. A. Wharam, T. J. Thornton, R. Newbury, M. Pepper, H. Ahmed, J. E. F. Frost, D. G. Hasko, D. C. Peacock, D. A. Ritchie, and G. A. C. Jones, J. Phys. C **21**, L209 (1988).

[5] L. I. Glazman, G. B. Lesovik, D. E. Khmel'nitskii, and R. I. Shekhter, Pis'ma Zh. Eksp. Teor. Fiz. **48**, 218 (1988) [JETP Lett. **48**, 238 (1988)].

[6] M. Büttiker, Phys. Rev. B, **41**, 7906 (1990).

[7] M. Büttiker, Phys. Rev. Lett. **57**, 1761, (1986).

[8] Y. Aharonov and D. Bohm, Phys. Rev. **115**, 485 (1959).

[9] M. Büttiker, Y. Imry, and R. Landauer, Phys. Lett. **96A**, 365, (1983).

[10] Y. Gefen, Y. Imry, and M. A. Azbel, Phys. Rev. Lett. **52**, 139, (1984).

[11] M. Büttiker, Y. Imry, and M. Ya. Azbel, Phys. Rev. A, **30**, 1982 (1984).

[12] B. L. Altshuler, A. G. Aronov and, D. Khmelnitskii, J. Phys. C **15**, 7367 (1982) ; B. L. Altshuler and A. G. Aronov, in *Electron-electron Interaction in Disordered Systems*, edited by A. L. Efros and M. Pollak, (North Holland, Amsterdam, 1985).

[13] J. J. Lin and J. P. Bird, J. Phys. Condens. Matter **14**, R501, (2002).

[14] J. P. Bird, K. Ishibashi, D. K. Ferry, Y. Ochiai, Y. Aoyagi, and T. Sugano, Phys. Rev. B **51**, 18 037, (1995) ;D. P. Pivin, Jr., A. Andresen, J. P. Bird, and D. K. Ferry, Phys. Rev. Lett. **82**, 4687 (1999).

[15] R. M. Clarke, I. H. Chan, C. M. Marcus, C. I. Duruöz and J. S. Harris, Jr., K. Campman, and A. C. Gossard, Phys. Rev. B **52**, 2656, (1995) ; A. G. Huibers, M. Switkes, C. M. Marcus, K. Campman, and A. C. Gossard, Phys. Rev. Lett. **81**, 200, (1998) ;A. G. Huibers, J. A. Folk, S. R. Patel, C. M. Marcus, C. I. Duruöz and J. S. Harris, Jr., Phys. Rev. Lett. **83**, 5090, (1999).

[16] A. E. Hansen, A. Kristensen, S. Pedersen, C. B. Sorensen, and P. E. Lindelof , Phys. Rev. B **64**, 045327 (2001).

[17] K. Kobayashi, H. Aikawa, S. Katsumoto, and Y.Iye, J. Phys. Soc. Jpn., **71** (9), 2094-2097, (2002).

[18] H. R. Zeller and I. Giaever, Phys. Rev. **181**, 789 (1969).

[19] I. O. Kulik and R. I. Shekhter, Zh. Eksp. Theor. Fiz. **62**, 623 (1975), [Sov. Phys. JETP **41**, 308, (1975)].

[20] D. A. Averin and K. K. Likharev, in *Mesoscopic Phenomena in Solids*, edited by B. A. Altshuler, P. A. Lee, and R. A. Webb, (North Holland, New York, 1991).

[21] Y. M. Blanter, Phys. Rev. B **54**, 12807 (1996).

[22] I. L. Aleiner, P. W. Brouwer and L. I. Glazman, Phys. Rep. **358**, 309, (2002).

[23] K. A. Matveev, Zh. Eksp. Teor. Fiz. **98**, 1598 (1990) [Sov. Phys. JETP **72**, 892, (1991)].

[24] K. A. Matveev, Phys. Rev. B **51**, 1743 (1995).

[25] K. Le Hur, Phys. Rev. B **64**, 161302(R) (2001).

[26] K. J. Thomas, J. T. Nicholls, M. Y. Simmons, M. Pepper, D. R. Mace and D. A. Ritchie, Phys. Rev. Lett. **77**, 135 (1996).

[27] K. J. Thomas, J. T. Nicholls, N. J. Appleyard, M. Y. Simmons, M. Pepper, D. R. Mace, W. R. Tribe, and D. A. Ritchie, Phys. Rev. B **58**, 4846 (1998).

[28] S. M. Cronenwett, H. J. Lynch, D. Goldhaber-Gordon, L. P. Kouwenhoven, C. M. Marcus, K. Hirose, N. S. Wingreen, and V. Umansky, Phys. Rev. Lett. **88**, 226805 (2002).

[29] A. Kristensen, H. Bruus, A. E. Hansen, J. B. Jensen, P. E. Lindelof, C. J. Marckmann, J. Nygard, C. B. Sørensen, F.Beuscher, A. Forchel, and M. Michel, Phys. Rev. B **62**, 10950 (2000).

Part I

Electron-electron interactions

CHAPTER 2

Dephasing in a mesoscopic interferometer

2.1 Introduction

Dephasing processes suppress quantum mechanical interference effects and generate the transition from a microscopic quantum coherent world in which interference is crucial to a macroscopic world characterized by the absence of quantum interference effects. Mesoscopic systems are neither entirely microscopic nor macroscopic but at the borderline between the two. Clearly, therefore, dephasing processes play a central role in mesoscopic physics. In this chapter we will address the question of dephasing in ballistic mesoscopic conductors using a mesoscopic interferometer as an example.

It is known [1] that the main mechanism for dephasing in *disordered* mesoscopic conductors in the low temperature regime is electron-electron scattering. In low-dimensional conductors the main contribution to the dephasing is due to scattering events with a small energy and momentum transfer. These processes can be understood as the interaction of an electron with the fluctuating electric field due to the presence of the other electrons in the conductor. [1] The theory by Altshuler, Aronov and Khmelnitskii predicts dephasing rates $\tau_\phi^{-1} \propto T^{2/3}$ for a one-dimensional disordered metal and a dephasing rate linear in temperature $\tau_\phi^{-1} \propto T$ in two dimensions. It should be mentioned, however, that the standard theory can not account for the saturation of the dephasing rate at very low temperatures that is observed experimentally. The origin of this saturation has been hotly debated over the last few years and the issue has not yet been settled. For an introduction to dephasing in mesoscopic physics, including the problem of zero temperature dephasing, and as a guide to further reading see Ref. [2].

While dephasing in disordered conductors is well understood at least above temperatures of the order of a few hundred mK the theoretical understanding of the processes responsible for dephasing in *open ballistic* mesoscopic conductors is less developed. On the experimental side, the situation seems quite clear since there have already been a number of experiments where the dephasing rate has been measured in ballistic quantum dots.[3, 4, 5, 6, 7] More recently, there have also been experiments on dephasing in mesoscopic rings.[8, 9] The main experimental findings can be summarized as follows: at the lowest temperatures reached in the experiments the dephasing rate saturates [3, 7, 6] exactly as in the experiments on disordered conductors. As temperature is increased the dephasing rate grows linearly with temperature $\tau_\phi^{-1} \propto T$ [3, 8, 9] (or according to $\tau_\phi^{-1} \propto AT + BT^2$ [5]). Before discussing dephasing in ballistic rings in detail, we will quickly describe the quantum dot experiments and summarize the current state of the theoretical understanding.

A convenient way[5, 7] to measure the dephasing time in a quantum dot is to extract it from the weak localization correction to the conductance (the dephasing rate can also be determined in different ways, e.g. from the universal conductance fluctuations, that will not be discussed further). Weak localization is very sensitive to magnetic fields, and the weak localization correction δG is the difference $\delta G = \langle G \rangle_{B=0} - \langle G \rangle_{B \neq 0}$ between the conductance measured without a magnetic field and the conductance measured with a field applied (more precisely, $B > B_C$, with a critical magnetic field B_C is needed to break time-reversal invariance). The observed correction can then be compared to the theoretical predictions based on the random matrix theory.[10, 11] Since dephasing can be introduced into the model based on the random matrix theory for non-interacting electrons through an extension of the voltage probe model of Ref. [12] it is possible to determine the dephasing time from the measured correction. Introducing the dephasing through a voltage probe model is a phenomenological approach that mimics the inelastic scattering processes responsible for the decoherence and the dephasing rate for a chaotic dot still needs to be derived from a microscopic model.

Brouwer and Aleiner have calculated the correction to the conductance of a chaotic dot due to electron-electron interactions and have found that the interactions *enhance* the weak-localization correction. Interactions were treated using a constant interaction model, which is a good approximation for a quantum dot in the universal (random matrix) regime.[14, 15] Still, to include a phase-breaking mechanism one would probably have to go beyond this approximation. Vavilov and Aleiner [16] solved the equation of motion for a Cooperon in an irradiated quantum dot and calculated the dephasing due to the external radiation. Takane[17] and Büttiker [18] calculated the phase diffusion time for an electron in or a scattering state of a chaotic quantum dot approximating the full electron-electron interactions by a constant interaction model. Both authors find a dephasing rate that is linear in temperature $\tau_\phi^{-1} \propto T$ and in addition predict that the dephasing rate is inversely proportional to the number of channels in

the leads connecting the dot to the reservoir. Since in these calculations the dephasing rate is introduced as an independent quantity, and not through the calculation of a physical observable like the conductance, the results obtained can not be directly related to the dephasing rates measured in weak localization type experiments.[5, 7] Also, to understand the decoherence of the weak localisation correction it is necessary to include spatially varying potential fluctuations. Still, a straightforward extension of these approaches [17, 18] that includes space-dependent fluctuations should allow us to understand dephasing in open quantum dots. The approach we will apply in our study of dephasing in mesoscopic rings is closely related to that of Ref. [18].

Now we turn our attention to the problem of decoherence in mesoscopic rings. As a consequence of the Aharonov Bohm effect [19] the conductance of a mesoscopic ring exhibits coherent oscillations as a function of the magnetic flux through the ring (For references to the early experimental and theoretical work on the Aharonov Bohm effect in disordered rings we refer the reader to the book by Imry [20]). Decoherence leads to a decrease in the visibility of the amplitude of the conductance oscillations. Dephasing due to a dynamic environment was considered in Refs. [21, 22]. Quite recently the decoherence of the persistent current in a ring [23, 24] as well as decoherence due to a fluctuating magnetic flux through the ring [25] were also investigated. Le Hur proposed to use a mesoscopic interferometer to measure the life-time of an electron in a Luttinger liquid.[26]

2.1.1 Decoherence in an interferometer

In this work, we investigate dephasing in a ballistic Aharonov-Bohm (AB) interferometer, in which electrons (in the absence of interactions) are subject only to forward scattering processes (see Fig. [2.1]). Our idealized setup consists of an AB-ring with four terminals, the arms of the ring being capacitively coupled to lateral gates (see Fig. [2.1]). For a recent experiment on a ballistic (two-terminal) AB-ring with lateral gates coupled to both arms see Ref.[27]. We will concentrate on a ballistic ring with a single transport channel. Although the one-channel limit is of actual experimental interest (see e.g. Refs. [8, 28, 29, 30]), this is mainly done for conceptual clarity. The approach we present can easily be extended to the multi-channel case.

The structure we examine has no closed orbits: as a consequence in its equilibrium state it exhibits no persistent current and in the transport state there is no weak localization correction to the conductance. It exhibits, however, an Aharonov-Bohm effect [19] due to superposition of partial waves in the out-going quantum channel. In fact this is the situation discussed in the original work of Aharonov and Bohm [19]. It is also sometimes assumed in mesoscopic physics without a detailed specification of the conditions (multi-terminal geometry, absence of backscattering) which are necessary for interference to appear only in the final outgoing channel. The system investigated here is the electric analog

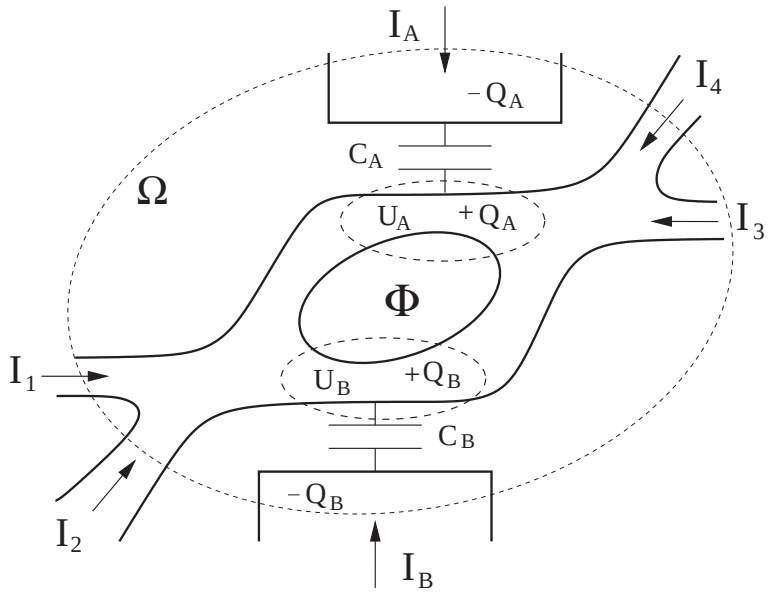

Figure 2.1: The figure shows the four-terminal AB-ring threaded by a magnetic flux. The two arms of the ring are each coupled to a side-gate via a capacitance C_G ($G = A, B$). We consider junctions which are perfectly transmitting and divide the incoming current into the upper and lower branches of the ring. The system then is the electronic equivalent of an optical Mach-Zehnder interferometer (MZI). The total charge in a Gauss sphere Ω drawn around the system of gates and ring is assumed to be zero, implying that current in the system is conserved. It is assumed that each arm is characterized by a single potential U_A (or U_B) and the charge $+Q_A$ (or $+Q_B$).

of an optical interferometer in which the path is divided by forward scattering only. An example of such an arrangement is the Mach-Zehnder[31] interferometer (MZI).

Our work is motivated by the following observations: instead of calculating a dephasing rate, as it was done for example in Refs. [17, 18, 21, 32] to treat dephasing in quantum dots, it is desirable to find a way to directly evaluate the quantity of interest (here the conductance). In small mesoscopic systems the dephasing rate might be a sample specific quantity [18] and there would be little justification in using an ensemble averaged dephasing rate even if we are interested only in the ensemble averaged conductance. Clearly to answer such conceptual questions it is useful to have a model which is as simple as possible.

Second, a mesoscopic conductor connects two or more electron reservoirs: inside a reservoir screening is effective and electron interactions are of little importance. In contrast, inside the mesoscopic structure screening is poor and interactions are important. Thus the process of a carrier entering or leaving the mesoscopic structure is essential since this process gives rise to potential fluctuations. We ask how this process affects the dephasing. In our approach the conductance and the dephasing time are not calculated separately but a dephas-

ing time will appear in the expression for the conductance in a natural way. It quantifies the degree of the attenuation of AB-oscillations due to randomization of the phases of the electrons going through the ring (as opposed to attenuation due to thermal averaging). From our calculations we find that the coherent part of the conductance is diminished by a factor $\exp(-\tau/\tau_\phi)$ relative to the ideal case due to temperature and coupling to the gates. Here τ is the traversal time for going through one arm of the ring. For temperatures $\hbar/\tau \ll kT$ we find a dephasing rate τ_ϕ^{-1} *linear* in temperature. In an experiment on a two-terminal AB-ring, a dephasing rate linear in temperature was measured by Hansen et al. [8]. Very recently a dephasing rate linear in temperature was also measured by Kobayashi et al. [9] in a four-terminal geometry.

We calculate the effect of internal potential fluctuations on the linear response dc-conductance in the ring as a function of the strength of the coupling between ring and gates and of temperature. As far as our treatment of the dephasing is concerned our approach is closely related to previous work by Büttiker and Martin [32] and by Büttiker.[18] Also, it is similar in spirit to the work by Altshuler et al.[1] since we consider dephasing due to (charge-fluctuation induced) Nyquist noise.

To simplify the discussion we assume that it is possible to draw a Gauss sphere around the system of gates and ring such that all electric field lines emanating within the sphere also end in it (see Fig. [2.1]). This implies that the total charge in the sphere is zero at any time. However, it is possible to charge up one part of the system (an arm of the ring) relative to another part (the nearby gate) creating *charge dipoles*. Charge fluctuations in the arms of the ring lead to fluctuations of the effective internal potentials. Electrons going through the ring are exposed to these potential fluctuations and scatter inelastically. The strength of the coupling between the gates and the arms determines the amount of screening and thus the strength of the effective electron-electron interaction. When the capacitance C between arm and gate becomes very large, the Coulomb energy e^2/C of the system goes to zero. This means that it is in principle possible to put any amount of charge on the ring without causing any reaction. The charge fluctuations in the ring are thus completely free. We say that in this limit ($C \to \infty$) gate and arm *decoupled*.

The gates are treated as macroscopic entities with perfect screening. The carrier dynamics in the gates is irrelevant for the discussion presented here. They do not represent an external bath or dephasing agent. The irreversible source necessary for dephasing is given by the electron dynamics of the ring itself: the phase and energy of a carrier exiting into a contact are unrelated to the phase and energy of a carrier entering the sample.

The chapter is structured as follows: in the following section (Sec. 2.2) we will present the scattering matrix description for the Mach Zehnder interferometer. Subsequently (see Sec. 2.3), a simple model for dephasing is presented and we will also discuss thermal averaging. The dephasing rate is related to the zero-

frequency potential fluctuation spectra. Fluctuation spectra and decoherence rates are then calculated in Sec. 2.4. The role of the external circuit and the probe configuration dependence of the dephasing times is addressed in Sec. 2.5. In Sec. 2.6 we calculate the conductance in the MZI using a more elaborate approach. Finally, Sec. 2.7 contains our conclusions.

2.2 The Mach Zehnder interferometer

We consider an MZI with a single transport channel threaded by a magnetic flux Φ. The interferometer is sketched in Fig. [2.2] where all current amplitudes are indicated. The amplitude of the current incoming at an intersection is A_α and the amplitude of the out-going current is B_α. The scattering matrix of the total interferometer is built up from the scattering matrices for the two intersections and the scattering matrices of the two arms. The two junctions are treated as simple beam-splitters: an electron arriving at one of them, coming from a reservoir can enter either of the two arms of the ring, but can not be reflected back to a reservoir. An electron coming to the intersection from the ring will enter one of the reservoirs. The amplitudes for going straight through the intersection and for being deflected to the adjacent lead in the forward direction are $\sqrt{T}$ and $i\sqrt{R}$ respectively, where $T + R = 1$. Transmission through the intersections is taken to be independent of energy. To summarize, the scattering matrix equations for the left and right beam-splitter are (see also Fig. [2.1]), respectively,

$$\begin{pmatrix} B_1 \\ B_2 \\ B_6 \\ B_5 \end{pmatrix} = \mathbf{S_0} \begin{pmatrix} A_1 \\ A_2 \\ A_6 \\ A_5 \end{pmatrix}, \quad \begin{pmatrix} B_8 \\ B_7 \\ B_3 \\ B_4 \end{pmatrix} = \mathbf{S_0} \begin{pmatrix} A_8 \\ A_7 \\ A_3 \\ A_4 \end{pmatrix}. \tag{2.1}$$

Here, the scattering matrix $\mathbf{S_0}$ for the beam-splitter has the very simple form

$$\mathbf{S_0} = \begin{pmatrix} 0 & \mathbf{s_0} \\ \mathbf{s_0} & 0 \end{pmatrix}, \quad \mathbf{s_0} = \begin{pmatrix} \sqrt{T} & i\sqrt{R} \\ i\sqrt{R} & \sqrt{T} \end{pmatrix}. \tag{2.2}$$

For symmetric intersections, a case we will often consider in the following, the transmission probabilities are $R = T = 1/2$. To construct the scattering matrix for the full interferometer we also need the equations relating the currents entering and leaving the two arms. These equations are most conveniently written in terms of the transfer matrices connecting the left and the right junction:

$$\begin{pmatrix} A_6 \\ A_5 \\ B_6 \\ B_5 \end{pmatrix} = \begin{pmatrix} 0 & \mathbf{T_1} \\ \mathbf{T_2} & 0 \end{pmatrix} \begin{pmatrix} A_8 \\ A_7 \\ B_8 \\ B_7 \end{pmatrix}. \tag{2.3}$$

The matrices $\mathbf{T_1}$ and $\mathbf{T_2}$ are, in turn, given by the expressions

$$\mathbf{T_1} = \begin{pmatrix} 0 & \mathrm{e}^{+i\Theta_B + i\Phi_B} \\ \mathrm{e}^{+i\Theta_A - i\Phi_A} & 0 \end{pmatrix}, \quad \mathbf{T_2} = \begin{pmatrix} 0 & \mathrm{e}^{-i\Theta_B + i\Phi_B} \\ \mathrm{e}^{-i\Theta_A - i\Phi_A} & 0 \end{pmatrix}.$$

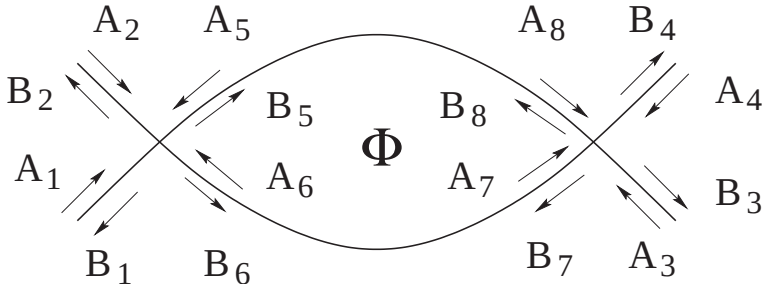

Figure 2.2: Schematic sketch of the Mach-Zehnder interferometer. The amplitude of the current incoming through contact α is A_α, the outgoing current amplitude in the same contact is B_β.

Here, the dynamic phases are $\Theta_i = \sqrt{2m(E - eU_i)}L_i/\hbar$ with a local potential eU_i in arm i of the interferometer (e is the electron charge and U_i has the dimension of a voltage). The index i takes the values $i = A, B$, where A refers to the upper and B to the lower arm. Furthermore, L_i is the length of arm i, m the effective electron mass and E the electrons energy. The magnetic phase picked up by a particle going through arm i clockwise is Φ_i. Then, $\Phi_A + \Phi_B = 2\pi\Phi/\Phi_0$, where Φ is the flux through the ring and Φ_0 is the flux quantum.

Combining Eqs. 2.1 and 2.3 the internal amplitudes (indices $\alpha = 5 - 8$) can be eliminated and the scattering matrix for the full MZI can be obtained. The result is

$$\begin{aligned}
S_{13}(E) &= i\sqrt{TR}\left(\mathrm{e}^{ikL_A - i\Phi_A} + \mathrm{e}^{ikL_B + i\Phi_B}\right) = S_{24}(E), \\
S_{14}(E) &= -R\,\mathrm{e}^{ikL_A - i\Phi_A} + T\mathrm{e}^{ikL_B + i\Phi_B}, \\
S_{23}(E) &= T\mathrm{e}^{ikL_A - i\Phi_A} - R\mathrm{e}^{ikL_B + i\Phi_B}, \\
S_{12}(E) &= S_{34}(E) = S_{21}(E) = S_{43}(E) = 0, \\
S_{\alpha\alpha}(E) &= 0.
\end{aligned} \tag{2.4}$$

The remaining non-zero matrix elements can be obtained from the reversibility relation $S_{\alpha\beta}(E; B) = S_{\beta\alpha}(E; -B)$. Inverting the magnetic field $\mathbf{B}$ has the effect of changing the sign of the magnetic phases Φ_A and Φ_B. For later convenience we here also list the transmission probabilities $T_{\alpha\beta}(E) = |S_{\alpha\beta}(E)|^2$:

$$\begin{aligned}
T_{13}(E) = T_{24}(E) &= 2RT\left(1 + \cos\left[k_A L_A - k_B L_B - 2\pi\Phi/\Phi_0\right]\right), \\
T_{14}(E) = T_{23}(E) &= R^2 + T^2 - 2RT\cos\left[k_A L_A - k_B L_B - 2\pi\Phi/\Phi_0\right], \\
T_{12}(E) = T_{34}(E) &= 0, \\
T_{\alpha\alpha}(E) &= 0.
\end{aligned} \tag{2.5}$$

The remaining elements of the transmission matrix can be obtain from the Onsager relations [33] which here can be written as $T_{\alpha\beta}(E; \Phi) = T_{\beta\alpha}(E; -\Phi)$.

2.3 Dephasing and thermal averaging

We now want to present a simple argument which will allow us to understand the decoherence of the Aharonov-Bohm oscillations.

To keep the notations simple we define $T(E) = T_{13}(E)$ and will use this element of the transmission matrix as a generic example throughout this section. Furthermore, we restrict the discussion to an MZI with symmetric junctions ($R = T = 1/2$) - it is straightforward to generalize the results to the case $R \neq T$ - and write

$$T(E) = \frac{1}{2}\left(1 + \cos\left[k_A L_A - k_B L_B - 2\pi\Phi/\Phi_0\right]\right).$$

In addition to the assumptions already made, we also take the arms of the ring to have the same length ($L_A = L_B = L$) and we expand the wave vectors $k_i = \sqrt{2m(E_F - eU_i)}$ ($i = A, B$) to the first order in the internal potentials. This can be done since these potentials are small compared to the Fermi energy. For the phase $k_i L$ we thus obtain $k_i L \approx k_F L - eU_i(\tau/\hbar)$ and for the transmission probability

$$T(E) = \frac{1}{2}\left(1 + \cos\left[\frac{\tau}{\hbar} e\Delta U + 2\pi\Phi/\Phi_0\right]\right). \tag{2.6}$$

Here we have introduced the traversal time $\tau = L/v_F$ and the potential difference $\Delta U = U_A - U_B$.

The internal potentials were introduced in an attempt to take into account electron-electron interactions in tractable way. So far (see e.g. Eq. 2.4) these potentials were implicitly treated as time-independent, or, more precisely, it was assumed that the characteristic frequencies of the fluctuations are smaller or, at best, comparable to the inverse traversal time $1/\tau$, such that transport is in fact adiabatic.

To account for potential fluctuations it is in principle necessary to solve the Schrödinger equation for the MZI with the time dependent potentials $U_A(t)$ and $U_B(t)$. Such an approach is presented in Sec. 2.6. The phenomenological approach we followed so far is simpler and also allows us to understand the effect of electron-electron interactions with small energy transfer on the coherent transport through the interferometer, as we will argue now.

As a first step we need to specify what we mean by the internal potentials used so far: in the adiabatic approximation made here, we use a potential

$$U_i = \frac{1}{\tau}\int_0^\tau dt U_i(t) \tag{2.7}$$

that is averaged over fluctuations takeing place on a time scale shorter than the traversal time instead of the fully time-dependent internal potential. Within this adiabatic approximation, the scattering matrix for the MZI is given by Eq. 2.4. Every electron, as it crosses the sample from one contact to the other, effectively sees a potential that is constant. However, the values for the potentials U_i are

different and uncorrelated for different electrons. Both, the introduction of a potential averaged over the traversal time and the assumption that potentials at different times are uncorrelated are of course justified only if the main frequencies of the potential fluctuations are of the order of or smaller than the traversal time.

This assumption is justified for open mesoscopic conductors connected to reservoirs through leads with many transport channels (see e.g. [34, 35]). There, the characteristic frequencies of potential and charge fluctuations are of the order of the inverse charge relaxation time $1/\tau_{RC}$ and $\tau_{RC} \ll \tau$. In the case of an interacting one-channel wire frequencies up to the plasmon frequency $\omega_p = 1/(g\tau)$ are important. Here $0 < g < 1$ is the interaction parameter and the adiabatic approximation is valid only in the weakly interacting regime $g \to 1$.

Also, we have made the simplifying assumption that each arm of the ring can be described by a single, space-independent potential. Again, this is a reasonable assumption if there is a time, say τ_{RC}, shorter than the traversal time τ after which potential differences between different points in the same arm i are washed out.

To characterize the potential fluctuations we introduce the fluctuation spectra $S_{U_iU_i}$ through

$$2\pi\delta(\omega+\omega')S_{U_iU_i}(\omega) = \langle \Delta u_i(\omega)\Delta u_i(\omega')\rangle. \tag{2.8}$$

Here $\Delta u_i(\omega) = u_i(\omega) - \langle u_i(\omega)\rangle$ and we will in the following always assume that the mean vanishes, $\langle u_i(\omega)\rangle = 0$. The Fourier transform $u_i(\omega)$ of the time-dependent potential $U_i(t)$ is

$$u_i(\omega) = \int dt \mathrm{e}^{+i\omega t} U_i(t). \tag{2.9}$$

If the potential fluctuations are correlated in time over a period τ_{RC} the half-width of the spectrum is of the order of the inverse $1/\tau_{RC}$ of the charge relaxation time [35].

Now that we defined the slowly varying internal potentials U_i (see Eq. 2.7), we can substitute them into the transmission probability Eq. 2.6, with the result

$$T(E) = \frac{1}{2}\left(1 + \cos\left[\frac{e}{\hbar}\int_0^\tau dt \Delta U(t) + \pi\Phi/\Phi_0\right]\right). \tag{2.10}$$

Note, that this expression could also have been guessed in an even simpler way: a particle in a time-dependent (infinitely extended) potential $U_i(t)$ that is switched on for a finite time τ picks up a phase

$$\phi_i(\tau) = \frac{e}{\hbar}\int_0^\tau U_i(t)dt.$$

If we equate the time during which this potential is switched on, with the traversal time we are lead to make the replacement $kL \to kL + \phi_i(\tau)$ for the phase in arm i in order to correct for the effect of the fluctuating potential $U_i(t)$. This argument gives some additional support to the solution proposed above.

Next we have to statistically average Eq. 2.10 with the probability distribution $P[U_i(t)]$ of the potential $U_i(t)$. We will assume that the potentials are distributed according to the Gaussian distribution

$$P[U_i] = \frac{1}{\sqrt{2\pi\sigma}} \mathrm{e}^{-\frac{1}{2\sigma}U_i^2} \tag{2.11}$$

which allows us to rewrite the transmission probability $T(E)$ in a particularly convenient fashion as

$$T(E) = \frac{1}{2}\left(1 + \mathrm{e}^{-\frac{1}{2}\langle\phi(\tau)^2\rangle} \cos\left[2\pi\Phi/\Phi_0\right]\right). \tag{2.12}$$

Pilgram and Büttiker [36] have shown, that the Gaussian approximation holds for the MZI. More generally, it is reasonable as long as the true probability distribution is relatively narrow. In Eq. 2.11 we have also used that the potential fluctuations in the two arms are uncorrelated as will be shown in Sec. 2.4.1. This is not true anymore if there is backscattering in the intersections or if there are closed orbits. Then, Eq. 2.11 has to be replaced by a multivariate Gaussian distribution $P[\{U_i(t)\}]$.

In Eq. 2.12 the origin of the decoherence is already obvious, but the damping factor can still be simplified. The time integrals can be done if the potential difference $\Delta U(t) = U_A(t) - U_B(t)$ is expressed through its Fourier transform. If we then invoke Eq. 2.8 we obtain

$$\frac{1}{2}\langle\phi(\tau)^2\rangle = \frac{e^2}{\pi\hbar^2}\int d\omega \frac{\sin(\omega\tau/2)^2}{\omega^2} S_{\Delta U\Delta U}(\omega) \approx \frac{e^2}{2\hbar^2}\,\tau S_{\Delta U\Delta U}(0). \tag{2.13}$$

The approximation made in the last step is good as long as the typical time scale τ_{RC} on which the potential fluctuations are correlated is short compared to the traversal time τ and becomes exact in the white noise limit. For the transmission probability we finally get

$$T(E) = \frac{1}{2}\left(1 + \mathrm{e}^{-\tau\Gamma_\phi} \cos\left[2\pi\Phi/\Phi_0\right]\right) \tag{2.14}$$

where the dephasing rate or inverse dephasing time $\Gamma_\phi = 1/\tau_\phi$ is related to the zero-frequency spectral function via

$$\Gamma_\phi = \frac{e^2}{2\hbar^2} S_{\Delta U\Delta U}(0). \tag{2.15}$$

Eqs. 2.14 and 2.15 contain the main results of this section. Once the relation Eq. 2.15 between the decoherence rate and the spectrum is established the problem of decoherence is reduced to the calculation of the zero-frequency spectrum.

It is important to emphasize, that not only dephasing but also thermal smearing leads to a decrease in the amplitude of the Aharonov-Bohm oscillations. Again, we will assume that the beam-splitters are symmetric $R = T = 1/2$ but

in contrast to the previous discussion we will allow for arms of different length $L_A \neq L_B$. Furthermore, we neglect the effect of interactions and set the internal potentials to $U_A = U_B = 0$. Then the transmission probability $T(E) = T_{13}(E)$ becomes

$$T(E) = \frac{1}{2}\left(1 + \cos\left[k_F \Delta L \left(1 + \frac{E - E_F}{2E_F}\right) + 2\pi\Phi/\Phi_0\right]\right). \tag{2.16}$$

Here $\Delta L = L_A - L_B$ is the length difference between the two arms and we have expanded the wave vector $k(E)$ to first order in the energy E around the Fermi energy E_F. The finite temperature, linear response conductance is given by

$$G/G_0 = \int dE \left(-\frac{\partial f}{\partial E}\right) T(E) \tag{2.17}$$

where $G_0 = 2e^2/h$ is the conductance quantum. Substituting Eq. 2.16 into Eq. 2.17 the energy integration can be performed exactly with the result

$$\frac{G}{G_0} = \frac{1}{2}\left[1 + \left(\frac{kT}{E_\Delta}\right)\frac{\cos\left(k_F \Delta L + 2\pi\Phi/\Phi_0\right)}{\sinh\left(kT/E_\Delta\right)}\right] \tag{2.18}$$

where $E_\Delta = (\lambda_F/\Delta L)E_F/\pi^2$ and the Fermi wave length $\lambda_F = 2\pi/k_F$. From Eq. 2.18 it is seen that the visibility of the AB-oscillations decays exponentially for temperatures $kT \gg E_\Delta$.

What is surprising about this result is that the characteristic energy of the exponential decay is given by E_Δ which diverges as $\Delta L \to 0$. For an interferometer with two arms of exactly the same length Eq. 2.18 thus predicts that temperature has no effect whatsoever. Instead of E_Δ one would much rather expect the characteristic temperature to be of the order of the ballistic Thouless energy $E_T = E_F(\lambda/L)$ which is comparable to E_Δ only if the length difference between the two pathes is of the order of the length of the path itself.

For our purposes it is very convenient that temperature effect can be neglected since in any case we are only interested in phase breaking. In Refs. [8] and [30] it is shown how the effect of thermal smearing can be taken into account when one is interested in extracting the decoherence rate from the experimentally accessible total decay rate due to decoherence and thermal smearing.

2.4 Dephasing time

2.4.1 Charge fluctuation spectra

In the previous section the internal potentials U_A and U_B of the two arms of the interferometer were introduced and it was shown that the decoherence rate of the Aharonov Bohm oscillations is proportional to the zero frequency spectrum.

Here, we will review how the internal potentials and their fluctuations can be expressed through the scattering matrix. In our discussion we closely follow the original work on this topic due to Pedersen, van Langen and Büttiker [37]. It should also be pointed out that all the results given in this section are valid for a wide set of mesoscopic conductors and their applicability is not restricted to the Mach Zehnder interferometer.

Also, we will make a point of writing all equations in a way that they are valid for conductors with many transport channels. So far, and in most of this work we will for conceptual clarity consider an interferometer with a single transport channel while in a typical experiment [8, 9] there are several (3-10, say) transport channels that contribute to the conduction. As we will see, the fluctuation spectra and consequently the dephasing rates can as well be obtained in the many-channel case. It is even so, that the entire formalism presented so far is better justified in the multi-channel case where screening is stronger and electron-electron interactions are correspondingly weaker.

Let's consider a mesoscopic structure, characterized by a set of charges Q_i and their associated internal potentials U_i. Every charge is capacitively coupled to a macroscopic back-gate via a geometrical capacitance C_i. In the case of the MZI a charge Q_i and a potential U_i belong to each of its arms (and $i = A, B$). For simplicity, we assume that the internal capacitances C_{ij} between the different parts i and j (the two arms, for the MZI) of the mesoscopic structure are infinitely large and that in consequence conductor i does not know about the charge in conductor j. This assumption can in principle be relaxed (see [38]), but it is reasonable as long as every mesoscopic conductor is close to a metallic gate that helps to screen the interactions with other conductors lying further away. With these assumptions there are two independent equations for the charge (and potential) in each conductor. They are

$$\begin{aligned} \hat{Q}_i(\omega) &= C_i \hat{U}_i(\omega), \\ \hat{Q}_i(\omega) &= e\hat{N}_i(\omega) - e^2 D_i(\omega)\hat{U}_i(\omega). \end{aligned} \tag{2.19}$$

The second equation states that the total charge in conductor i is the difference between the bare charge $e\hat{N}_i(\omega)$ injected from the reservoirs through the contacts attached to conductor i and the screening charge $-e^2 D_i(\omega)\hat{U}_i(\omega)$ that builds up in response to this external perturbation. In the Fermi-Thomas approximation the screening charge is proportional to the local, frequency-dependent, density of states $D_i(\omega)$ in conductor i and it is also proportional to the local potential $\hat{U}_i(\omega)$. Solving Eqs. 2.19 for the potential $\hat{U}_i(\omega)$ gives

$$\hat{U}_i(\omega) = \frac{\hat{N}_i(\omega)}{e^2 D_i(\omega) + C_i} = \frac{C_{\mu,i}(\omega)}{C e^2 D_i(\omega)} \hat{N}_i(\omega). \tag{2.20}$$

The electrochemical capacitance $C_{\mu,i}(\omega)$ is the series capacitance of the geometrical capacitance C_i and the density of states $D_i(\omega)$ [41]:

$$C_{\mu,i}^{-1}(\omega) = C_i^{-1} + \left(e^2 D_i(\omega)\right)^{-1}. \tag{2.21}$$

Eq. 2.20 relates the internal potential in a simple way to the bare charge. In the present model $\hat{U}_i(\omega)$ is a function of $\hat{Q}_i(\omega)$ only (and not of $\hat{Q}_j(\omega)$). This would change if non-infinite internal capacitances were introduced. We now proceed to the calculation of the fluctuation spectra. From Eq. 2.20 it can be seen that we need to know the spectra of the bare charge fluctuations in order to obtain the spectral functions for the potentials.

Our next step will be to express the charge operators through the scattering matrix.[37] To this end we first consider the operator $\hat{N}(\omega) = \sum_i \hat{N}_i(\omega)$ for the total charge in the sample. Current conservation implies that

$$i\omega e\hat{N}(\omega) = \sum_\gamma \hat{I}_\gamma(\omega) \tag{2.22}$$

where the sum is over all the contacts of the sample. The current operator in terms of the scattering matrix of the sample is given by [40],

$$\hat{I}_\gamma(\omega) = e\sum_{\alpha\beta}\int dE\hat{\mathbf{a}}^\dagger_\alpha(E)\left[\delta_{\gamma\alpha}\delta_{\gamma\beta}\mathbb{1}_\gamma - \mathbf{s}^\dagger_{\gamma\alpha}(E)\mathbf{s}_{\gamma\beta}(E+\hbar\omega)\right]\hat{\mathbf{a}}_\beta(E+\hbar\omega).$$

Here the vector $\hat{\mathbf{a}}^\dagger_\alpha(E)$ ($\hat{\mathbf{a}}_\beta(E+\hbar\omega)$) with elements $\hat{a}^\dagger_{\alpha m}(E)$ ($\hat{a}_{\beta n}(E+\hbar\omega)$) has the length of the number N_α (N_β) of channels in contact α (β) and $\mathbb{1}_\alpha$ is the unit matrix of dimension N_α. The operator $\hat{a}^\dagger_{\alpha m}(E)$ creates a scattering state at energy E that enters the conductor through channel m in lead α while $\hat{a}_{\beta n}(E+\hbar\omega)$ destroys a scattering state at energy $E+\hbar\omega$ incoming through channel n of lead β. Furthermore, $\mathbf{s}_{\gamma\alpha}(E)$ is a sub-matrix of dimension $N_\gamma \times N_\alpha$ of the total scattering matrix.

With the help of Eq. 2.22 and using the unitarity of the scattering matrix, it can be shown that the quantum mechanical operator for the total charge (in units of the elementary charge e) can be written as [37]

$$\hat{N}(\omega) = h\sum_{\alpha\beta,mn}\int dE\hat{a}^\dagger_{\alpha m}(E)D_{\alpha\beta,mn}(E,E+\hbar\omega)\hat{a}_{\beta,n}(E+\hbar\omega) \tag{2.23}$$

where $D^{(i)}_{\alpha\beta,mn}(E,E+\hbar\omega)$ is an element of the density of states matrix. From the above calculations it follows that the density of states matrix is related to the scattering matrix through

$$D_{\alpha\beta}(E,E') = \frac{1}{2\pi i}\sum_\gamma \mathbf{s}^\dagger_{\gamma\alpha}(E)\frac{\mathbf{s}_{\gamma\beta}(E)-\mathbf{s}_{\gamma\beta}(E')}{E-E'}.$$

Further down we will only need the zero frequency limit of this expression which is simply given by

$$D_{\alpha\beta}(E) = \frac{1}{2\pi i}\sum_\gamma \mathbf{s}^\dagger_{\gamma\alpha}(E)\frac{\mathbf{s}_{\gamma\beta}(E)}{dE} = -\frac{1}{2\pi i}\sum_\gamma\int_\Omega d^3\mathbf{r}\,\mathbf{s}^\dagger_{\gamma\alpha}(E)\frac{\mathbf{s}_{\gamma\beta}(E)}{edU(\mathbf{r})}. \tag{2.24}$$

The second equation is correct in the semiclassical limit where we can replace the derivative with respect to the charge by a derivative with respect to a local potential. The integral is over the volume included by the Gauss sphere Ω (see Fig. [2.1]). From this equation it becomes clear how we can make the transition from global to local quantities in the zero-frequency limit. Namely, to obtain an expression for the local charge operator in conductor i we restrict the integration to a smaller volume that only includes conductor i.

The quantities we eventually want to calculate are the spectra $S_{Q_iQ_k}(\omega)$ of the bare charge fluctuations ($i = k$) and correlations ($i \neq k$) respectively. Quite generally, they are defined through the relation

$$2\pi\delta(\omega+\omega')S_{N_iN_k}(\omega) = \frac{1}{2}\langle\Delta\hat{N}_i(\omega)\Delta\hat{N}_k(\omega') + \Delta\hat{N}_k(\omega')\Delta\hat{N}_i(\omega)\rangle. \tag{2.25}$$

So far we have not been able to express the local charge operators through the scattering matrix and as we will see below, this becomes possible only in the zero frequency limit. Luckily, to obtain the dephasing rates, this is all we need. Let us assume for the moment that the operator for the local charge can be written in the form of Eq. 2.23 but with the elements of the global density of states matrix $D_{\alpha\beta,mn}(E, E+\hbar\omega)$ replaced by the elements $D^{(i)}_{\alpha\beta,mn}(E, E+\hbar\omega)$ of the *local* density of states matrix. Substituting the operator Eq. 2.23 for the charge in conductor i into the symmetrized correlator Eq. 2.25 leads to

$$\begin{aligned} S_{N_iN_k}(\omega) &= \frac{h}{2}\sum_{\alpha\beta,mn}\int dE D^{(i)}_{\alpha\beta,mn}(E, E+\hbar\omega)D^{(k)}_{\beta\alpha,nm}(E+\hbar\omega, E) \\ &\times \left[f_\alpha(E)(1-f_\beta(E+\hbar\omega) + (1-f_\alpha(E))f_\beta(E+\hbar\omega\right]. \end{aligned} \tag{2.26}$$

Since the density of states varies only slowly around the Fermi energy on a scale set by the temperature T or the bias $\Delta\mu_{\alpha\beta} = \mu_\alpha - \mu_\beta$ ($\Delta\mu_{\alpha\beta}, T \ll E_F$) the matrix elements $D^{(i)}_{\alpha\beta,mn}(E, E+\hbar\omega)$ can be evaluated at the Fermi energy. The energy integration over the products of Fermi functions can then be done exactly and we find

$$\begin{aligned} S_{N_iN_k}(\omega) &= \frac{h}{2}\sum_{\alpha\beta,mn} D^{(i)}_{\alpha\beta,mn}(E_F, E_F+\hbar\omega)D^{(k)}_{\beta\alpha,nm}(E_F+\hbar\omega, E_F) \\ &\times (\hbar\omega+\Delta\mu_{\alpha\beta})\coth\left[(\hbar\omega+\Delta\mu_{\alpha\beta})/2kT\right] \end{aligned} \tag{2.27}$$

where T is temperature and $\Delta\mu_{\alpha\beta} = \mu_\alpha - \mu_\beta$. In the low-frequency limit, of interest to us, these matrix elements of the local density of states matrix become (see Eq. 2.24)

$$D^{(i)}_{\alpha\beta}(E) = -\frac{1}{2\pi i}\sum_\gamma \mathbf{s}^\dagger_{\gamma\alpha}(E)\frac{d\mathbf{s}_{\gamma\beta}(E)}{edU_i}. \tag{2.28}$$

Here, we have made use of our assumption that the mesoscopic system we are studying can be described by a set of discreet potentials that are themselves

space-independent. The total local density of states D_i to which we have already refered repeatedly is the sum

$$D_i = \sum_\gamma Tr\left[D_{\gamma\gamma}\right] = -\frac{1}{2\pi i}\sum_{\alpha,\gamma} Tr\left[\mathbf{s}^\dagger_{\gamma\alpha}(E)\frac{d\mathbf{s}_{\gamma\alpha}(E)}{edU_i}\right]$$

of the diagonal elements of the local density of states matrix. The trace is over the quantum channels. If we do not explicitly indicate the frequency-dependence we always mean the zero-frequency limit of a frequency dependent quantity.

With the help of Eq. 2.20 fluctuations of the bare charge are readily related to those of the potential and, in the zero-frequency limit, we get

$$S_{U_iU_k}(0) = \frac{1}{D_iD_k}\left(\frac{C_{\mu,i}C_{\mu,k}}{C_iC_k}\right) S_{N_iN_k}(0). \tag{2.29}$$

Eq. 2.29 can be further simplified and at finite temperature in equilibrium and zero bias we find from Eqs. 2.27 and 2.29

$$S_{U_iU_k}(0) = 2kTR_q^{ik}\left(\frac{C_{\mu,i}C_{\mu,k}}{C_iC_k}\right) \tag{2.30}$$

for the low-frequency limit of the spectral function. The charge relaxation resistance R_q^{ik} is [37]

$$R_q^{ik} = \frac{h}{2e^2}\frac{\sum_{\alpha,\beta} Tr\left[D^{(i)}_{\alpha\beta}D^{(k)\dagger}_{\alpha\beta}\right]}{D_iD_k} \tag{2.31}$$

where we have used the short notation $D^{(i)}_{\alpha\beta}(E_F, E_F) \equiv D^{(i)}_{\alpha\beta}$. In the case where a finite bias eV is applied to contact α while all other contacts are kept at the same chemical potential, the fluctuation spectrum is

$$S_{U_iU_k}(0) = 2|eV|R_V^{ik}\left(\frac{C_{\mu,i}C_{\mu,k}}{C_iC_k}\right), \tag{2.32}$$

with the Schottky resistance

$$R_V^{ik} = \frac{h}{2e^2}\frac{\sum_{\alpha\neq\beta}\left(Tr\left[D^{(i)}_{\alpha\beta}D^{(i)\dagger}_{\alpha\beta}\right] + Tr\left[D^{(i)}_{\beta\alpha}D^{(i)\dagger}_{\beta\alpha}\right]\right)}{D_iD_k}. \tag{2.33}$$

In conclusion, we have here rederived Eqs. 2.30 and 2.32 for the zero-frequency noise of the potential fluctuations in equilibrium and in the driven case. These results are still written in a very general form and we will now apply them to the Mach Zehnder interferometer.

2.4.2 Dephasing rate for the MZI

It thus remains to calculate the charge relaxation (see Eq. 2.31) and Schottky resistances (Eq. 2.33) for the Mach-Zehnder Interferometer. For completeness

and for later use we first give the local density of states matrices that can be obtained substituting the scattering matrix Eq. 2.4 into Eq. 2.28. They are

$$\mathbf{D}^{(A)} = \frac{L_A}{hv_F} \begin{pmatrix} R & -i\sqrt{RT} & 0 & 0 \\ +i\sqrt{RT} & T & 0 & 0 \\ 0 & 0 & T & -i\sqrt{RT} \\ 0 & 0 & +i\sqrt{RT} & R \end{pmatrix} \tag{2.34}$$

for the upper arm and, very similarly,

$$\mathbf{D}^{(B)} = \frac{L_B}{hv_F} \begin{pmatrix} T & +i\sqrt{RT} & 0 & 0 \\ -i\sqrt{RT} & R & 0 & 0 \\ 0 & 0 & R & i\sqrt{RT} \\ 0 & 0 & -i\sqrt{RT} & T \end{pmatrix} \tag{2.35}$$

for the lower arm. The total density of states in arm i is the sum of all diagonal elements of the respective density of states matrix $D^{(i)} = \sum D^{(i)}_{\alpha\alpha} = 2L_i/(hv_F)$ where the factor of two is due to the presence of left- and right-moving states and spin is not yet accounted for. The diagonal element $D^{(i)}_{\alpha\alpha}$ is refered to as the injectivity [37] of contact alpha since it is the contribution to the total local DOS due to injection from contact α. With these results and using Eqs. 2.31 and 2.33 we immediately find

$$R_q^{AA} = R_q^{BB} = \frac{h}{4e^2}, \tag{2.36}$$

$$R_q^{AB} = R_q^{BA} = 0, \tag{2.37}$$

$$R_V^{AA} = R_V^{BB} = \frac{h}{16e^2}, \tag{2.38}$$

$$R_V^{AB} = R_V^{BA} = -\frac{h}{16e^2}, \tag{2.39}$$

for the Schottky and charge relaxation resistances. Combining these equations with Eqs. (2.30) and (2.32) we get potential correlations for the equilibrium and out-of-equilibrium situations. It is interesting to note that at equilibrium the potentials in the two arms are *uncorrelated*. This is a consequence of the absence of closed electronic orbits in the ring and the fact that we have not introduced a Coulomb coupling between the two branches of the ring. For the same reason correlations are independent of the magnetic field. This implies, that despite the fact that AB-oscillations are observed in the currents measured at one of the contacts, the interior of the ring behaves like a classical system. In contrast, the charge fluctuations generated by the shot noise are correlated. Like the equilibrium charge fluctuations they are for the geometry investigated here independent of the AB-flux.

In Eq. (2.36) we have introduced the *charge-relaxation* resistance $R_q = h/(4e^2)$ of the interferometer. The charge relaxation resistance [41] is a measure of the dissipation generated by the relaxation of excess charge on the conductor into the

reservoirs. For a structure with perfect channels connected to a reservoir each reservoir channel connection contributes with a conductance $G_q^{(1)} = 2e^2/h$: the conductances of different channels add in parallel since each channel reservoir connection provides an additional path for charge relaxation. For example, a ballistic wire connected to two reservoirs has a charge relaxation resistance $R_q = (G_q^{(1)} + G_q^{(1)})^{-1} = h/4e^2$. For the MZI considered here an excess charge in the upper or lower branch has the possibility to relax into the four reservoirs of the MZI. But at each junction the two connections are only open with probability T and R (see Eq. 2.4). Thus the two connections act like one perfect channel. As a consequence, the charge relaxation resistance for our MZI is just that of a perfect wire and also given by $R_q = h/(4e^2)$.

From Eq. 2.15 we know that the dephasing rate for the MZI with two arms of equal length is proportional to the zero frequency limit $S_{\Delta U \Delta U}(0)$ of the spectrum of the difference $\Delta U = \Delta U_A - \Delta U_B$ between the potentials in the two arms. Since in the MZI there are no cross-correlations between the potentials in the two arms (see Eq. 2.36) we simply have

$$S_{\Delta U \Delta U}(0) = S_{U_A U_A}(0) + S_{U_B U_B}(0). \tag{2.40}$$

Substituting Eq. 2.40, the dephasing rate Eq. 2.15 becomes

$$\Gamma_\phi = \frac{2kTe^2}{\hbar^2} \sum_{i=1,2} \left(\frac{C_{\mu,i}}{C_i} \right)^2 R_q^i. \tag{2.41}$$

In addition we will explicitly give the result for the most symmetric case where both arms have the same length ($L_A = L_B = L$), both capacitances are the same ($C_A = C_B = C$) and, consequently also the electrochemical capacitances are identical $C_{\mu,A} = C_{\mu,B} = C_\mu$. Then $S_{U_A U_A} = S_{U_B U_B}$ and the dephasing rate becomes

$$\Gamma_\phi = \frac{2kTe^2}{\hbar^2} \left(\frac{C_\mu}{C} \right)^2 R_q. \tag{2.42}$$

From this result, together with Eq. 2.14 we see that we reproduce at least two of the main characteristics of the experimental results of Hansen et al. [8] and of Kobayashi et al. [9], namely, the linear temperature dependence of the decoherence rate and the proportionality of the total suppression factor to the traversal time (see Eq. 2.14).

In the limit of vanishing level spacing the electrochemical capacitance Eq. 2.21 tends towards the geometrical capacitance and thus $C_\mu/C \to 1$. In this limit the decoherence rates Eqs. 2.41 and 2.42 become independent of the coupling strength and are determined by the charge relaxation resistance and the temperature. Although we have here only calculated the charge relaxation resistance and decoherence rate for the one-channel limit it is possible to estimate the effect of adding additional transport channels. The charge relaxation resistance typically is inversely proportional to the total number of channels in all contacts of the

sample, that is $R_q \propto 1/N$. As was said before, the charge relaxation resistance measures the ease with which an excess charge in the conductor can relax into the reservoirs. If we consider an MZI with $N/4$ channels in each contact, and a probability T or $R = 1 - T$ for entering any given contact, the total charge relaxation *conductance*, i.e. the parallel addition of the conductances of the individual channels is $G_q = (2e^2/h)N/4(R + T + R + T) = (2e^2/h)N/2$ and the charge relaxation resistance in consequence is $R_q^{(N)} = 2(h/2e^2)/N$. Then, the dephasing time $\tau_\phi = 1/\Gamma_\phi$ should increase linearly with the number of channels. It is well known that interactions become weaker the more channels can contribute to the screening and it thus seems reasonable that decoherence due to electron-electron interactions should become gradually less important as the coupling to the reservoirs is improved.

It should be emphasized that decoherence rates very similar to Eqs. 2.41 and 2.42 have been obtained before (see Refs. [32], [18] and also Ref. [17] for a similar result). What is new here, is that we have calculated an observable quantity (the conductance) and have not defined the dephasing rate independently.

2.5 Probe configuration dependent decoherence

Until now, we have always assumed that the MZI is part of an external circuit with zero impedance. Here, we will extend the theory developed so far to include the case where only two of the contacts, the current probes, are part of a zero impedance circuit, while the two other contacts are voltage probes with an infinitely large impedance. Voltage fluctuations at the voltage probes can inject charge into the sample and consequently influence the internal potentials and their spectra.

The investigation presented here is motivated by an interesting recent experiment by Kobayashi and co-workers [9] who studied the probe-configuration dependence of the decoherence rate in a four-terminal Aharonov-Bohm geometry. Surprisingly, decoherence was found to be considerably stronger if the two voltage probes where on opposite sides of the ring, the so-called local configuration, than when they where arranged in the non-local configuration next to each other on the same side of the ring (see Fig. [2.3]). Note, that the terms local and non-local do not refer to the location of the voltage probes relative to each other but to their location with regard to the current probes.

The local configuration corresponds to the conventional setup for an Aharonov-Bohm type experiment, with the current probes on different sides of the ring and the voltage drop also being measured across the ring. In the non-local setup the current is flowing between two probes attached next to each other while the voltage drop is measured at the other end of the interferometer.

In the following, we will calculate the potential fluctuation spectra and then, using Eq. 2.15, the dephasing rates for the MZI, for the two different voltage probe

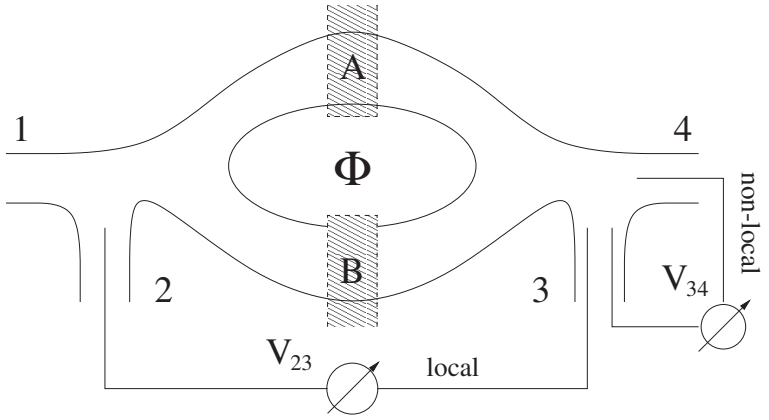

Figure 2.3: In the figure the local and the non-local voltage probe configuration are indicated. In the experiment of Ref. [9], narrow metallic top-gates, labelled A and B here, allowed to control the number of open transport channels in the arms.

configurations described above. Our main point is to show that the additional charge and potential fluctuations, induced through the voltage fluctuations at the voltage probes, depend on the measurement geometry. On the basis of this observation, we can propose an explanation [39] for the results of Kobayashi et al. [9].

The starting point for our investigation is the relation

$$\Delta I_\alpha = \delta I_\alpha + G_0 \left[(M_\alpha - T_{\alpha\alpha}) \Delta V_\alpha - \sum_{\beta \neq \alpha} T_{\alpha\beta} \Delta V_\beta \right] \tag{2.43}$$

between currents and voltages proposed by Büttiker in Ref. [40]. It is assumed that the $T_{\alpha\beta}$ are the thermally averaged transmission probabilities. Then, the validity of this equation is not restricted to zero temperature (for an MZI with two arms of equal length, temperature effects can of course be neglected, see Eq. 2.18). In this Langevin-like equation $\Delta I_\alpha = I_\alpha - \langle I_\alpha \rangle$ are the full current fluctuations at the current-carrying contact α, δI_α are the fluctuations of the bare (particle) current and ΔV_α are the voltage fluctuations. Also, we have written the equation in a form that is valid for the many-channel case: M_α is the number of channels in contact α. The transmission probabilities $T_{\alpha\beta}$ for the MZI are given in Eq. 2.5. For better comparison with the experiment of Ref. [9], at this point we include a non-zero probability $T_{12} = T_{21} = T_{34} = T_{43} = T_0 \neq 0$ for an electron coming in through contact α to be backscattered *incoherently* into the adjacent contact β. Current conservation and gauge invariance then imply that we have to make the replacement $M_\alpha \to M_\alpha + T_0$. From now on we choose $M_\alpha = 1$ and for notational convenience we introduce an effective (non-integer) channel number $\tilde{M}_\alpha = 1 + T_0$. We always assume that the transport voltage applied to the current source and the reference voltage at the current sink do not fluctuate and that we thus have the boundary conditions $\Delta V_\alpha = 0$ for current probes. In

addition we can also use the condition $\delta I_\alpha = 0$ for voltage probes.

To include the effect of the voltage fluctuations at the voltage probes, Eq. 2.19 for the charge $\Delta Q_i = Q_i - \langle Q_i \rangle$ in arm i has to be replaced by

$$\Delta Q_i = C_i \Delta U_i, \tag{2.44}$$

$$\Delta Q_i = \delta Q_i^b - e^2 D_i \Delta U_i + e^2 \sum_{\alpha, I_\alpha = 0} D_{\alpha\alpha}^{(i)} \Delta V_\alpha. \tag{2.45}$$

The sum is over the two voltage probes and the injectivity $D_{\alpha\alpha}^{(i)} = \partial \langle Q_i \rangle / \partial V_\alpha$ of contact α is simply the α-th diagonal element of the local density of states matrix Eq. 2.28. The injectivity can thus be understood as the contribution to the density of states that is due to injection from contact α. Note that we distinguish between the bare charge fluctuations δQ_i^b that are due to particles entering and leaving the sample trough the current carrying contacts and those charge fluctuations related to the fluctuations of the external voltages. In this section we will concentrate on the most simple case where the two arms of the ring have the same length ($L_A = L_B = L$) and the two capacitances are equal ($C_A = C_B = C$). As a consequence of the first assumption we can also write $D_A = D_B = D = 2D_0 = 2L/hv_F$ for the local densities. If we solve Eq. 2.44 for the potential we get

$$\Delta U_i = \frac{C_\mu}{Ce^2 D} \left(\delta Q_i^b + e^2 \sum_{\alpha, I_\alpha = 0} D_{\alpha\alpha}^{(i)} \Delta V_\alpha \right) \tag{2.46}$$

where the electrochemical capacitance was defined in Eq. 2.21. From Eq. 2.46 we can see that for the calculation of the potential fluctuations it will not be enough any more to know the fluctuations of the bare charge, but the fluctuations of the voltages and the correlator of charge and voltage fluctuations also have to be calculated. As usual for an MZI with two arms of equal length and equal coupling between arms and gates, to calculate the dephasing rate we only need to know the zero-frequency spectrum $S_{\Delta U \Delta U}(0)$ of the potential *difference* $\Delta U = \Delta U_A - \Delta U_B$. We will now calculate this quantity for the two different probe configurations.

2.5.1 Local configuration

In the local configuration one of the two contacts on each side of the ring acts as a current probe, the other as a voltage probe. For concreteness we assume that contacts 1 and 4 are the current probes while contacts 2 and 3 are the voltage probes (see Fig. [2.3]). The corresponding boundary conditions are

$$\Delta V_1 = \Delta V_4 = 0, \tag{2.47}$$

$$\Delta I_2 = \Delta I_3 = 0.$$

Substituting the boundary conditions for the voltages into Eqs. 2.46, we find

$$\Delta U = \frac{C_\mu}{Ce^2 D} \left[\Delta Q^b + e^2 D_0 (T - R) \big(\Delta V_2 + \Delta V_3 \big) \right] \tag{2.48}$$

where we have used that for the MZI $D_{22}^{(A)} = D_{33}^{(A)} = TD_0$ and $D_{22}^{(B)} = D_{33}^{(B)} = RD_0$ ($D_0 = L/hv_F$) (see Eqs. 2.34 and 2.35). For the difference of the bare charges in the two arms the short notation $\Delta Q^b = \delta Q_A^b - \delta Q_B^b$ was used. Solving the system of equations given in Eq. 2.43 for $\Delta V_2 + \Delta V_3$ with the boundary conditions on the current Eq. 2.47 gives

$$\Delta V_2 + \Delta V_3 = -\frac{\left(\tilde{M}_3 + T_{32}\right)\delta I_2^b + \left(\tilde{M}_2 + T_{23}\right)\delta I_3^b}{G_0\left(\tilde{M}_2\tilde{M}_3 - T_{23}T_{32}\right)}. \tag{2.49}$$

We have here used that due to the absence of backscattering in the MZI $T_{22} = T_{33} = 0$. Also note that Eq. 2.49 can be simplified further if it is used that $\tilde{M}_2 = \tilde{M}_3 = 1 + T_0$ and (cf. Eq. 2.5)

$$T_{23} = T_{32} = T^2 + R^2 - 2RT\cos(2\pi\Phi/\Phi_0) \tag{2.50}$$

for an interferometer with two arms of equal length. At this point we have made an important simplification: as it can be seen from Eqs. 2.5 and 2.6 that the argument of the cosine in Eq. 2.50 should rather be $\tau e\Delta U/\hbar \pm 2\pi\Phi/\Phi_0$ where the different signs are for T_{23} and T_{32}. With T_{23} and T_{32} depending on ΔU we would have to solve a non-linear equation to determine the potential difference ΔU. Instead, with the approximation made in Eq. 2.50 we can proceed in a much simpler way. If Eq. 2.49 is substituted into Eq. 2.48, the potential difference $\Delta U = \Delta U_A - \Delta U_B$ becomes

$$\Delta U = \frac{C_\mu}{Ce^2D}\left(\Delta Q^b - \frac{e^2D_0(T-R)}{G_0(\tilde{M}_2 - T_{23})}\left(\delta I_2^b + \delta I_3^b\right)\right). \tag{2.51}$$

From Eq. 2.51 we can see that the spectrum of the potential fluctuations can be expressed through the fluctuation spectra $S_{\alpha\beta}$ of the bare currents and the spectral function $S_{\Delta Q^b\Delta Q^b}$ of the bare charge fluctuations. The resulting expression for the spectral function is

$$S_{\Delta U\Delta U}(0) = \left(\frac{C_\mu}{Ce^2D}\right)^2\left[S_{\Delta Q^b\Delta Q^b} + \left(\frac{e^2D_0}{G_0}\right)^2\frac{(T-R)^2}{(\tilde{M}_2 - T_{23})^2}\sum_{\alpha,\beta=2,3}S_{\alpha\beta}\right] \tag{2.52}$$

since the cross-correlations $S_{i\alpha}$ between the bare charge in arm i and the bare current in contact α vanish, as can be checked by direct calculation. Remembering that in the MZI there are also no cross-correlations between the charges in the two arms $e^2S_{N_AN_B} = 0$ (cf. Eq. 2.36), the spectrum of the bare charge fluctuations

$$S_{\Delta Q^b\Delta Q^b}(0) = e^2S_{N_AN_A}(0) + e^2S_{N_BN_B}(0) = kTh(eD_0)^2 \tag{2.53}$$

is simply the sum of the spectra (see Eq. 2.26) of the bare charges in the two arms. The zero-frequency spectral function of the bare current fluctuations in the two arms is well known, and is given by the generalized Nyquist formula

$$S_{\alpha\beta}(0) = kT\left(G_{\alpha\beta} + G_{\beta\alpha}\right). \tag{2.54}$$

For the Mach-Zehnder interferometer we obtain from this formula

$$\sum_{\alpha,\beta=2,3} S_{\alpha\beta}(0) = 2kTG_0(\tilde{M}_2 - T_{23}). \tag{2.55}$$

Substituting the results Eqs. 2.53 and 2.55 for the zero-frequency spectra of the bare charge and current fluctuations into Eq. 2.52 we find for the potential fluctuations

$$S_{\Delta U\Delta U}(0) = 4kTR_q \left(\frac{C_\mu}{Ce^2D}\right)^2 \left[1 + \frac{(T-R)^2}{\tilde{M}_2 - T_{23}}\right] \tag{2.56}$$

where $R_q = h/(4e^2)$ is the charge relaxation resistance.

To get an idea of the symmetry dependence of the spectrum we can average T_{23} (see Eq. 2.50) over one period of the magnetic field (i.e. drop the coherent part) which gives us the approximate result

$$S_{\Delta U\Delta U}(0) = 4kTR_q \left(\frac{C_\mu}{Ce^2D}\right)^2 \left[1 + \frac{(2T-1)^2}{2T(1-T)+T_0}\right]. \tag{2.57}$$

The most interesting feature of this result is the strong dependence of the potential fluctuation spectrum on the symmetry of the MZI. For a totally symmetric interferometer $T = R = 1/2$ the part of the spectrum that is due to the fluctuations of the voltages vanishes and we recover the result we have obtained earlier for an interferometer integrated in a zero impedance circuit. This is not surprising, since we have calculated the spectrum of the *difference* $\Delta U = \Delta U_A - \Delta U_B$ of the two potentials in the two arms and since for a symmetric MZI both arms are identical with respect to any given contact. The spectrum $S_{U_kU_k}$ of the fluctuations in arm k on the other hand knows about the fluctuating voltages even if $T = R = 1/2$. If we had considered an interferometer with arms of different length, the dephasing rate would not depend only on the fluctuations of the difference between the two potentials. Then, voltage fluctuations affect the dephasing rate even in an interferometer with symmetric beam-splitters. Any type of asymmetry between the two arms will lead to an observable contribution of the voltage fluctuations to the dephasing rate.

If there is no backscattering $T_0 = 0$, the spectrum diverges for $T = 0$ and $T = 1$. From the argument just given, it seems natural that the fluctuations of the potential difference grow with increasing asymmetry. This divergence does not have any unphysical consequences since in any case there is no interference if the transmission in the beamsplitter is either $T = 0$ or $T = 1$.

It is helpful to split up the total decoherence rate

$$\Gamma_\phi^l = \gamma_\phi^0 + \gamma_\phi^l$$

into the contribution γ_ϕ^0 that we found already for a zero-impedance external circuit (see Eq. 2.42) and the correction γ_ϕ^l due to voltage fluctuations. From

Eq. 2.15 we obtain

$$\gamma_\phi^0 = \frac{2kTe^2}{\hbar^2}\left(\frac{C_\mu}{C}\right)^2 R_q, \tag{2.58}$$

$$\gamma_\phi^l = \frac{2kTe^2}{\hbar^2}\left(\frac{C_\mu}{C}\right)^2 R_q \frac{(2T-1)^2}{2T(1-T)+T_0}. \tag{2.59}$$

For comparison, we now want to calculate the spectrum for an MZI with the voltage probes in the non-local configuration.

2.5.2 Non-local configuration

In the non-local configuration both voltage probes are on the same side of the ring. Following Ref. [9] we choose the voltage probes to be contacts 3 and 4 (cf. Fig. [2.3]). The boundary conditions thus imposed on the voltage and current fluctuations are

$$\begin{aligned} \Delta V_1 = \Delta V_2 &= 0, \\ \Delta I_3 = \Delta I_4 &= 0. \end{aligned} \tag{2.60}$$

With the boundary conditions for the voltages and with Eq. 2.46 we find for the difference of the potentials in the two arms

$$\Delta U = \frac{C_\mu}{Ce^2N}\left(\Delta Q^b + e^2 D_0(T-R)(\Delta V_3 - \Delta V_4)\right). \tag{2.61}$$

Eq. 2.61 is quite similar to the corresponding equation (Eq. 2.48) for the local case apart from the fact that here the difference of the two fluctuating voltages enters instead of their sum. The relation between current and voltage fluctuations that are obtained combining the boundary conditions Eq. 2.60 with Eq. 2.43 are particularly simple in the non-local case, namely

$$\Delta V_3 - \Delta V_4 = -\frac{\delta I_3^b - I_4^b}{G_0\left(\tilde{M}_3 + T_0\right)} \tag{2.62}$$

where we have used $G_{33} = G_{44} = \tilde{M}_3 G_0$ and $G_{34} = G_{43} = T_0 G_0$. Note that there is no field-dependent part in the denominator. As we will see, this will lead to a striking difference between the spectra for the local and the non-local case. Combining Eqs. 2.61 and 2.62 gives for the potential difference

$$\Delta U = \frac{C_\mu}{Ce^2N}\left(\Delta Q^b + \frac{e^2 D_0(T-R)}{G_0\left(\tilde{M}_3 + T_0\right)}\left(-\delta I_3^b + \delta I_4^b\right)\right) \tag{2.63}$$

and for the spectrum we thus have

$$S_{\Delta U \Delta U}(0) = \left(\frac{C_\mu}{Ce^2N}\right)^2 \left[S_{\Delta Q^b \Delta Q^b} + \left(\frac{e^2 D_0(T-R)}{G_0\left(\tilde{M}_3 + T_0\right)}\right)^2 \sum_{\alpha,\beta=1,2} (-1)^{\alpha+\beta} S_{\alpha\beta}\right]. \tag{2.64}$$

With the help of Eqs. 2.53 and 2.54 the spectrum of charge fluctuations in the non-local case becomes

$$S_{\Delta U \Delta U}(0) = 4kTR_q \left(\frac{C_\mu}{Ce^2N}\right)^2 \left[1 + \frac{(2T-1)^2}{1+2T_0}\right]. \tag{2.65}$$

As in the local case, the spectrum reduces to the result in the zero impedance limit if the MZI is symmetric ($R = T = 1/2$). However, in contrast to the result in the nonlocal case the symmetry-dependent (divergent) denominator is absent. As for the non-local setup, it is instructive to consider the two contributions to the dephasing rate $\Gamma_\phi^{nl} = \gamma_\phi^0 + \gamma_\phi^{nl}$ independently. The contribution γ_ϕ^0 due to charge fluctuations is the same in the local and the nonlocal case. For the voltage fluctuation part we here find

$$\gamma_\phi^{nl} = \frac{2kTe^2}{\hbar^2}\left(\frac{C_\mu}{C}\right)^2 R_q \left[\frac{(2T-1)^2}{1+2T_0}\right]. \tag{2.66}$$

The main difference to the result for the local case is the absence of a symmetry-dependent denominator in the configuration specific part of the dephasing rate. The decoherence rates for the two probe configurations are shown in Fig. [2.4] as a function of the transmission probability T of the beamsplitters.

2.5.3 Four-terminal resistance

So far, we have investigated how the coherent part of the transmission probabilities is attenuated due to decoherence in the local and non-local setup. However, the transmission probabilities or conductances are not the quantities that are actually accessible in a four-terminal measurement. Rather, in such an experiment the four-terminal resistance [33] $R_{\alpha\beta,\gamma\delta} = (V_\gamma - V_\delta)/I_\alpha$ ($I_\beta = -I_\alpha$) relating the current flowing at the current probes to the voltage-drop between the two voltage probes is measured. Solving the equations $I_\alpha = \sum_{\beta=1}^4 G_{\alpha\beta}V_\beta$ ($\alpha = 1-4$) for a four-terminal conductor for the voltage differences $V_\gamma - V_\delta$ one can express the four-terminal resistances

$$R_{\alpha\beta,\gamma\delta} = \frac{G_{\gamma\alpha}G_{\delta\beta} - G_{\gamma\beta}G_{\delta\alpha}}{D} \tag{2.67}$$

through the conductance matrix elements $G_{\alpha\beta} = G_0(M_\alpha\delta_{\alpha\beta} - T_{\alpha\beta})$. [33] Here D is any sub-determinant of rank three of the total conductance matrix.

Kobayashi et al. [9] measured the four-terminal resistances for the local and the non-local setup and the decoherence rates were extracted from a simple model for the transmission probabilities $T_{\alpha\beta}$. First, in the absence of interactions ($\Delta U = 0$, and thus $T_{\alpha\beta} = T_{\beta\alpha}$) and for an MZI including a finite incoherent transmission probability between neighbouring contacts the four terminal resistances for the

local and non-local case become, respectively,

$$\begin{aligned} R^l = R_{14,23} &= \frac{h}{2e^2}\frac{T_0 - T_{13}}{T_0 + T_{23}}, \\ R^{nl} = R_{12,43} &= \frac{h}{2e^2}\frac{T_{23} - T_{13}}{(T_0 + T_{13})(T_0 + T_{23})}. \end{aligned} \tag{2.68}$$

The four-terminal resistances given in Eq. 2.68 are exactly as in Ref. [9] if we define $T_1 = T_{23}$ and $T_2 = T_{13}$ and if we use $T_{13} + T_{23} = 1$. In fact, the model used for the transmission probabilities in Ref. [9] is very similar to the symmetric MZI. As was pointed out there, in the four-terminal resistance $R_{12,43}$ for the non-local case the incoherent contributions in the numerator tend to cancel each other. In fact, the cancellation is exact for $T = 1/2$ in our model. In the local case on the other hand the coherent part in the numerator is only a small correction to the large incoherent contribution. These observations provide a simple explanation for the much larger contribution of the coherent AB-oscillations to the total resistance in the non-local case that was observed in the experiment .[9].

If non-zero potentials in the arms are included the relation $T_{\alpha\beta} = T_{\beta\alpha}$ does not hold anymore and we only have the reversibility condition $T_{\alpha\beta}(\Phi) = T_{\beta\alpha}(-\Phi)$ (see Eqs. 2.5 and 2.6 as well as the discussion below Eq. 2.50). The equations for the four-terminal resistances then become correspondingly more complicated. Eq. 2.68 would remain true only if, in the presence of interactions, we could make the replacement $T_{\alpha\beta} \to \langle T_{\alpha\beta}\rangle$ since $\langle T_{\alpha\beta}\rangle = \langle T_{\beta\alpha}\rangle$. The angular brackets as usual imply statistical averaging. However, this is probably not the quantity that is accessible in an experiment. In the experiment the voltage difference $V_\gamma - V_\delta$ is measured at a constant driving current $I_\alpha = -I_\beta$. In such a measurement an average voltage difference $\langle V_\gamma - V_\delta\rangle$ and, consequently the averaged four-terminal resistance $\langle R_{\alpha\beta,\gamma\delta}\rangle = \langle V_\gamma - V_\delta\rangle / I_\alpha$ is observed. To compare theory and experiment it is thus best to average the four-terminal resistances R^l and R^{nl} (see Eq. 2.68) over the potential fluctuations instead of averaging each transmission matrix element independently. The decay of the coherent contribution to the local and non-local four-terminal resistances will be governed by the local and non-local decoherence rates respectively. Note, that in a current measurement at a constant voltage difference one could obtain information about the average of the inverse $\langle R^{-1}_{\alpha\beta,\gamma\delta}\rangle = \langle I_\alpha\rangle/(V_\gamma - V_\delta)$ of the four-terminal resistances.

If interactions and thus a finite potential difference ΔU are included the average four-terminal resistances become

$$\begin{aligned} \langle R^l\rangle &= \frac{h}{2e^2}\left\langle \frac{T_0^2 - T_{13}T_{31}}{2T_0(1+T_0) + T_{13} + T_{31} - 2T_{13}T_{31}}\right\rangle, \\ \langle R^{nl}\rangle &= \frac{h}{2e^2}\left\langle \frac{2T_{31} - 1}{2T_0(1+T_0) + T_{13} + T_{31} - 2T_{13}T_{31}}\right\rangle \end{aligned} \tag{2.69}$$

where T_{13} and T_{31} are functions of ΔU (see Eq. 2.6). It can be checked that Eqs. 2.68 and 2.69 agree if we use $T_{13} = T_{31}$ (and omit the angular brackets)

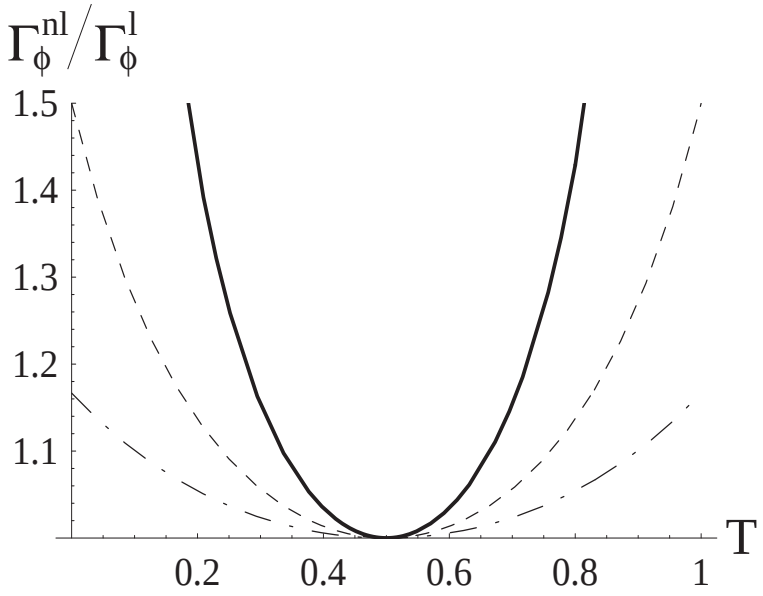

Figure 2.4: Ratio of the local to the non-local decoherence rate as a function of the transmission T at the beam-splitters for different values of the incoherent parallel resistance. The full line is for $T_0 = 0.1$, the dashed line for $T_0 = 1$ and the dashed-dotted line for $T_0 = 3$. The difference between the two rates becomes smaller as the incoherent contribution is increased.

in the former and $T_{23} = 1 - T_{13}$ in the latter. We will explicitly perform the statistical averaging only in the particularly simple limit where we can assume that $1 \ll T_0$ and where we thus can expand the resistances in a series in the small parameter $1/T_0$. If we go to the first non-vanishing coherent contribution we get

$$\begin{aligned} \langle R^l \rangle &\approx \frac{h}{4e^2}\left(1 - \frac{1}{T_0} + \frac{1 - \langle T_{13}\rangle}{T_0^2}\right), \\ \langle R^{nl} \rangle &\approx \frac{h}{4e^2}\frac{2\langle T_{13}\rangle - 1}{T_0^2}. \end{aligned}$$

In this simple limit we have thus reduced the problem of averaging the four-terminal resistances to that of averaging the transmission matrix elements. The decoherence rates that determine the attenuation of the coherent contributions to the resistances in the local and non-local case are given in Eqs. 2.58 and 2.66 respectively.

In conclusion, we have calculated the dephasing rates for the local and the non-local probe configuration for an electronic interferometer and have discussed how the decoherence influences the measured four-terminal resistances. In Fig. [2.4] we compare the two results for different values of the incoherent parallel resistance. The differences between the two setups quickly disappear as the parallel resistance is decreased. However, other types of asymmetry like a different capacitive coupling of the two arms to the gates will increase the difference between

our results for the two configurations.[39]

Finally, it should be mentioned again that the results for the dephasing rates Eqs. 2.58 and 2.66 were obtained after averaging the transmission probabilities over one period of the field. This procedure has allowed us to study the symmetry-dependence of the decoherence rate at a simple example. In principle, however, the potential fluctuation spectrum and thus the dephasing rate are field-dependent and it would be very interesting to study such a dependence in an experiment.

2.6 A scattering approach to dephasing

In this section we will present an alternative approach to calculating the interaction-induced attenuation of the Aharonov-Bohm oscillations in the interferometer. As before, we will assume that interaction effects can be included through the internal potentials $U_A(t)$ and $U_B(t)$ for the upper and lower arm. Instead of reducing the problem to an effectively time-independent one, as we have done in Sec. 2.3 we will now solve the time-dependent problem directly. The scattering from the time-dependent potentials gives rise to inelastic transitions, or, in other words, a scattering state with a well defined energy E in the incoming channel will contain side-bands at many different energies E' in the out-going channels (see Fig. [2.5] for an illustration). The scattering is completely coherent (we are only solving a one-particle Schrödinger equation) and we will extend the scattering matrix approach that we have used so far to include also time-dependent scattering. In the next subsection we will demonstrate how the inelastic scattering can be included into the scattering formalism. In Sec. 2.6.2 we will derive the scattering matrix elements for the MZI from a time-dependent WKB approach. In the final part of this section the average conductance in the interferometer is calculated and we will obtain the decoherence time.

2.6.1 Scattering matrix

Here we will discuss the general framework needed for the calculation of the conductance in the interferometer in the presence of inelastic scattering. To account for inelastic transitions we introduce a scattering matrix with two energy arguments through the relation

$$\hat{b}_\alpha(E) = \sum_\beta \int \frac{dE'}{2\pi\hbar} S_{\alpha\beta}(E, E')\hat{a}_\beta(E'). \tag{2.70}$$

The operators $\hat{a}^\dagger_\alpha(E)$ ($\hat{a}_\alpha(E)$) create (destroy) an electron in a scattering state with energy E entering the system through contact α and the operators $\hat{b}^\dagger_\alpha(E)$ and $\hat{b}_\alpha(E)$ respectively create and annihilate an electron leaving the mesoscopic conductor at energy E through contact α. The usual scattering matrix relation

between incoming and outgoing states in different contacts and channels at the same energy is recovered if

$$S_{\alpha\beta}(E,E') = 2\pi\hbar\delta(E-E')S^{(0)}_{\alpha\beta}(E) \tag{2.71}$$

with the on-shell scattering matrix $S^{(0)}_{\alpha\beta}(E)$. The on-shell scattering matrix for the MZI is given in Eq. 2.4 (there the superscript was omitted). The formulation of the inelastic scattering we use here, based on a scattering matrix connecting scattering states at different energies, follows previous work by Büttiker and co-workers [41, 42]. Alternatively, it is possible to formulate a theory for time-dependent scattering using scattering matrices with two time arguments instead of two energy arguments. Such an approach is completely equivalent to ours and was used by Aleiner and Vavilov [16] as well as by Polianski and Brouwer [43] to discuss time-dependent scattering in chaotic quantum dots.

As above, our final goal is the calculation of the statistically averaged dc conductance for the interferometer. The averaged linear response conductance is defined through the equation

$$\langle G_{\alpha\beta}\rangle = \langle I_\alpha\rangle / V_\beta. \tag{2.72}$$

We want to emphasize again that the angular brackets mean statistical averaging. The starting point for our calculation of the conductance is the following expression for the current in contact α [44]:

$$\begin{aligned} \hat{I}_\alpha(t) &= \frac{e}{h}\int dE\, dE' \mathrm{e}^{i(E-E')t/\hbar} \\ &\times \left[\hat{a}^\dagger_\alpha(E)\hat{a}_\alpha(E') - \hat{b}^\dagger_\alpha(E)\hat{b}_\alpha(E')\right], \end{aligned} \tag{2.73}$$

We then substitute the scattering matrix relation Eq. 2.71 into the current operator Eq. 2.73 and perform quantum statistical averaging using $\langle \hat{a}^\dagger_\alpha(E)\hat{a}_\beta(E')\rangle_{QM} = \delta_{\alpha\beta}\delta(E-E')f(E-\mu_\alpha)$ where $f(E)$ is the Fermi distribution and μ_α is the chemical potential at contact α. The subscript QM is used to distinguish the quantum statistical average from the classical statistical average. If a voltage is applied to contact β, the resulting linear response conductance at contact $\alpha \neq \beta$ is

$$G_{\alpha\beta} = \frac{e^2}{h^3}\int dE dE' dE_1 \left(-\frac{\partial f}{\partial E_1}\right) S^*_{\alpha\beta}(E,E_1)S_{\alpha\gamma}(E',E_1). \tag{2.74}$$

The unusual prefactor is a consequence of the normalization we have used in the definition of the scattering matrix (see Eq. 2.71). As it is written, Eq. 2.74 is valid for a conductor with a single transport channel. Our next step will be to express the scattering matrix in terms of the internal potentials $u_A(\omega)$ and $u_B(\omega)$. Once a relation between the scattering matrix and the potentials is established, we can average Eq. 2.74 over the probability distribution of the potentials.

As in the preceding sections we consider an MZI with a single transport channel. There is no backscattering in the beamsplitters (cf. Eq. 2.2) and transmission

through the intersections is taken to be independent of energy. In the remainder, we assume symmetric intersections, that is $R = T = 1/2$ in Eqs. 2.2, 2.4. Due to the potential fluctuations in the arms of the ring a carrier can gain or loose energy. This process is described by a scattering matrix $S_i(E', E)$ for each arm which depends on both the energy E of the incoming and the energy E' of the exiting carrier. We assume that interactions are weak and we only take into account scattering processes with a small momentum $q \ll 2k_F$and energy $\hbar\omega \ll E_F$ transfer. Therefore, also in the leads, there is no backscattering.

As a consequence of the inelastic transitions in the arms of the ring, the full scattering matrix $S_{\alpha\beta}(E', E)$ describing transmission through the entire interferometer from contact β to contact α is also a function of two energy arguments. As an example we give the matrix element

$$S_{13}(E', E) = \frac{i}{2}\left[S_A(E', E)\mathrm{e}^{-i\Phi_A} + S_B(E', E)\mathrm{e}^{+i\Phi_B}\right]. \tag{2.75}$$

connecting the amplitude of the current incoming through contact 3 to the amplitude of the current leaving the conductor trough contact 1. With Eq. 2.75 and with Eq. 2.4 it is straight forward to construct the remaining elements of the scattering matrix in the presence of inelastic scattering in the arms. Here Φ_i is the magnetic phase picked up by a particle going through arm i clockwise. Then $\Phi_A + \Phi_B = 2\pi\Phi/\Phi_0$, where Φ is the flux through the ring and Φ_0 is the flux quantum. The on-shell (one-energy) scattering matrix element $S_{13}^{(0)}(E)$ (see Eq. 2.4) for the (free) one-channel interferometer in the absence of interactions is found by substituting $S_i(E', E) = 2\pi\hbar\delta(E' - E)S_i^{(0)}(E)$ with $S_i^{(0)}(E) = \exp(ik_E L_i)$ into Eq. 2.75.

2.6.2 S matrix for a time-dependent potential

In this section we will show how the scattering matrix for the interacting ring system can be calculated explicitly. We first solve the Schrödinger equation for a single branch of the interferometer using a WKB approach. The amplitude for a transition from energy E to energy $E + \hbar\omega$ of a particle passing through this arm and the corresponding scattering matrix element $S_i(E, E')$ are determined. Subsequently the scattering matrices for the two arms are included into a scattering matrix for the full interferometer. A WKB approach similar to ours has been used previously to discuss photon-assisted transport in a quantum point contact [45] and to the investigation of traversal times for tunnelling [46]. The influence of a time-dependent bosonic environment on transport through a QPC was addressed in Refs. [47] and [48] also applying a WKB ansatz.

The gate situated opposite to arm i ($i = A, B$) is assumed to be extended over the whole length of this arm. Fluctuations of the charge in the gate capacitively couple to the charge in the neighbouring arm of the MZI and influence electron transport through this arm (the setup is exactly as described before, see

Fig. [2.1]). The one-dimensional Schrödinger equation for arm i of the MZI is

$$i\hbar\partial_t\Psi_i(E;x,t) = \left(-\frac{\hbar^2}{2m}\,\partial_x^2 + h_i(x)eU_i(t)\right)\Psi_i(E;x,t). \tag{2.76}$$

Here x is the coordinate along the arm and m is the effective mass of the electron. We have made the assumption that the fluctuating potential factorizes in a space- and a time-dependent part. For the ballistic structure considered here the internal potential is a slowly varying function of x. We will, however, sometimes employ a rectangular potential barrier ($h_i(x) = const.$ for $0 \le x \le L_i$, where L_i is the length of arm i). Using a space-independent internal potential is a valid approximation [49] at least in the low frequency limit $\omega\tau_i \le 1$ where a passing electron sees a constant or slowly changing barrier. Remember, that $\tau_i = L_i/v_{i,F}$ is the traversal time for arm i.

If we make the ansatz $\Psi_i(E;x,t) = \mathrm{e}^{i\sigma_i(x,t)/\hbar}$ we obtain a differential equation for the phase $\sigma_i(x,t)$. To leading order in $\hbar$, this equation is the Hamilton-Jacobi equation

$$\partial_t\sigma_i(x,t) + \frac{1}{2m}\left(\partial_x\sigma_i(x,t)\right)^2 + h_i(x)eU_i(t) = 0. \tag{2.77}$$

For simplicity we have assumed that there is no time-independent contribution to the total potential. Then, the solutions to the unperturbed ($U_i(t) = 0$) Schrödinger equation are just plane wave states. If the fluctuating potential is small we can expand the phase $\sigma_i(x,t)$ in a perturbation series in $U_i(t)$. Going to second order we have

$$\sigma_i(x,t) = -Et + \hbar kx + r_{i,1}(x,t) + r_{i,2}(x,t) \tag{2.78}$$

where $r_{i,1}(x,t)$ is linear in the potential and $r_{i,2}(x,t)$ is a second order term.

It is assumed that transmission is perfect: the potential fluctuations cause only forward scattering. This is justified if the energy transfer in a single scattering process is much smaller than the Fermi energy E_F, $\hbar\omega \ll E_F$.

From Eqs. 2.77 and 2.78 we obtain two linear differential equations for $r_{i,1}(x,t)$ and $r_{i,2}(x,t)$, namely

$$\begin{aligned} -\partial_t r_{i,1}(x,t) &= v_F\partial_x r_{i,1}(x,t) + h_i(x)eU_i(t), \\ -\partial_t r_{i,2}(x,t) &= v_F\partial_x r_{i,2}(x,t) + \frac{1}{2m}\left(\partial_x r_{i,1}(x,t)\right)^2 \end{aligned} \tag{2.79}$$

where v_F is the Fermi velocity. Although these equations can be solved quite easily as they are, it is convenient to Fourier transform with respect to time and to solve for the Fourier coefficients $r_{i,1}(x,\omega)$ and $r_{i,2}(x,\omega_1,\omega_2)$. They are defined through

$$\begin{aligned} r_{i,1}(x,t) &= \int\frac{d\omega}{2\pi}\mathrm{e}^{-i\omega t}r_{i,1}(x,\omega), \\ r_{i,2}(x,t) &= \int\frac{d\omega_1}{2\pi}\int\frac{d\omega_2}{2\pi}\mathrm{e}^{-i(\omega_1+\omega_2)t}r_{i,2}(x,\omega_1,\omega_2). \end{aligned}$$

Substituting into Eq. 2.79 and also Fourier transforming the potential with regard to time (see Eq. 2.9), we get two simple differential equations for $r_{i,1}(x,\omega)$ and $r_{i,2}(x,\omega_1,\omega_2)$. To solve these equations we impose the initial conditions $r_{i,1}(x_0,\omega)=0$ and $r_{i,2}(x_0,\omega_1,\omega_2)=0$. This corresponds to saying that the solution to the Schrödinger Equation is a plane wave, at a point $x_0 \ll 0$ far to the left of the center of the barrier $h(x)$, such that $h(x_0)=0$. With these initial conditions we obtain the formal solution

$$r_{i,1}(x,\omega) = -\frac{eu(\omega)}{v_F}\int_{x_0}^{x} dx' h_i(x') \mathrm{e}^{i\omega(x-x')} \tag{2.80}$$

for the linear term in the phase (this result can also be found in Ref. [46]) while the result for the second order term is

$$r_{i,2}(x,\omega_1,\omega_2) = -\frac{1}{2mv_F}\int_{x_0}^{x} dx' \partial_{x'} r_{i,1}(x'\omega_1)\partial_{x'} r_{i,1}(x'\omega_2)\mathrm{e}^{i(\omega_1+\omega_2)(x-x')}. \tag{2.81}$$

Here $r_{i,1}$ gives the contribution to the action due to absorption or emission of a single modulation quantum $\hbar\omega$, while $r_{i,2}$ corresponds to the absorption and emission of two modulation quanta $\hbar\omega_1$ and $\hbar\omega_2$.

We now proceed to the formulation of the scattering problem in terms of a scattering matrix with elements of the form $S_i(E',E)$ describing transitions between states at different energies. The amplitude $t_i(E',E)$ for a transition from a state with energy E to a state with energy E' of an electron is found from the boundary condition at $x=L_i$, $\Psi^i_E(L_i,t)=\chi^i_E(L_i,t)$. Here L_i is an arbitrary point on the right of the barrier where the fluctuating potential is negligible. If $h_i(x)$ is a rectangular barrier we can of course identify L_i with the length of the barrier and with the length of arm i. If $h(x)$ is a smooth barrier we can still assume that L_i is the length of arm i, but we will also have a second, shorter length-scale, namely the typical length over which the potential decays to zero. Physically, this corresponds to saying that interactions are stronger at the center of the arms than in the intersections, which is reasonable since the wires become wider as they approach the intersection.

For the matching we expand the WKB wave function in $x=L_i$ to the second order in the perturbing potential

$$\begin{aligned}\Psi^i_E(x,t) &= \mathrm{e}^{-iEt/\hbar+ik_{i,E}x}\Big[1+\frac{i}{\hbar}r_{i,1}(L_i,t) \\ &+ \frac{i}{\hbar}r_{i,2}(L_i,t)-\frac{1}{2\hbar^2}r^2_{i,1}(L_i,t)\Big].\end{aligned} \tag{2.82}$$

Furthermore the wave function at the right-hand side of the barrier (outside the fluctuating potential region) is

$$\chi^i_E(x,t) = \int \frac{dE'}{2\pi\hbar} t_i(E',E)\mathrm{e}^{ik_{E'}x-iE't/\hbar}. \tag{2.83}$$

In principle, also the derivatives of the wave function should be matched. However, here we describe transmission through the fluctuating potential region as reflectionless which is accurate up to corrections of the order of $\hbar\omega/E_F$. To determine the transmitted wave with the same accuracy it is sufficient to match amplitudes only. The transmission amplitude is found by Fourier transforming the WKB wave function Eq. (2.82) and comparing with the wave function Eq. (2.83) at $x = L_i$. To second order in the potential we have

$$\begin{aligned} t_i(E', E) &= \mathrm{e}^{i(k_E - k_{E'})L_i} \Bigg[2\pi\hbar\delta(E' - E) + \frac{i}{\hbar} r_{i,1}(L_i, (E' - E)/\hbar) \\ &+ \int \frac{d\omega}{2\pi} \Bigg[\frac{i}{\hbar} r_{i,2}\left(L_i, \omega, (E' - E)/\hbar - \omega\right) \\ &- \frac{1}{2\hbar^2} r_{i,1}(L_i, \omega) r_{i,1}\left(L_i, (E' - E)/\hbar - \omega\right) \Bigg] \Bigg]. \end{aligned} \tag{2.84}$$

The scattering matrix connecting incoming wave amplitudes (at $x = 0$) to outgoing wave amplitudes (at $x = L_i$) is related to the transmission amplitude $t_i(E', E)$ through

$$S_i(E', E) = \mathrm{e}^{ik_{E'}L_i} t_i(E', E). \tag{2.85}$$

The transmission amplitude $t_i(E', E)$ was determined through the continuity of the wave function in the point $x = L_i$. It thus connects amplitudes at the same point. In contrast, the scattering matrix $S_i(E', E)$ connects amplitudes at $x = 0$ to amplitudes at $x = L_i$. This difference in the definitions of the two quantities leads to the phase factor $\exp(ik_{E'}L_i)$ in Eq. (2.85). The scattering matrix as it is derived here a priori relates wave function amplitudes and not current amplitudes. To be consistent with the usual definition of the scattering matrix as a relation between current amplitudes, $S_i(E', E)$ should be multiplied by $\sqrt{v_{E'}/v_E}$. The deviation from unity, however, is of the order $\hbar\omega/E_F$ and can thus be neglected. The scattering matrices found to describe a single arm can now be integrated into the full scattering matrix for the MZI (see Eq. (2.75)).

In the discussion presented here the transmission of the carrier through the fluctuating potential region is described as a unitary scattering process. The "final" scattering channels are always open. We emphasize that up to now we have investigated a perfectly coherent process. Decoherence in our model will be introduced through the statistical averaging (cf. Sec. 2.6.3).

2.6.3 Average conductance

We now come to the discussion of the dephasing of the coherent part of the dc-conductance in the linear transport regime due to (equilibrium) charge fluctuations. Electron-electron interactions affect the coherent part of the dc-conductance only. This can be understood from the well known result [50] that interactions do not change the conductance of a one-dimensional wire attached to reservoirs. To

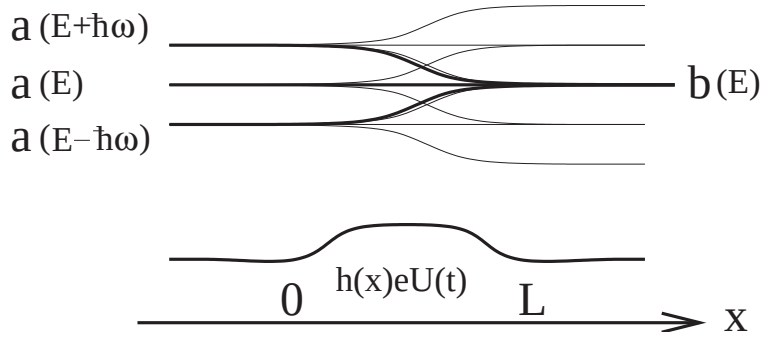

Figure 2.5: Scattering states Ψ^i_E and $\Psi^i_{E\pm\hbar\omega}$ with amplitudes $a(E)$ and $a(E \pm \hbar\omega)$ respectively due to electrons incident from the left at energies E and $E\pm\hbar\omega$ are indicated in the figure. For didactic purposes the special case of a harmonically oscillating barrier $U(t) \propto \cos(\omega t)$ is considered and only first order side-bands are drawn. In the rest of this section we discuss the case of a randomly oscillating barrier and include second order corrections. The scattering state which may be described by a simple (outgoing) plane wave at energy E with amplitude $b(E)$ to the right of the barrier is emphasized in the figure. The amplitudes $a(E)$ and $b(E)$ are related through the scattering matrix via $b(E) = \sum_{\sigma=0,\pm} S(E, E + \sigma\hbar\omega)a(E + \sigma\hbar\omega)$.

keep the notation simple, we consider throughout this section a situation where a voltage is applied only to contact 3, $\mu_3 = \mu_0 + eV$, and the current is measured at contact 1 ($\mu_1 = \mu_2 = \mu_4 = \mu_0$). We will first assume that only arm A is coupled to a gate ($C_B \to \infty$). This assumption corresponds to saying that interactions take place only in arm A and is made for purely technical purposes. The generalization to the case where both arms are coupled to gates is straight forward and will be discussed at the end of this section.

We now substitute the scattering matrix element $S_{13}(E, E')$ (see Eq. 2.75) into the expression for the linear conductance Eq. 2.74. The scattering matrix for arm A is given in Eqs. 2.84 and 2.85. Since we have chosen $C_B \to \infty$ there are no interactions in arm B and there are no transition between states at different energies in this arm.

Statistical averaging (remember $\langle U_A(t)\rangle = 0$ and thus $\langle r_{A,1}(L_A, t)\rangle = 0$) then leads to the following expression for the conductance:

$$\langle G\rangle = \frac{e^2}{h}\int dE \left(-\frac{\partial f}{\partial E}\right)\langle T(E)\rangle, \tag{2.86}$$

where we have introduced the statistically averaged transmission probability

$$\begin{aligned}\langle T(E)\rangle &= \frac{1}{2}\Big[1 + \cos\left(\Theta(E) - 2\pi\Phi/\Phi_0\right) \\ &\times \left(1 - \langle r^2_{A,1}(L_A, 0)\rangle/2\hbar^2\right) \\ &- \sin\left(\Theta(E) - 2\pi\Phi/\Phi_0\right)\langle r_{A,2}(L_A, 0)\rangle/\hbar\Big].\end{aligned} \tag{2.87}$$

As in Sec.2.3 we use the short notation $T(E) = T_{13}(E)$. Here $\Theta = k_{A,E}L_A - k_{B,E}L_B$ is the dynamic phase, Φ is the magnetic flux enclosed by the ring and Φ_0 is the flux quantum. In deriving this result we have used that the phases $r_{A,1}(L_A,t)$ and $r_{A,2}(L_A,t)$ are real. Also, note that $\langle r_{A,2}(L_A,t)\rangle = \langle r_{A,2}(L_A,0)\rangle$ and, similarly, $\langle r^2_{A,1}(L_A,t)\rangle = \langle r^2_{A,1}(L_A,0)\rangle$. In the absence of interactions the transmission probability simply is $\langle T(E)\rangle = (1+\cos(\Theta(E) - 2\pi\Phi/\Phi_0))/2$ (compare Eq. (2.5)). Interactions thus decrease the amplitude of the AB-oscillations and lead to an additional out-of-phase contribution.

Eq. (2.87) can be rewritten in an approximate but more convenient form as

$$\begin{aligned}\langle T(E)\rangle &= \frac{1}{2}\Bigg[1+\mathrm{e}^{-\langle r^2_{A,1}(L_A,t)\rangle/2\hbar^2} \\ &\times \cos\left(\Theta(E) - 2\pi\Phi/\Phi_0 + \frac{1}{\hbar}\langle r_{A,2}(L_A,t)\rangle\right)\Bigg].\end{aligned} \tag{2.88}$$

The calculations we have presented here can easily be generalized to the calculation of the full conductance matrix $\langle G_{\alpha\beta}\rangle$. It can then be checked, that current is conserved, $\sum_\alpha \langle G_{\alpha\beta}\rangle = 0$, and that the system is gauge invariant, $\sum_\beta \langle G_{\alpha\beta}\rangle = 0$, also in the presence of interactions.

Eq. (2.88) has a rather intuitive interpretation since, essentially, $\langle T_{\beta\alpha}(E)\rangle \sim \langle|\Psi^A_E(x,t) + \Psi^B_E(x,t)|^2\rangle$, where $\Psi^A_E(x,t)$ and $\Psi^B_E(x,t)$ are wave functions for the upper and lower path respectively. Here the wave function $\Psi^i_E(x,t)$ is the WKB wave-function for arm i to energy E multiplied by the amplitudes for going through the intersections and by the magnetic phase picked up going through arm i. Note, that Eq. (2.88) is strictly correct only to second order in the fluctuating potential.

2.6.4 Dephasing time

We can now proceed to further evaluate Eq. (2.88). So far, we did not need to specify the shape of the potential $h_A(x)$ or to actually calculate $r_{A,1}(L_A,t)$ or $r_{A,2}(L_A,t)$. We only needed to know that the scattering matrix for arm A is of the form given in Eq. 2.85 and that the phases are real. Our first goal is to show for a few specific examples that the total suppression factor can be written in the form

$$\langle r^2_{A,1}(L_A,t)\rangle/2\hbar^2 = \tau_\Delta/\tau_\phi \tag{2.89}$$

where τ_Δ is an effective traversal time to be introduced below and $\Gamma_\phi = 1/\tau_\phi$ is the decoherence rate.

For a first example we will assume that $h_A(x) = 1/\cosh(x/\Delta)^2$ where Δ is the characteristic length of the potential. For $L_A \gg \Delta$ we find from Eq. 2.80

$$r_{A,1}(L_A,t) = -\pi\tau_\Delta^2 \int_{-\infty}^{\infty} \frac{d\omega}{2\pi} u_A(\omega) \frac{\omega \mathrm{e}^{-i\omega(t-L_A/v_F)}}{\sinh(\pi\omega\tau_\Delta/2)}. \tag{2.90}$$

In this expression, only the length Δ has a physical meaning, L_A is just an arbitrary point to the right of the barrier, where the potential is negligibly small. We have also defined the physical traversal time as $\tau_\Delta = \Delta/v_F$. In principle, the integral over the x-coordinate in Eq. 2.80 can be done exactly for any values of the upper and lower boundaries, but the result is cumbersome. To give an idea of the full x-dependence of the Fourier transform $r_{i,1}(x,\omega)$ of the first order correction to the phase, this quantity is shown as a function of x ($x_0 \to -\infty$ in Eq. 2.80) for one particular value of ω in Fig. [2.6]. The figure shows how the phase factor approaches its asymptotic (large x) value for $x \gg \Delta$ ($\Delta = 1$ in the figure) and quickly goes to zero to the left of the barrier.

Using the definition of the spectrum Eq. 2.8 and Eq. 2.90 it is possible to calculate $\langle r_{A,1}^2(L_A,t)\rangle$ for which we get

$$\langle r_{A,1}^2(L_A,t)\rangle = e^2\pi^2\tau_\Delta^4 \int \frac{d\omega}{2\pi} S_{U_AU_A}(\omega) \frac{\omega^2}{\sinh(\pi\omega\tau_\Delta/2)} \approx \frac{4e^2}{3}\tau_\Delta S_{UU}(0). \quad (2.91)$$

In writing the second equation we have assumed that the spectral function is a smooth function of ω and that it decays to zero for large frequencies. The integral then is fast converging due to the exponential decay of the form-factor for $\omega \gg 1/\tau_\Delta$. From Eq.2.91 we can see that the exponential suppression factor that enters the average conductance Eq. 2.88 is indeed of the form Eq. 2.89 with a dephasing rate (compare also Eq. 2.15)

$$\Gamma_\phi = \frac{2e^2}{3\hbar^2} S_{UU}(0). \quad (2.92)$$

As in our earlier calculations we find a suppression factor that is linear in the traversal time and proportional to the zero-frequency spectral function. The numerical prefactor is of order one but depends on the details of the barrier shape.

A Lorentzian barrier $h(x) = (1+x^2/\Delta^2)^{-1}$ can be used for comparison. Then, the first order correction to the phase (cf. Eq. 2.80) is

$$r_{A,1}(L_A,t) = -\pi\tau_\Delta \int_{-\infty}^{\infty} \frac{d\omega}{2\pi} u_A(\omega) \mathrm{e}^{-i\omega(t-L_A/v_F)-|\omega|\tau_\Delta}. \quad (2.93)$$

Again, this result is only valid asymptotically ($L_A \gg \Delta$). The suppression factor can be evaluated similarly to Eq. 2.91 and can be written in the form given in Eq. 2.89. The dephasing rate for the Lorentzian barrier is $\Gamma_\phi = e^2\pi S_{UU}(0)/2\hbar^2$. Not surprisingly, the numerical prefactor is different from the that in Eq. 2.92. Of course, no particular choice for $h(x)$ can be considered more realistic than any other and the shape-dependent features of the dephasing rate should not be taken too seriously (the true shape of the potential would have to be found from a self-consistent solution of the Poisson equation).

So far, we have not calculated the second order correction Eq. 2.81 to the phase of the semi-classical wave function. This has several reasons: first, we

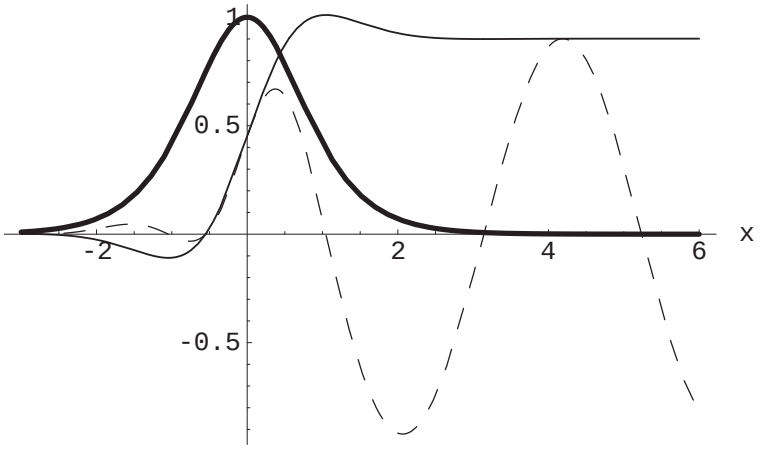

Figure 2.6: The thick line is the potential barrier $1/\cosh(x)^2$. The dashed line shows the real part of the first order correction $r_{i,1}(\omega)$ (cf. Eq. 2.80) as a function of x, for $\omega\tau_\Delta = 1.5$. The thin solid line shows the real part of $r_{i,1}(\omega)$ without the oscillating prefactor.

could do the integral over the x-coordinate in Eq. 2.81 only numerically (note that it is necessary to know the first order correction not only for large x, but for any x). A more serious objection is that the integral does not converge if the integration is extended over the whole real axis. For negative x convergence is no problem, since $r_{2,A}(x,t)$ quickly goes to zero for $x \ll 0$. For $x \gg a$ on the other hand the integral grows roughly linearly with the upper boundary. This can be seen through substitution of the asymptotically valid result for the first order correction (see Eq. 2.90 or Eq. 2.93) into Eq. 2.81. The integral can then be done from a lower boundary $x_1 \gg a$ to an upper boundary $x_2 \to \infty$ which allows us to check the convergence or rather the absence of convergence. The observed divergence may be understood from the following argument: due to the fluctuating potential the incoming plane wave state acquires side-bands at different energies. The wave packet quickly decays as its components propagate with different velocities. Eventually, the wave function can not be approximated anymore by a plane wave plus a small correction, as we have assumed when writing Eq. 2.78, and, consequently, perturbation theory breaks down.

2.6.5 A rectangular barrier

As we will show now, this breakdown of perturbation theory does not invalidate our approach. What we need is the transition amplitude from a plane wave state at energy E incoming at $x = 0$ to a plane wave state at E' at $x = L_A$. Using a rectangular barrier ($h_A(x) = 1$, $0 \le x \le L_A$ as an example we can demonstrate that our perturbation theory gives a satisfactory solution to this problem. Note that for this case there is only one length scale $L_A = \Delta$. While the semiclassical

approach should not be applied if the barrier is not smooth, we can always use such a simplification to get an order of magnitude estimate.

For the rectangular barrier $r_{A,1}(x,\omega)$ and $r_{A,2}(x,\omega_1,\omega_2)$ are

$$\begin{aligned} r_{i,1}(x,\omega) &= i\frac{u_i(\omega)}{\omega}\left(\mathrm{e}^{ix\omega/v_F}-1\right), \\ r_{i,2}(x,\omega_1,\omega_2) &= -\frac{x}{2m^*v_F^3}\,u_i(\omega_1)u_G(\omega_2)\mathrm{e}^{ix(\omega_1+\omega_2)/v_F}. \end{aligned} \tag{2.94}$$

These results are valid for $0 \le x \le L_A$ which is sufficient for our purposes. Note that for the rectangular barrier $r_{i,2}(x,t)$ grows linearly with x as is also the case for the smooth barriers we have discussed before.

Again, we start with a discussion of the real suppression factor for which we get

$$\frac{1}{2\hbar^2}\langle r_{A,1}^2(L_A,t)\rangle = \frac{e^2}{\pi\hbar^2}\int d\omega S_{U_AU_A}(\omega)\frac{\sin^2(\omega\tau/2)}{\omega^2}. \tag{2.95}$$

This is almost the same expression that we had already encountered in our simpler treatment of dephasing in Sec. 2.3 (see Eq. 2.13). This is not quite surprising, since we are in fact solving the same problem. Namely, dephasing of a particle that is exposed to a spatially constant potential during a finite time τ. The only difference to Eq. 2.13 is due to the auxiliary assumption we made in this section that interactions take place only in one arm. This is, why here the suppression factor contains the spectrum $S_{U_AU_A}$ instead of $S_{\Delta U\Delta U}$.

Note that the convergence of the integral is comparably weak for this particular choice of potential, since there is no exponentially decaying part in the kernel of the ω-integral. This is a consequence of the fact that there is no length-scale Δ different from L_A over which the potential decays.

We could now proceed with the evaluation of the dephasing time exactly as we did after Eq. 2.13. For concreteness we will instead consider a particular choice for the spectrum. In Ref. [51] we have calculated the spectrum for the lowest (spatially constant) mode of charge fluctuations in a single channel wire capacitively coupled to a gate. In the weak interaction limit we obtained

$$S_{U_AU_A}(\omega) = 2kTR_q\frac{C_{\mu,A}^2}{C_A^2}\frac{\sin(\omega\tau_A/2)^2}{(\omega\tau_A/2)^2}. \tag{2.96}$$

The same expression can also be obtained from the results of Blanter et al. [49]. With this particular choice of the spectrum the integral in Eq. 2.95 can be done exactly and we obtain for the dephasing rate

$$\Gamma_\phi = \left(\frac{\pi}{3}\right)\frac{kT}{\hbar}(1-g_A^2)^2 = \left(\frac{2\,e^2}{3\,\hbar^2}\right)\frac{C_{\mu,A}^2}{C_A^2}kTR_q. \tag{2.97}$$

For comparison with the notation conventionally used in the discussion of interacting single-channel wires we have introduced the Luttinger liquid parameter

g_A that measures the strength of the interactions in arm A. If interactions are strong $g \to 0$ and $g \to 1$ for weak coupling between arm and gate. The relation between the interaction parameter and the capacitance for a gated single-channel wire

$$g_A^2 = \frac{1}{1 + e^2 D_A / C_A}$$

was established by Blanter et al. [49]. The electrochemical capacitance [41] $C_{\mu,A}$ of arm A is $C_{\mu,A}^{-1} = C_A^{-1} + (e^2 D_A)^{-1}$.

We would like to emphasize again, that very recently experimental results were reported by Hansen et al. [8] and by Kobayashi et al. [9] on the temperature dependence of the decoherence of AB-oscillations in ballistic rings. In both measurements a dephasing rate linear in temperature was found. In our calculations the dephasing rate Γ_ϕ (Eq. (2.97)) also depends on the coupling parameter g_A. Dephasing goes to zero when gate and ring are completely decoupled ($g_A \to 1$).

Finally we can also evaluate the (second order) phase shift $r_{A,2}(L_A, t)/\hbar$. From Eq. 2.94 we get

$$\delta\Theta = \langle r_2(L_A, t)\rangle/\hbar = -\frac{L_A}{2 m v_F^3 \hbar} \int \frac{d\omega}{2\pi} S_{U_A U_A}(\omega)$$

and using the spectrum of Eq. 2.96 we find

$$\delta\Theta = -\frac{\pi}{4} \frac{C_{\mu,A}^2}{C_A^2} \left(\frac{kT}{E_F}\right).$$

If we compare the size of the two corrections due to scattering from the internal potential we find that $(\tau/\tau_\phi)/\delta\Theta \sim k_F L \gg 1$ which implies that taking scattering into account to the first order in the potential is a surprisingly good approximation. Combining the information gathered so far allows us to rewrite the transmission matrix elements Eq. (2.88) in the more convenient form

$$\langle T(E)\rangle = \frac{1}{2}\left[1 + \mathrm{e}^{-\tau/\tau_\phi} \cos\left(\Theta(E) - 2\pi\Phi/\Phi_0\right)\right]. \tag{2.98}$$

Our theory can be readily adapted to the case where both arms are coupled to gates ($g_i \neq 0, i = A, B$) by making the replacement

$$\frac{\tau_A}{\tau_\phi} \to \left(\frac{\tau_A}{\tau_{\phi,A}} + \frac{\tau_B}{\tau_{\phi,B}}\right) \tag{2.99}$$

in Eq. (2.98). The simple result Eq. (2.99) is an immediate consequence of the fact that potential fluctuations in the two arms are uncorrelated ($S_{U_A U_B} = S_{U_B U_A} = 0$). Of course, it is exactly the same result that we have found previously in Sec. 2.3

2.7 Conclusions

In this work we have examined dephasing due to electron-electron interactions in a simple Mach-Zehnder interferometer (MZI). Without interactions the MZI exhibits only forward scattering.

Using the assumption that the interaction effects in each arm of the interferometer can be taken into account through a single fluctuating internal potential we have calculated interaction corrections to the dc-conductance. In the expression for the averaged dc-conductance a dephasing time τ_ϕ occurs in a natural way. It is a measure of the strength of the attenuation of the AB-oscillations as a function of temperature and coupling strength between ring and gates. The dephasing rate $\Gamma_\phi = \tau_\phi^{-1}$ was found to be *linear* in temperature and to be proportional to the zero-frequency spectral function of the fluctuations of the internal potentials (see Sec. 2.3 and Sec. 2.6.4). The fluctuation spectra were calculated combining a scattering matrix approach with an electrically self-consistent treatment of the interactions (cf. Sec. 2.4.1).

It was found that the fluctuation spectra depend on the interaction through the ratio of the electrochemical capacitance C_μ and the geometrical gate capacitance C like $(C_\mu/C)^2$. Alternatively, in the case of a single channel wire, the spectrum depends on the Luttinger liquid interaction parameter g through $\Gamma_\phi \propto (1-g^2)^2$, at least in the weak coupling limit. In terms of the Coulomb energy $E_c = e^2/2C$ needed to charge the wire and the density of states (inverse level spacing) $D = 2L/hv_F$ this ratio is $(1 + 1/(2DE_c))^{-2}$. Such a dependence on E_c cannot be obtained from a Golden rule argument in which the coupling between the ring and the gate is treated perturbatively. Such a treatment would lead to a dephasing rate proportional to E_c^2. A dephasing rate proportional to E_c^2 is obtained only in the (unrealistic) limit that the level spacing far exceeds the Coulomb energy.

Recently the temperature dependence of AB-oscillations in ballistic rings was investigated experimentally by Cassé et al. [28]. Since both thermal averaging and dephasing of the electronic wave functions lead to a decrease in the visibility of the AB-oscillations as temperature is increased a separation of these different effects is of interest. Such an analysis of experimental data was carried out by Hansen et al. [8] and by Kobayashi et al. [9]. They find that the dephasing rate is *linear* in temperature in agreement with our work. We have seen (see Sec. 2.3) that the effect of thermal averaging is very small in the MZI if the two arms have a similar length. The dephasing length ($l_\phi = v_F\tau_\phi$) we have calculated can be of the order of the dephasing length observed in the experiments [8, 9].

In the experiment of Ref. [9] the dependence of the dephasing rate on the voltage-probe configuration in a four-terminal geometry was studied and large differences in the strength of the dephasing were observed for the so-called local and non-local configuration (see Sec. 2.5). We have calculated the dephasing rates for the MZI for these two configurations taking into account charge fluctuations

induced by the external voltages and have obtained a strong symmetry dependence of the dephasing rate in the local configuration. In a MZI with asymmetric beam-splitters (or any other type of asymmetry, e.g. different coupling of the two arms to the gates) the dephasing rate is larger for the local setup as was also observed in the experiment.

As we mentioned already in the introduction a linear temperature dependence has also been observed in experiments on chaotic cavities [3, 4, 5, 6, 7]. Theoretical work which gives a linear temperature dependence for the dephasing rate in chaotic cavities connected to open leads is presented in Refs. [17, 18]. Takane [17] finds $\Gamma_\phi = c(\lambda_F/W)kT/\hbar$ with c a constant of order one and W the width of the leads. Using the approach of Ref. [32] the dephasing rate of a chaotic cavity coupled via a geometrical capacitance C to a gate is given by $\Gamma_\phi = (e/\hbar)^2 kT(C_\mu/C)^2 R_q$ where C_μ is the electrochemical capacitance and R_q is the charge relaxation resistance (see Eq. (14.15) in Ref. [18]). Since in the experimentally relevant regime $(C_\mu/C) \approx 1$ and the ensemble averaged charge relaxation resistance R_q is $R_q = (h/e^2)(N_1 + N_2)^{-1}$ for a quantum dot coupled via $N_1 \gg 1$ and $N_2 \gg 1$ open channels to reservoirs, the dephasing rate is

$$\Gamma_\phi = \frac{2\pi kT}{\hbar(N_1 + N_2)}.$$

In contrast to the conductance which is determined by the smaller of the two contacts the charge relaxation resistance and hence the dephasing rate is dominated by the larger of the two contacts. Since the overall width of the two contacts is given by $W \propto \lambda_F(N_1 + N_2)$ it is seen that the two results are in fact identical. Both theories also make similar assumptions. In particular it is assumed that the dominant effect comes from uniform potential fluctuations inside the cavity. Taken together these results suggest that a linear temperature dependence can be expected whenever self-polarization effects are unimportant. Since the electrochemical capacitance and more importantly the charge relaxation resistance are sample specific quantities [37] even for chaotic cavities coupled to perfect leads this discussion leads to a distribution of dephasing rates in the few channel limit [18]. The mechanism for dephasing in our interferometer is exactly the same (potential fluctuations) as the mechanism proposed for dephasing in quantum dots in Refs. [17, 18]. In contrast to those calculations we have, however, directly calculated an observable quantity, namely the conductance.

It is also interesting to note that our dephasing time shows features similar to the life-time of an electron in a one-dimensional wire. The life time of Ref. [26] is also inversely proportional to temperature and, in the weak coupling limit, exhibits the same dependence on the interaction parameter g as our one-channel result for the dephasing time.

We hope that the work reported here stimulates further experimental and theoretical investigations.

2.8 Bibliography

[1] B. L. Altshuler, A. G. Aronov and, D. Khmelnitskii, J. Phys. C **15**, 7367 (1982); B. L. Altshuler and A. G. Aronov, in *Electron-electron Interaction in Disordered Systems*, edited by A. L. Efros and M. Pollak, (North Holland, Amsterdam, 1985).

[2] J. J. Lin and J. P. Bird, J. Phys. Condens. Matter **14**, R501, (2002).

[3] J. P. Bird, K. Ishibashi, D. K. Ferry, Y. Ochiai, Y. Aoyagi, and T. Sugano, Phys. Rev. B **51**, 18 037, (1995).

[4] R. M. Clarke, I. H. Chan, C. M. Marcus, C. I. Duruöz and J. S. Harris, Jr., K. Campman, and A. C. Gossard, Phys. Rev. B **52**, 2656, (1995).

[5] A. G. Huibers, M. Switkes, C. M. Marcus, K. Campman, and A. C. Gossard, PRL **81**, 200, (1998).

[6] D. P. Pivin, Jr., A. Andresen, J. P. Bird, and D. K. Ferry, Phys. Rev. Lett. **82**, 4687 (1999).

[7] A. G. Huibers, J. A. Folk, S. R. Patel, C. M. Marcus, C. I. Duruöz and J. S. Harris, Jr., PRL **83**, 5090, (1999).

[8] A. E. Hansen, A. Kristensen, S. Pedersen, C. B. Sorensen, and P. E. Lindelof , Phys. Rev. B **64**, 045327 (2001).

[9] K. Kobayashi, H. Aikawa, S. Katsumoto, and Y.Iye, J. Phys. Soc. Jpn. **71** (9), 2094, (2002).

[10] H. U. Baranger and P. A. Mello, Phys. Rev. B **51**, 4703, (1995).

[11] P. W. Brouwer and C. W. J. Beenakker, Phys. Rev. B **55**, 4695, (1997).

[12] M. Büttiker, Phys. Rev. B **33**, 3020, (1986); IBM J. Res. Dev. **32**, 63, 1988.

[13] P. W. Brouwer and I. L. Aleiner, Phys. Rev. Lett. **82**, 390 (1999).

[14] I. L. Aleiner, P. W. Brouwer and L. I. Glazman, Phys. Rep. **358**, 309, (2002).

[15] Y. M. Blanter, Phys. Rev. B **54**, 12807 (1996).

[16] M. G. Vavilov and I. L. Aleiner, Phys. Rev. B **60**, R16 311, (1999).

[17] Y. Takane, J. Phys. Soc. Jap. **67**, 3003 (1998).

[18] M. Büttiker, in "Quantum Mesoscopic Phenomena and Mesoscopic Devices", edited by I. O. Kulik and R. Ellialtioglu, (Kluwer, Academic Publishers, Dordrecht, 2000). Vol. 559, p. 211, cond-mat/9911188.

[19] Y. Aharonov and D. Bohm, Phys. Rev. **115**, 485 (1959).

[20] Y. Imry, *Introduction to mesoscopic physics*, Oxford University Press, 1997.

[21] A. Stern, Y. Aharonov, and Y. Imry, Phys. Rev. A **41**, 3436 (1990).

[22] D. Loss and K. Mullen, Phys. Rev. B **43**, 13252-13261 (1991).

[23] P. Cedraschi, V. V. Ponomarenko, and M. Büttiker, Phys. Rev. Lett. **84**, 346 (2000).

[24] P. Cedraschi and M. Büttiker, Phys. Rev. B **63**, 165312 (2001).

[25] F. Marquardt and C. Bruder, Phys. Rev. B **65**, 125 315 (2002).

[26] K. Le Hur, Phys. Rev. B **65**, 223 314 (2002).

[27] B. Krafft, A. Förster, A. van der Hart, and Th. Schäpers Physica E **2**, 635 (2001).

[28] M. Cassé, Z. D. Kvon, G. M. Gusev, E. B. Olshanetskii, L. V. Litvin, A. V. Plotnikov, D. K. Maude, and J. C. Portal, Phys. Rev. B **62**, 2624 (2000).

[29] S. Pedersen, A. E. Hansen, A. Kristensen, C. B. Sorensen, and P. E. Lindelof Phys. Rev. B **61**, 5457 (2000).

[30] A. E. Hansen, PhD Thesis, University of Copenhagen.

[31] L. Zehnder Zeitschr. f. Instrumentenkunde **11**, 275 (1891); L. Mach Zeitschr. f. Instrumentenkunde **12**, 89 (1892);

[32] M. Büttiker and A. M. Martin, Phys. Rev. B **61**, 2737, (2000).

[33] M. Büttiker, Phys. Rev. Lett. **57**, 1761, (1986).

[34] P. W. Brouwer and M. Büttiker, Europhys. Lett. **37**, 441 (1997).

[35] M. Büttiker, J. Low. Temp. Phys. **118**, 519, (2000).

[36] S. Pilgram and M. Büttiker, unpublished.

[37] M. H. Pedersen, S. A. van Langen, and M. Büttiker, Phys. Rev. B **57**, 1838 (1998).

[38] A. M. Martin and M. Büttiker, Phys. Rev. Lett. **84**, 3386 (2000).

[39] S. Pilgram, A. N. Jordan, G. Seelig and M. Büttiker, unpublished.

[40] M. Büttiker, PRB **46**, 12 458, (1992).

[41] M. Büttiker, H. Thomas, and A. Prêtre, Phys. Lett. A **180**, 364 (1993).

[42] M. Büttiker, H. Thomas, and A. Prêtre, Z. Phys. B **94**, 133 (1994).

[43] M. L. Polianski and P. W. Brouwer, cond-mat/0208408 (unpublished).

[44] M. Büttiker, Phys. Rev. B **46**, 12485 (1992).

[45] F. W. J. Hekking and Yu. V. Nazarov, Phys. Rev. B **44**, 11 506 (1991).

[46] M. Büttiker and R. Landauer, Phys. Rev. Lett. **49**, 1739 (1982).

[47] F. W. J. Hekking, Yu. V. Nazarov, and G. Schön, Europhys. Lett **14**, 489 (1991).

[48] G. Steinebrunner, F. W. J. Hekking, and G. Schön, Physica B **210**, 420 (1995).

[49] Ya. M. Blanter, F. W. J. Hekking, and M. Büttiker, Phys. Rev. Lett. **81**, 1925 (1998).

[50] D. L. Maslov and M. Stone, Phys. Rev. B **52**, R5539 (1995); V. V. Ponomarenko, Phys. Rev. B 52, R8666 (1995); I. Safi and H. J. Schulz *ibid* **52**, R17040 (1995).

[51] G. Seelig and M. Büttiker, Phys. Rev. B **64**, 245 313 (2001).

CHAPTER 3

Capacitance of a quantum dot from the Kondo model

3.1 Introduction

Although this chapter is again dedicated to the study of electron-electron interactions in ballistic mesoscopic conductors, we will focus on a limit that is very different from the one investigated in the last chapter. In our treatment of dephasing in mesoscopic rings we have assumed that interactions are relatively weak. This has allowed us to reduce the intricate many-particle problem to a one-particle problem where the interactions were absorbed into a fluctuating time-dependent potential. Such a treatment is appropriate for open conductors that can easily exchange electrons with a reservoir and where screening is consequently effective.

If, on the other hand, the mesoscopic conductor is well isolated, the phenomenon of Coulomb blockade is important. In this chapter we will be interested in a quantum dot (QD) in the Coulomb blockade regime and will, in particular, study the transition from weak to strong coupling between dot and reservoir. In our discussion we will exploit and expand a useful connection between the Coulomb blockade and the Kondo model mainly due to Matveev [1, 2, 3].

The setup we have in mind consists of a large quantum dot coupled to a reservoir via a quantum point contact (QPC) and capacitively coupled (with a capacitance C_{gd}) to a back-gate (see Fig. [3.1]). The electrostatic energy E_Q of the dot is a function of the voltage applied to the gate and is given by

$$E_Q(N) = E_C(Q/e - N)^2 \tag{3.1}$$

where N is a dimensionless parameter proportional to the gate voltage, Q is the charge on the dot and e is the elementary charge. Furthermore, $E_C = e^2/2C_\Sigma$

is the charging energy and C_Σ is the dot's total capacitance. Only when N is close to a half-integer value and two neighboring charge states - with n and $n+1$ electrons on the dot, say - are energy degenerate the number of electrons can fluctuate (between the two values n and $n+1$ in that case, all other charge states having an energy E of the order of or larger than the charging energy ($E_C \lesssim E$) for this particular value of the gate voltage). As a consequence of this so-called Coulomb blockade, the charge on the dot increases in steps of the size of the unit charge as a function of the gate voltage: an electron is added every time N passes through a half-integer value. The Coulomb blockade is effective only in the low temperature regime $T \ll E_C$ where thermal fluctuations of the number of charges on the dot show an activated behavior with activation energy of the order of E_C. As temperature is increased and becomes comparable to the charging energy, the steps of the Coulomb staircase are progressively smeared out. Also, for the observation of well-defined steps the dot has to be well separated from its environment. If the dot is strongly connected to its environment, charge can easily be exchanged and the Coulomb blockade is lifted.

The ground-state energy $\epsilon(N)$, the average charge $\langle Q(N)\rangle$ and the capacitance between dot and lead $C(N) = \partial\langle Q(N)\rangle/\partial V_G$ are all periodic functions of the dimensionless gate voltage N with a period corresponding to a change of the grain charge of e. It is interesting to ask how these quantities depend on the transparency of the connection between dot and reservoir. Experimentally, this question was addressed in a nice paper by Berman et al. [4]. Following Matveev [2, 3], we will study the case of a quantum dot that is coupled to the reservoir trough a quantum point contact with two transport channels (meaning here: one channel for electrons with spin or two channels for spin-less electrons). In particular we will be interested in the two limits of week reflection $|r|^2 = 1 - |t|^2 \ll 1$, r and t being the reflection and transmission amplitudes at the QPC respectively, and week transmission $|t|^2 \ll 1$. In these two limits one can try to calculate the average charge on the dot perturbatively treating either r or t as a small parameter. However, it turns out that perturbation theory breaks down at least close to charge degeneracy points $N = n + 1/2$ and consequently an exact solution of the problem is needed. Such a solution was provided in Refs. [2, 3] where the Coulomb blockade problem was mapped on a Kondo problem.

In the past few years a great amount of work has been devoted to studying the Kondo effect in mesoscopic systems [5]. A motivation for these efforts was the recent experimental observation of the Kondo effect in tunnelling through a small quantum dot [6, 7]. In these experiments the effective (or excess) electronic spin of the dot acts as a magnetic impurity. It should be emphasized, that the Kondo physics we will encounter here is quite different from this standard case. First, we are here interested in a large quantum dot with correspondingly small level spacing Δ such that the life-time $\hbar/\Delta$ of an electronic state in the dot far exceeds the time $\hbar/E_C$, it takes for the Coulomb blockade to build up. In contrast, for the observation of the standard Kondo effect one relies on small quantum dots with well separated levels. More importantly, we are not interested

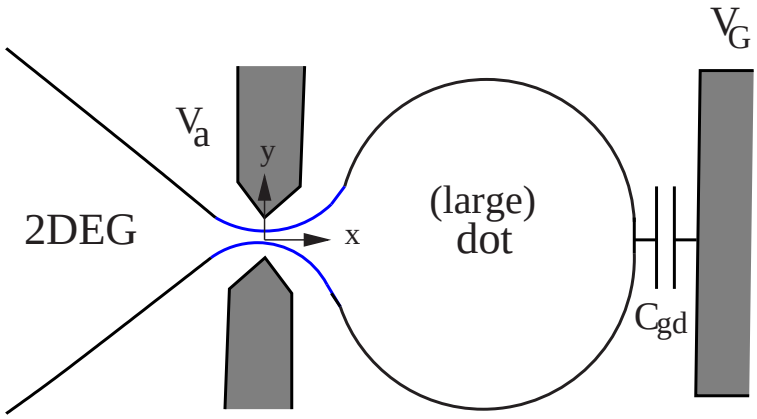

Figure 3.1: A large quantum dot is coupled to a 2DEG via a quantum point contact. The number of electrons in the dot can be controlled through the gate voltage V_G. The auxiliary voltage V_a can be used to open or close the point contact and thus to adjust the reflection amplitudes for the transport channels in the QPC.

in spin dynamics but in charge dynamics and the mapping on the Kondo effect is only a mathematical tool that allows for an exact solution of the Coulomb blockade problem.

There are two limits -corresponding to the cases of very strong and very weak reflection at the QPC - in which a mapping to a Kondo Hamiltonian can be used to calculate the average charge on the quantum dot. Before elaborating on this point we will here give the standard multi-channel Kondo Hamiltonian

$$\begin{aligned} H_K &= H_{Kin} + \sum_{\alpha} \left[J_{\alpha,z} s_{\alpha,z}(0) S_z^i \right. \\ &+ \left. J_{\alpha,\perp} \left(s_{\alpha,x}(0) S_x^i + s_{\alpha,y}(0) S_y^i \right) \right] \end{aligned} \tag{3.2}$$

in a very general form to be used as a point of reference for later discussions [8]. Here $\vec{S}$ is an impurity spin and $\vec{s}_\alpha(0)$ is the spin of conduction electrons with flavor α at the place of the impurity. We will consider only the two-channel case $\alpha = 1, 2$. In the discussion of the Coulomb blockade problem we will encounter Kondo Hamiltonians which are both spin- ($J_{\alpha,z} \neq J_{\alpha,\perp}$) and channel-anisotropic ($J_{1,\perp} \neq J_{2,\perp}$).

Matveev demonstrated the equivalence of the effective Hamiltonian describing the charge dynamics of a quantum dot, tunnel-coupled ($t \ll 1$) to a reservoir, close to a charge degeneracy point to a spin-anisotropic Kondo Hamiltonian [2]. If the dot and the reservoir are connected by m transport channels with the same transmission probability the problem can be mapped on a channel-isotropic m-channel Kondo model [9] with $J_{\alpha,z} = 0$ and $J_{\alpha,\perp} \ll 1$ [2]. The similarity of the charge dynamics on the dot to the spin dynamics in a Kondo model was already observed by Glazman and Matveev in their discussion on the conductance of a metallic grain (a quantum dot) tunnel-coupled to two reservoirs [1].

The limit of a point contact with one (electrons without spin) or two (electrons with spin) transport channels close to perfect transmission ($r \ll 1$) has also been treated. An effectively one-dimensional model for the dot-QPC system, which makes it possible to calculate the average charge on the dot using bosonization, was developed b y Flensberg [10] and by Matveev [3]. Matveev [3] also calculated the dot's capacitance as a function of the gate voltage and the reflection amplitude at the point contact. In his calculation he demonstrated that the Hamiltonian of the original problem can be mapped onto a Kondo Hamiltonian in the generalized Toulouse limit ($J_{1,z} = J_{2,z} = 2\pi v_F$). In this limit the two-channel Kondo model is exactly solvable, as was shown by Emery and Kivelson [11]. It was one of the main results of Ref. [3] that Coulomb blockade oscillations (accompanied by a logarithmic singularity in the expressions for the charge or the capacitance close to "half-integer" values of the number of electrons in the dot) persist also in the limit of weak reflection, as recently checked experimentally by Berman et al. [4]. They are completely smeared out only if at least one transport channel is at perfect transmission, the charge in the dot then increases linearly with the gate voltage [3, 10, 12]. A review of these results and more generally of interaction effects in quantum dots can be found in Ref. [13].

Extending previous work by Le Hur [14] we here want to discuss the effect of *channel-anisotropy* on the results for the capacitance in the two limits of almost perfect transmission and almost total reflection discussed above. We will show that the Coulomb staircase behavior is smeared out by a small channel anisotropy both in the weak and strong reflection limit. We will concentrate on the case of two transport channels. Channel-anisotropy then means that the reflection (or transmission) amplitudes for the two channels are different. Such a situation can be realized applying a magnetic field to the sample. A weak in-plane magnetic field leads to different reflection amplitudes for spin-up and spin-down electrons. In a strong magnetic field electrons are spin polarized and the number of open channels in the QPC and their respective reflection amplitudes depend on the opening of the QPC. The confinement potential at the QPC and thus its opening can be tuned changing the auxiliary gate voltage V_a (see Fig. [3.1]). In the limit of small reflection an intuitive physical picture for the transition from the channel symmetric case [3] to the case of a weak asymmetry between the two channels can be obtained [14] from the use of the *channel-anisotropic* two-channel Kondo model at the Emery-Kivelson line [15]. The two coupling constants of the asymmetric Kondo model are directly related to the reflection amplitudes of the two transport channels in the QPC. In this chapter we will elaborate on this mapping and discuss its limitations. Although the physical picture associated with the *channel-anisotropic* two-channel Kondo model is very appealing, the Coulomb blockade problem in the high transparency limit with two transport channels with different reflection coefficients can also be solved through a mapping on the *channel-isotropic* two-channel Kondo model as we will show. Such a procedure was applied by Matveev and Furusaki [16] when they calculated the inelastic cotunneling through a quantum dot strongly coupled to two

quantum point contacts with one transport channel each (electrons in a strong magnetic field). Furthermore, we will show that in the case of tunnel-coupling (small transmission) an asymmetry between transmission amplitudes of different channels will lead to a mapping of the Hamiltonian on a channel-anisotropic Kondo model with $J_{1,z} = J_{2,z} = 0$.

This chapter is structured as follows: In a first part we consider the weak coupling limit. We start by developing the model Hamiltonian in Sec. 3.2. In Sec. 3.3 we discuss the mapping on the channel-anisotropic two-channel Kondo model and use it to calculate the capacitance of the quantum dot in a weak magnetic field. In the following section (Sec. 3.4) we show that the same results can also be found from a mapping to a channel-isotropic Kondo model and in addition look at the case of a strong magnetic field applied to the QPC-dot system. In Sec. 3.5 a simple scaling argument is used to rederive the main (exact) results of Secs. 3.3 and 3.4. The limit of small transmission through the quantum dot will finally be considered in Sec. 3.6.

3.2 The model

We here consider a large quantum dot weakly coupled to a 2DEG via a point contact[3] (see Fig. [3.1]). The shape of the QPC is defined trough metallic gates placed on top of the 2DEG. A change in the voltage applied to these gates changes the lateral confinement potential in the QPC. As a consequence of the lateral confinement the conductance of the QPC is quantized and electron motion in the vicinity of the QPC is essentially one-dimensional. The one-dimensional wave-function Ψ_σ^n for motion along the x axis is characterized by the spin index $\sigma = \uparrow, \downarrow$ and the (orbital) channel quantum number n due to the lateral confinement [17]. Note, that from here on we will use the word channel to mean electrons with a certain pair of indices σ, n. As a short notation we introduce the channel index $\alpha = \sigma, n$ and we denote the wave-function of an electron in this channel by Ψ_α. In the further analysis we neglect transport channels that are totally reflected at the QPC, since electrons from these channels are confined to the reservoir and will not contribute to the charging of the dot. We will concentrate on the case where only two channels are open. This can be realized in two different ways. If a weak (or zero) in-plane magnetic field is applied (see Sec. 3.3), the two channels correspond to the two spin polarizations of electrons in the lowest ($n = 1$) energy eigenstate of the lateral Hamiltonian ($\Psi_1 = \Psi_\uparrow^1, \Psi_2 = \Psi_\downarrow^1$). The role of the magnetic field is to introduce an asymmetry between the reflection coefficients for spin-up and spin-down electrons [14]. In a strong magnetic field the electrons are spin-polarized and the two-channel case corresponds to two orbital channels entering the constriction (e.g. $\Psi_1 = \Psi_\uparrow^1, \Psi_2 = \Psi_\uparrow^2$), see Sec. 3.4.

Since we are interested in energies much smaller than the Fermi energy we linearize the spectrum around the Fermi points. Furthermore it is convenient to decompose the wave-function into a right-going and a left-going contribution

$\Psi_\alpha = \exp(ik_F x)\Psi_{\alpha,R}(x) + \exp(-ik_F x)\Psi_{\alpha,L}(x)$. For two open transport channels the Hamiltonian for the electrons in the point contact is

$$H_{Kin} = -iv_F \sum_{\alpha=1,2} \int_{-\infty}^{\infty} dx \left[\Psi^\dagger_{\alpha,R}(x)\partial_x \Psi_{\alpha,R}(x) - \Psi^\dagger_{\alpha,L}(x)\partial_x \Psi_{\alpha,L}(x)\right] \tag{3.3}$$

where the sum is over (open) quantum channels. Electron interactions in the quantum dot are taken into account via the Coulomb Hamiltonian

$$H_C = E_C(Q/e - N)^2. \tag{3.4}$$

The parameter $eN = V_G C_{gd}$ is proportional to the gate voltage and $E_C = e^2/2C$ is the charging energy ($eN = V_G C_{gd}$ holds for a single electron box, in a more complicated geometry the ratio $\beta = N/V_G$ will be more involved). Note that the total capacitance C of the quantum dot is different from the capacitance C_{gd} between gate and dot. In addition we allow for a weak backscattering[28] in the point contact,

$$H_{bs} = v_F \sum_{\alpha=1,2} |r_\alpha| \left[\Psi^\dagger_{\alpha,R}(0)\Psi_{\alpha,L}(0) + h.c.\right]. \tag{3.5}$$

The transmission is supposed to be globally adiabatic [18]. The reflection amplitudes $|r_1|$ and $|r_2|$ can be tuned applying a voltage to the gates defining the QPC. The main goal in the following will be to calculate the shift in the ground state energy $\delta\epsilon(N)$ due to the backscattering in the point contact. From the correction $\delta\epsilon(N)$ it is possible to obtain the corrections to the average charge on the dot and to dot's capacitance via

$$\begin{aligned} \langle Q(N)\rangle &= eN + \frac{\partial}{\partial V_G}\,\delta\epsilon(N), \\ \delta C(N) &= \frac{\partial}{\partial V_G}\langle \delta Q(N)\rangle = \frac{\partial^2}{\partial {V_G}^2}\,\delta\epsilon(N). \end{aligned} \tag{3.6}$$

To manipulate the Hamiltonian of the one-dimensional interacting system we have introduced above, it is convenient to use the bosonization technique. Bosonizing in the standard way we express the Fermi field operators through the bosonic fields $\phi_\alpha(x)$ and $\theta_\alpha(x)$ and write [19, 20]

$$\Psi_{\alpha,R/L}(x) = \frac{1}{\sqrt{2\pi a}} \mathrm{e}^{i\sqrt{\pi}(-p\phi_\alpha(x) + \theta_\alpha(x))}. \tag{3.7}$$

Here $p = 1$ for right-movers (R) and $p = -1$ for left-movers (L). The bosonic fields obey the commutation relations

$$\begin{aligned} [\phi_\alpha(x), \theta_\beta(y)] &= \frac{i}{2}\mathrm{sign}(x-y)\delta_{\alpha,\beta}, \\ [\phi_\alpha(x), \partial_y\theta_\beta(y)] &= i\delta(x-y)\delta_{\alpha,\beta}, \\ [\phi_\alpha(x), \phi_\beta(y)] &= [\theta_\alpha(x), \theta_\beta(y)] = 0. \end{aligned}$$

In the new variables the kinetic energy takes the form

$$H_{Kin} = v_F \sum_{\alpha=1,2} \int_{-\infty}^{\infty} dx \left[(\partial_x \phi_\alpha)^2 + (\partial_x \theta_\alpha)^2 \right]. \tag{3.8}$$

To bosonize the Coulomb Hamiltonian we make use of $: \Psi^\dagger_{\alpha,L}\Psi_{\alpha,L} + \Psi^\dagger_{\alpha,R}\Psi_{\alpha,R} := -\partial_x\phi_\alpha/\sqrt{\pi}$. The total charge in the dot then is

$$Q = \sum_{\alpha=1,2} \int_0^{\infty} dx \left(: \Psi^\dagger_{\alpha,R}\Psi_{\alpha,R} + \Psi^\dagger_{\alpha,L}\Psi_{\alpha,L} : \right).$$

The charge in the dot is now measured in units of e. We neglect both finite size effects in the dot [13, 21] (supposed to be ideal with no dephasing process) and mesoscopic corrections to the capacitance C [22, 23]. Expressing the charge in terms of the bosonic variables we obtain $Q = (\phi_1(0) + \phi_2(0))/\sqrt{\pi}$. The term at spatial infinity is independent of the gate voltage; We choose $\phi_i(\infty) = 0$ in such a way that the total charge Q on the dot is zero when $N = 0$. Consequently we get

$$H_C = \frac{E_C}{\pi} \left(\sum_{\alpha=1,2} \phi_\alpha(0) - \sqrt{\pi} N \right)^2 \tag{3.9}$$

for the Coulomb Hamiltonian. In writing Eq. (3.9) we have only considered the charge-dependent part of Eq. (3.4). Finally we also have to bosonize the backscattering Hamiltonian which leads us to

$$H_{bs} = \frac{v_F}{\pi a} \sum_{\alpha=1,2} |r_\alpha| \cos\left(\sqrt{4\pi}\phi_\alpha(0) \right). \tag{3.10}$$

Now it is convenient to introduce the new variables $\phi_{c,s} = \frac{1}{\sqrt{2}} (\phi_1(x) \pm \phi_2(x))$ and $\theta_{c,s} = \frac{1}{\sqrt{2}} (\theta_1(x) \pm \theta_2(x))$ where the positive sign belongs to the label c (charge) and the negative sign belongs to s (spin). Note that in the case of a strong magnetic field electrons are spin-polarized. The index s then labels a "pseudospin" and not physical spin states.

The kinetic energy in the new variables has the standard form of Eq. (3.8). The Coulomb Hamiltonian

$$H_C = \frac{2E_C}{\pi} \left(\phi_c(0) - \sqrt{\pi/2} N \right)^2 \tag{3.11}$$

is a function of the charge field only which is the main motivation for the introduction of this new set of variables. Furthermore we get for the backscattering part

$$\begin{aligned} H_{bs} &= \frac{v_F}{\pi a} (|r_1| + |r_2|) \cos\left(\sqrt{2\pi}\phi_c(0) \right) \cos\left(\sqrt{2\pi}\phi_s(0) \right) \\ &- \frac{v_F}{\pi a} (|r_1| - |r_2|) \sin\left(\sqrt{2\pi}\phi_c(0) \right) \sin\left(\sqrt{2\pi}\phi_s(0) \right). \end{aligned} \tag{3.12}$$

We now introduce the charge fluctuation field $\hat{\phi}_c(0) = \phi_c(0) - \sqrt{\pi/2}N$. The total charge in the dot is pinned at its classical value $Q_{cl} = \phi_c(0) = \sqrt{\pi/2}N$ to minimize the Coulomb energy. For weak backscattering $|r_1|, |r_2| \ll 1$ and for energies below the charging energy we can average over the charge fluctuations $\hat{\phi}_c(0)$. When averaging over the term $\cos\left(\sqrt{2\pi}\phi_c(0)\right) = \cos\left(\sqrt{2\pi}\hat{\phi}_c(0) + \pi N\right)$ in Eq. (3.12) we obtain the expression

$$\mathrm{e}^{-\pi\langle\hat{\phi}_c(0)^2\rangle}\cos(\pi N) = \sqrt{\frac{a\gamma E_C}{v_F}}\cos(\pi N).$$

Here the angular brackets mean averaging with regard to the ground-state of the free Hamiltonian Eq. (3.8). An analogous expression can also be found for the term $\sin\left(\sqrt{2\pi}\phi_c(0)\right)$ in Eq. (3.12). When calculating the correlator

$$\langle\hat{\phi}_c(0)^2\rangle = -\frac{1}{2\pi}\ln\frac{a\gamma E_C}{v_F}$$

we have taken into account that only fluctuation modes with energies larger than the charging energy E_C can enter into the dot. Here γ is defined through $\gamma = \mathrm{e}^{\mathcal{C}}$ where $\mathcal{C} \approx 0.577$ is Euler's constant. After the averaging the backscattering part of the Hamiltonian can be written as

$$\begin{aligned} H_{bs} &= \frac{\sqrt{\gamma a E_C v_F}}{\pi a}(|r_1| + |r_2|)\cos(\pi N)\cos\left(\sqrt{2\pi}\phi_s(0)\right) \\ &- \frac{\sqrt{\gamma a E_C v_F}}{\pi a}(|r_1| - |r_2|)\sin(\pi N)\sin\left(\sqrt{2\pi}\phi_s(0)\right). \end{aligned} \tag{3.13}$$

Alternatively, the Hamiltonian Eq. (3.13) can also be written in the form[16]

$$H_{bs} = \frac{\sqrt{a\gamma E_C v_F}}{\pi a}\left(r\mathrm{e}^{i\sqrt{2\pi}\phi_s(0)} + r^*\mathrm{e}^{-i\sqrt{2\pi}\phi_s(0)}\right), \tag{3.14}$$

where r is the complex parameter $r = (|r_1|\mathrm{e}^{i\pi N} + |r_2|\mathrm{e}^{-i\pi N})/2$. The first form of the backscattering term Eq. (3.13) will be used in Sec. 3.3 when discussing the two-channel anisotropic version of the Kondo model, while Eq. (3.14) will be useful as a starting point for the mapping on the isotropic form of the two-channel Kondo model (see Sec. 3.4). The charge part of the kinetic energy can now be dropped since it is completely decoupled from the perturbation due to the backscattering.

3.3 Channel-anisotropic Kondo model

In this section we will concentrate on the case where the reflection amplitudes $|r_1|$ and $|r_2|$ are very close to each other. It is convenient to introduce the parameters $|R| = |r_1| + |r_2|$ and $|\delta r| = |r_2| - |r_1|$ where $|\delta r| \ll |R| \ll 1$. For the sake of clarity we have split up this section into three subsections. In the first subsection we

will discuss the relation between our problem and the channel-anisotropic (two-channel) Kondo model[14]. In the second subsection we will derive an expression for the impurity correction to the ground state energy while a physical realization of the case $|\delta r| \ll |R| \ll 1$ is discussed in the third subsection. There we will also explicitly calculate the charge in the dot and the dot's capacitance.

3.3.1 Equivalence to the Kondo model

We will now see that our theory for the Coulomb blockade problem can be mapped on the anisotropic two-channel Kondo model at the Emery-Kivelson line i.e. $J_{\sigma,z} = 2\pi v_F$ with $\sigma = 1, 2$. The solution of this model [15, 24] is due to Fabrizio, Gogolin and Nozières[15].

Introducing the auxiliary impurity-spin operators $\hat{S}_x$ and $\hat{S}_y$ we rewrite the backscattering term (Eq. (3.13)) as

$$H_{bs} = \frac{J_x}{\pi a} \cos\left(\sqrt{2\pi}\phi_s(0)\right) \hat{S}_x + \frac{J_y}{\pi a} \sin\left(\sqrt{2\pi}\phi_s(0)\right) \hat{S}_y, \tag{3.15}$$

where the Kondo coupling parameters are defined through

$$\begin{aligned} J_x &= 2|R|\sqrt{a\gamma E_C v_F}\cos(\pi N), \\ J_y &= 2|\delta r|\sqrt{a\gamma E_C v_F}\sin(\pi N). \end{aligned} \tag{3.16}$$

In terms of the Kondo Hamiltonian Eq. 3.2 we get $J_x \propto (J_{1,\perp} + J_{2,\perp})$ and $J_y \propto (J_{1,\perp} - J_{2,\perp})$, where $J_{\sigma,\perp}$ denotes the transverse Kondo coupling of each conduction band channel with the magnetic impurity. The total Hamiltonian which we will denote H^A_{EK} is given by $H^A_{EK} = H_{Kin}(\phi_s, \theta_s) + H_{bs}(\phi_s)$, where the kinetic term is of the form Eq. (3.8). Both $\hat{S}_x$ and $\hat{S}_y$ can be considered as good quantum numbers since their commutators with the Hamiltonian H^A_{EK} are small close to perfect transmission through the quantum point contact:

$$\begin{aligned} \left[H^A_{EK}, \hat{S}_x\right] &\propto -i|R|\hat{S}_z, \\ \left[H^A_{EK}, \hat{S}_y\right] &\propto i|\delta r|\hat{S}_z. \end{aligned}$$

The impurity spin in H^A_{EK} can oscillate between the two values $\hat{S}_x = 1/2$ and $\hat{S}_y = -1/2$. It is important to note that the backscattering part of the total Hamiltonian (Eq. (3.13)) and the coupling term of the two-channel anisotropic Kondo model (Eq. (3.15)) are exactly equivalent only in the channel symmetric case $|\delta r| = 0$, since $\hat{S}_x$ and $\hat{S}_y$ do not commute. However, we will see in the following section that the approximation made in writing Eq. (3.15) is good as long as $|\delta r| \ll |R|$ or $N \sim 0, \pm 1/2, \pm 1 \ldots$.

We now want to find the shift of the energy due to the backscattering or, in the language of the Kondo problem, the impurity correction to the ground state energy. To make further progress it is useful to refermionize the Hamiltonian.

Since we have eliminated one degree of freedom, namely the charge field ϕ_c from our problem, a refermionization of our Hamiltonian will not take us back to the original fermionic Hamiltonian (Eqs. 3.3, 3.4, 3.5). Also, the fermionic excitations that will be introduced are not electrons, but a kind of spin-fields. The backscattering part of the bosonic Hamiltonian to be refermionized is given in Eq. (3.15). The kinetic energy is of the form

$$H_{Kin} = v_F \int_{-\infty}^{\infty} dx \left[(\partial_x \phi_s(x))^2 + \pi_s(x)^2 \right]. \tag{3.17}$$

It is convenient to use the field $\pi_s(x) = \partial_x \theta_s(x)$ instead of $\theta_s(x)$ for the moment. The commutation relations for the fields $\phi_s(x)$ and $\pi_s(x)$ are $[\phi_s(x), \pi_s(y)] = i\delta(x-y)$, $[\phi_s(x), \phi_s(y)] = 0$ and $[\pi_s(x), \pi_s(y)] = 0$. Furthermore we will use the Majorana representation

$$\begin{aligned} \sqrt{2}\hat{S}_x &= a = (d + d^\dagger)/\sqrt{2}, \\ \sqrt{2}\hat{S}_y &= -b = (d^\dagger - d)/(i\sqrt{2}) \end{aligned} \tag{3.18}$$

to express the spin-operators through fermionic operators. The d operators ($d = a + ib$) obey $\{d^\dagger, d\} = 1$ and $\{d, \psi(x)\} = 0$.

The basic idea of the refermionization procedure is to introduce an operator $\psi(x)$ such that $\cos(\sqrt{2\pi}\phi_s(0)) \propto \psi(0) + \psi^\dagger(0)$ and $\sin(\sqrt{2\pi}\phi_s(0)) \propto \psi(0) - \psi^\dagger(0)$. It is clear that for such an operator

$$\psi(0) = \frac{1}{\sqrt{2\pi a}} \exp(i\sqrt{2\pi}\phi_s(0)).$$

For the operator $\psi(x)$ to represent a Fermion it must in addition obey anti-commutation relations. Using the relation $\mathrm{e}^A \mathrm{e}^B = \mathrm{e}^B \mathrm{e}^A \mathrm{e}^{[A,B]}$ it can be seen that the obvious choice for ψ, namely $\psi(x) = (2\pi a)^{-1/2} \exp(i\sqrt{2\pi}\phi_s(x))$ does not obey anti-commutation relations. To construct an operator that does obey anti-commutation relations we introduce the auxiliary fields

$$\begin{aligned} \phi_\pm(x) &= \frac{1}{\sqrt{2}} \left(\phi_s(x) \pm \phi_s(-x) \right), \\ \pi_\pm(x) &= \frac{1}{\sqrt{2}} \left(\pi_s(x) \pm \pi_s(-x) \right). \end{aligned}$$

In terms of these new fields the kinetic energy is

$$H_{Kin} = v_F \sum_{\alpha=\pm} \int_0^{\infty} dx \left[(\partial_x \phi_\alpha)^2 + (\partial_x \theta_\alpha)^2 \right]. \tag{3.19}$$

We thus arrive at a theory which is confined to positive values of x. The advantage of this restriction becomes clear when we introduce the two additional right-going and left-going fields

$$\begin{aligned} \Phi_{R,\pm}(x) &= \phi_\pm(x) - \int_0^x dy\ \pi_\pm(y), \\ \Phi_{L,\pm}(x) &= \phi_\pm(x) + \int_0^x dy\ \pi_\pm(y)). \end{aligned} \tag{3.20}$$

At $x = 0$ we have $\Phi_{R,+}(0) = \Phi_{L,+}(0) = \sqrt{2}\phi_s(0)$ and also $\Phi_{R,-}(0) = \Phi_{L,-}(0) = 0$ which makes these fields candidates for the construction of our new fermions. The backscattering Hamiltonian can be expressed through the fields $\Phi_{R,+}(x)$ and $\Phi_{L,+}(x)$ only. There are in fact many ways in which this can be done. However, we will soon get rid of this ambiguity. The fields $\Phi_{L,-}(x)$ $\Phi_{R,-}(x)$ occur only in the kinetic part of the Hamiltonian and are thus of little interest to us. Later on we will need the commutation relations

$$\begin{aligned}[\Phi_{R,+}(x), \Phi_{R,+}(y)] &= +i\,\mathrm{sign}(x-y),\\ [\Phi_{L,+}(x), \Phi_{L,+}(y)] &= -i\,\mathrm{sign}(x-y).\end{aligned}$$

We also give the correlation functions $G_{R(L)} = \langle \Phi_{R(L),+}(x)\Phi_{R(L),+}(0) - \Phi_{R(L),+}(0)^2 \rangle$ which take the standard form

$$G_{R(L)} = \frac{1}{\pi} \ln\left(\frac{a}{a \pm ix}\right).$$

The plus sign belongs to the label R while the minus sign belongs to L. The kinetic energy in terms of these new fields takes the form

$$H_{Kin} = \frac{v_F}{2} \sum_{\alpha=\pm} \int_0^\infty dx \left[(\partial_x \Phi_{R,\alpha})^2 + (\partial_x \Phi_{L,\alpha})^2 \right]. \tag{3.21}$$

We now drop the $\Phi_{R(L),-}(x)$ part of the kinetic energy since these fields are not coupled to the backscattering term. To refermionize the $\Phi_{R(L),+}(x)$ part we introduce the operators

$$\begin{aligned}\psi_R(x) &= \frac{1}{\sqrt{2\pi a}} \mathrm{e}^{i\sqrt{\pi}\Phi_{R,+}(x)},\\ \psi_L(x) &= \frac{1}{\sqrt{2\pi a}} \mathrm{e}^{i\sqrt{\pi}\Phi_{L,+}(x)}.\end{aligned} \tag{3.22}$$

Using the commutation relations for the bosonic fields we can verify that the fields $\psi_{R,+}(x)$ and $\psi_{L,+}(x)$ really are fermions and obey

$$\psi_{p,+}(x)\psi_{p,+}(y) = -\psi_{p,+}(y)\psi_{p,+}(x),$$

where $p = R, L$. Note, that for $x = 0$ we have $\psi_{L,+}(0) = \psi_{R,+}(0)$ (see Eqs. (3.20) and (3.22)) and there thus seems to be more than one way to refermionize the backscattering Hamiltonian Eq. (3.15). To lift this ambiguity we reextend our theory on the full x-axis via the definition

$$\psi(x) = \mathcal{P} \begin{cases} \psi_R(x) & x > 0,\\ \psi_L(-x) & x < 0. \end{cases} \tag{3.23}$$

In the above definition of the fermion $\psi(x)$ (Eq. (3.23)) we have introduced an additional phase factor

$$\mathcal{P} = \exp(i\pi d^\dagger d) = 1 - 2d^\dagger d \tag{3.24}$$

to ensure that $\psi(x)$ anticommutes with the spin operators $\hat{S}_x$ and $\hat{S}_y$ written in terms of Majorana fermions d and $d^\dagger$ (cf. Eq. (3.18)). The second equality in Eq. (3.24) holds because $d^\dagger d = 0, 1$ at zero temperature. In the fermionic operators we have defined above, the kinetic energy finally takes the simple form

$$H_{Kin} = -iv_F \int_{-\infty}^{\infty} dx\ \psi^\dagger(x)\partial_x\psi(x), \tag{3.25}$$

while the backscattering part of the Hamiltonian is

$$\begin{aligned} H_{bs} &= \frac{J_x}{\sqrt{2\pi a}} \left(\psi(0) + \psi^\dagger(0)\right) \mathcal{P}\hat{S}_x \\ &- \frac{iJ_y}{\sqrt{2\pi a}} \left(\psi(0) - \psi^\dagger(0)\right) \mathcal{P}\hat{S}_y. \end{aligned}$$

Using Eqs. (3.24) and (3.18) together with the commutation relations for the operators d and $d^\dagger$ we can show that $\mathcal{P}\hat{S}_x = -i\hat{S}_y$ and $\mathcal{P}\hat{S}_y = -i\hat{S}_x$ and, expressing the spin-operators through the Majorana Fermions a and b, we get

$$\begin{aligned} H_{bs} &= \frac{iJ_x}{\sqrt{4\pi a}} \left(\psi(0) + \psi^\dagger(0)\right) b \\ &+ \frac{J_y}{\sqrt{4\pi a}} \left(\psi(0) - \psi^\dagger(0)\right) a. \end{aligned} \tag{3.26}$$

So, we finally arrive at a solvable resonant level type of model for the two Majorana fermions a and b [15, 24].

3.3.2 Impurity corrections and scattering phase shifts

Our next step is to calculate the impurity corrections to the ground state energy from the impurity Green's functions $G_a = -\langle T_\tau a(\tau)a(0)\rangle$ and $G_b = -\langle T_\tau b(\tau)b(0)\rangle$.

Although this is rather standard material (see e.g. Ref. [24]) we believe that it is useful to give a short derivation of the Green's functions. The Fourier transforms of the impurity Green's functions $G_a(\tau) = -\langle T_\tau a(\tau)a(0)\rangle$ and $G_b(\tau) = -\langle T_\tau b(\tau)b(0)\rangle$ can conveniently be found from the equations of motion. We will here only derive the correlation function for a, the correlator for b can be found along the same lines. The Hamiltonian $H^A_{EK} = H_{Kin} + H_{bs}$ of our system is given in Eqs. (3.25) and (3.26). The fields ψ and $d = a + ib$ (see Eq. (3.18)) obey standard fermionic anti-commutation relations. Introducing the Majorana components of the field ψ through $z_1(x,\tau) = \left(\psi^\dagger(x,\tau) + \psi(x,\tau)\right)/\sqrt{2}$ and $z_2(x,\tau) = \left(\psi(x,\tau) - \psi^\dagger(x,\tau)\right)/(i\sqrt{2})$ we see already from the Hamiltonian in Eq. (3.26) that a couples only to z_2. We introduce the additional propagator $G_{z_2a}(x,\tau) = -\langle T_\tau z_2(x,\tau)a(0)\rangle$. The equations of motion for the two coupled correlators $G_a(\tau)$ and $G_{z_2a}(x,\tau)$ are

$$\begin{aligned} \partial_\tau G_a(\tau) &= -\delta(\tau) + i\frac{J_y}{\sqrt{2\pi a}} G_{z_2a}(0,\tau), \\ \partial_\tau G_{z_2a}(x,\tau) &= +iv_F\partial_x G_{z_2a}(x,\tau) - i\frac{J_y}{\sqrt{2\pi a}}\delta(x)G_a(\tau). \end{aligned}$$

To solve these equations it is best to go to Fourier space making use of the relations

$$\begin{aligned} G_a(\tau) &= \frac{1}{\beta}\sum_{\omega_n} \mathrm{e}^{-i\omega_n\tau} G_a(\omega_n), \\ G_{z_2a}(x,\tau) &= \frac{1}{\beta}\sum_{\omega_n}\int \frac{dp}{2\pi}\mathrm{e}^{-i\omega_n\tau+ipx} G_{z_2a}(p,\omega_n) \end{aligned}$$

where the sum is over the fermionic Matsubara frequencies $\omega_n = (2n+1)\pi/\beta$. To calculate the correlator $G_a(\tau)$ we only need to understand the local physics in $x = 0$. The local equations of motion in Fourier space are

$$i\omega_n G_a(\omega_n) = 1 - i\frac{J_y}{\sqrt{2\pi a}} G_{z_2a}(\omega_n), \tag{3.27}$$

$$G_{z_2a}(\omega_n) = i\frac{J_y}{\sqrt{2\pi a}} G^{(0)}(\omega_n) G_a(\omega_n). \tag{3.28}$$

To alleviate the notation we have introduced $G^{(0)}(\omega_n) = -i\,\mathrm{sgn}(\omega_n)/2v_F$ (To find $G^{(0)}(\omega_n)$ we Fourier transform the free electron propagator $G^{(0)}(p,\omega_n) = (i\omega_n - v_F p)^{-1}$ with regard to p and take the limit $x \to 0$). Furthermore we have defined $G_{z_2a}(\omega_n) = G_{z_2a}(x = 0, \omega_n)$.

Substituting Eq. (3.28) into Eq. (3.27) we can solve for $G_a(\omega_n)$ and obtain

$$G_a(\omega_n) = \frac{1}{i\omega_n + i\Gamma_a sgn(\omega_n)}.$$

After an analytic continuation $i\omega_n \to \omega + i\delta$ we get

$$G_k(\omega) = \frac{1}{\omega + i\Gamma_k sgn(\omega)} \tag{3.29}$$

where the label k is $k = a, b$. The width $\Gamma_a(\Gamma_b)$ of the resonant level $a(b)$ is related to the respective Kondo coupling constant $J_y(J_x)$ via

$$\begin{aligned} \Gamma_a &= \frac{{J_y}^2}{4\pi a v_F} = \frac{E_C\gamma}{\pi}|\delta r|^2 \sin^2(\pi N), \\ \Gamma_b &= \frac{{J_x}^2}{4\pi a v_F} = \frac{E_C\gamma}{\pi}|R|^2 \cos^2(\pi N). \end{aligned} \tag{3.30}$$

The impurity correction to the ground state energy at zero temperature is

$$\delta\epsilon = -\int_{\omega_{min}}^{E_C} \frac{d\omega}{2\pi}\omega\left(n_a(\omega) + n_b(\omega)\right). \tag{3.31}$$

The occurrence of a high energy cut-off at E_C in Eq. (3.31) is an intrinsic property of the theory developed so far. The low energy cut-off ω_{min} needs some additional explanation. We can distinguish two different situations: In the neighborhood of

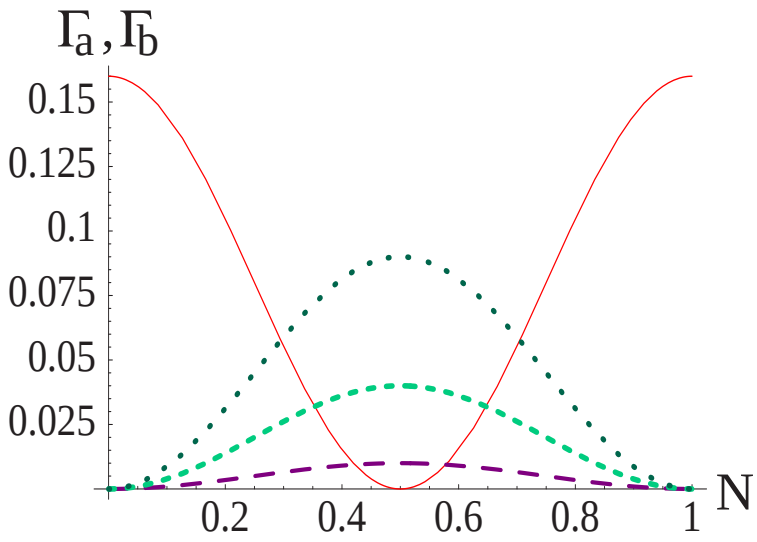

Figure 3.2: The resonance energies Γ_a and Γ_b of Eq. (3.30) are shown. The parameter $|R|$ in Γ_b (full line) is $|R| = 0.4$. The size of the resonance Γ_a grows with increasing anisotropy and thus with increasing $|\delta r|$. The lowest (dotted) line in the graph corresponds to $|\delta r| = 0.1$ the second lowest (short dashes) to $|\delta r| = 0.2$ and the third (long dashes) to $|\delta r| = 0.3$. The energies are measured in units of $E_C\gamma/\pi$.

integer values of N the resonance width Γ_a is negligibly small. Already at temperatures of the order of Γ_b spin fluctuations will get pinned, since the coupling constant J_x goes to strong coupling (compare Sec. 3.5). Very close to half-integer values of N however, we have $\Gamma_b \ll \Gamma_a$ even though $|\delta r| \ll |R|$. Thus the coupling J_y will go to strong coupling before J_x and spin fluctuations will be frozen at Γ_a. An expression for ω_{min} that correctly reproduces these two limits is $\omega_{min} = max\{\Gamma_a, \Gamma_b\}$. The density of states $n_k(\omega)$ of impurity k in Eq. (3.31) is related to the corresponding impurity Green's function through

$$n_k(\omega) = -2\mathrm{Im}\{G_k(\omega)\} = \frac{2\Gamma_k \mathrm{sgn}(\omega)}{\omega^2 + {\Gamma_k}^2}. \tag{3.32}$$

With this expression for $n_k(\omega)$ the integration in Eq. (3.31) can easily be performed and we get

$$\delta\epsilon = -\frac{1}{2\pi} \sum_{k=a,b} \left[\Gamma_k \ln \left(\frac{{E_C}^2 + {\Gamma_k}^2}{\max\{\Gamma_a, \Gamma_b\}^2 + {\Gamma_k}^2} \right) \right]. \tag{3.33}$$

For most purposes it is sufficient to approximate this expression by the simpler form [25]

$$\delta\epsilon = -\frac{1}{\pi} (\Gamma_a + \Gamma_b) \ln \left(\frac{E_C}{\max\{\Gamma_a, \Gamma_b\}} \right). \tag{3.34}$$

We have used $\Gamma_k \ll E_C$ and have dropped an additive constant. A quantity which is interesting is the scattering phase shift (extracted from the Friedel sum

rule)

$$\delta(\omega) = \frac{1}{2}\sum_{k=a,b} \arctan\left(\frac{\Gamma_k}{\omega}\right)$$

of the conduction electrons ψ due to the impurity scattering. In the channel symmetric case we have $\Gamma_a = 0$ and $\delta(\omega \ll \Gamma_b) = \pi/4$. The Friedel sum rule can also be rewritten $Z = 2\sum_l (2l+1)\,\delta_l/\pi$ where Z is the impurity charge screened by the electrons. For s-wave scattering ($l = 0$) and $Z = 1/2$ we recover $\delta = \pi/4$. The particular value of δ can thus be understood as a consequence of the fact that only "half" of the fermion d (the part a) is coupled to the conduction electrons. In general, if both Γ_a and Γ_b are finite we find $\delta = \pi/2$ in the limit $\omega \to 0$ and $Z = 1$ since now a and b are screened. Here, (even) for a *finite* channel asymmetry, we still find $\delta = \pi/4$ at the fixed point because close to $N = 1/2$ we have $\Gamma_b \to 0$ and close to $N = 0, \pm 1$ we have $\Gamma_a \to 0$. This gives a physical justification on the validity of the mapping in Sec. IV. It is important to remember that the "spin-fermions" ψ are not the real electrons but are related to the spin degrees of freedom of the original electronic wave-functions. However, they play the part of the conduction electrons of the real Kondo problem. In the case of spin-less electrons (electrons in a strong magnetic field) and for a single transmitted channel $|r| \ll 1$ the scattering phase shift of the real electrons is related to the average charge on the dot via $\delta = \pi\langle Q\rangle$, again as a consequence of Friedel's rule. It was shown by Aleiner and Glazman[13] that in the one-channel limit this relation can be used to calculate the impurity correction (see Eq. (3.37)) in an intuitive way.

3.3.3 Applications

The case $|\delta r| \ll |R| \ll 1$ can be realized in our setup by applying a weak in-plane magnetic field. In a non-zero field the reflection amplitudes $|r_1|$ and $|r_2|$ for electrons with spin-up and spin-down are different due to the Zeeman effect. The channel index α here distinguishes between spin-up and spin-down electrons in the lowest orbital channel $n = 1$. The (original) electronic wave-functions for electrons in the two channels are $\Psi_{\alpha=1} = \Psi_\uparrow^{n=1}$ and $\Psi_{\alpha=2} = \Psi_\downarrow^{n=1}$. We first want to consider the special case of zero magnetic field which was solved by Matveev in Ref. [3]. The reflection amplitudes for the two channels, corresponding to spin-up and spin-down electrons are equal ($|r_1| = |r_2| = |R|/2$) and thus $|\delta r| = 0$. It follows from Eqs. (3.16) and (3.30) that $J_y = 0$ and $\Gamma_a = 0$. Furthermore from Eq. (3.30) we know that $\Gamma_b = |R|^2\gamma E_C \cos^2(\pi N)/\pi$. Calculating the energy with Eq. (3.34) we find[3]

$$\delta\epsilon(N) = -\frac{\gamma E_C}{\pi^2}|R|^2 \ln\left(\frac{\pi}{\gamma|R|^2\cos^2(\pi N)}\right)\cos^2(\pi N).$$

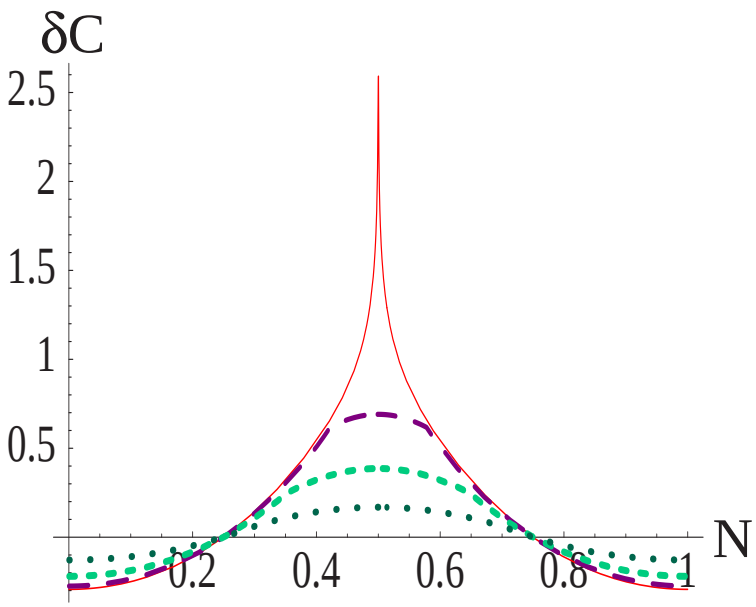

Figure 3.3: The correction to the capacitance Eq. (3.36) is shown for different values of the anisotropy parameter $|\delta r| = |r_2| - |r_1|$. The parameter $|R| = |r_1| + |r_2|$ is set to $|R| = 0.4$. The full line corresponds to the channel isotropic case $|\delta r| = 0$ where the capacitance is logarithmically divergent. In order of decreasing peak height the remaining three curves correspond to $|\delta r| = 0.1$, $|\delta r| = 0.2$ and $|\delta r| = 0.3$. The units of the capacitance are arbitrary.

The correction to the capacitance can then easily be calculated using Eq. (3.6) and is found to be

$$\delta C(N) = -2\gamma E_C |R|^2 \beta^2 \ln\left(\frac{1}{|R|^2\cos^2(\pi N)}\right)\cos(2\pi N).$$

Here we have kept only the logarithmically divergent contribution which will dominate all other terms close to $N = 1/2$. The parameter β is the geometry-dependent ratio of the dimensionless parameter N and the gate voltage V_G, $\beta = N/V_G$. This result is in reasonable agreement with the recent capacitance experiment of Ref. [4]. As we can see from Eq. (3.15) in the channel-symmetric case only fermion b is coupled to the field ψ. If we allow for a weak magnetic field the reflection coefficients for spin-up and spin-down electrons are slightly different and $|\delta r| \neq 0$. As a consequence the Kondo coupling J_y does not vanish anymore and both Majorana fermions a and b are coupled to the bath. The total energy shift $\delta\epsilon$ from Eqs. (3.30) and (3.34) is found to be[14]

$$\begin{aligned}\delta\epsilon(N) &= -\frac{\gamma E_C}{\pi^2}\ln\left(\frac{\pi}{\gamma\max\{|\delta r|^2\sin^2(\pi N), |R|^2\cos^2(\pi N)\}}\right) \\ &\times \left(|R|^2\cos^2(\pi N) + |\delta r|^2\sin^2(\pi N)\right).\end{aligned} \tag{3.35}$$

Due to the appearance of the max the logarithm does not diverge anymore. Still it can be very large due to the smallness of $|\delta r|$ and the logarithmic term will

dominate in the capacitance (See Fig. [3.3]):

$$\begin{aligned}\delta C(N) &= -2\gamma E_C \beta^2 \left(|R|^2 - |\delta r|^2\right) \cos(2\pi N) \\ &\times \ln\left(\frac{1}{\max\{|\delta r|^2 \sin^2(\pi N), |R|^2 \cos^2(\pi N)\}}\right).\end{aligned} \tag{3.36}$$

We see from Eqs. (3.35) and (3.36) that an arbitrary weak anisotropy between the two reflection coefficients is sufficient to cut off the logarithmic divergence. At the degeneracy point $N = 1/2$, we find $\delta C \propto \ln|\delta r|$. There is some similarity [3] with the behavior of the magnetic susceptibility of the impurity $\chi = \partial^2(\delta\epsilon)/\partial h^2$ away from the Emery-Kivelson line [15] and with that of the local magnetic susceptibility $\chi_l = \partial\langle\hat{S}_z\rangle/\partial h$ at the Emery-Kivelson line (the magnetic field h would only act on the impurity) [24], even though for weak backscattering at the QPC there is no real correspondence between the charge in the dot Q and $\hat{S}_z$. From the two-channel anisotropic Kondo model we see that the appearance of the second energy scale which leads to the suppression of the divergence follows in a natural manner from the coupling of the second Majorana fermion to the conduction electrons.

At this point it is also interesting to compare these results to the result obtained in the case of a single transmitted channel (reflection amplitude $|r_1| \ll 1$ and $|r_2| \to 1$). Such a situation can be realized in a strong magnetic field [14] (spinless electrons) and was also treated in Ref.[3]. The energy-shift for this case is

$$\delta\epsilon \propto |r_1| E_C \cos(2\pi N) \tag{3.37}$$

and therefore no logarithmic contribution occurs anymore in the expressions for the charge and the capacitance, we only get periodic oscillations as a function of the gate voltage.

In the next section we want to demonstrate that the approximation made in writing Eq. (3.15) is justified. Furthermore we will address the case of strong asymmetry between the conduction channels.

3.4 Mapping to a channel-isotropic Kondo model

We have seen in the last section that the backscattering term Eq. (3.15) is not exactly equivalent to the original Hamiltonian Eq. (3.13). We will now justify the approximation made and will rederive the results we have found from the two-channel anisotropic Kondo model in an exact way, following in our derivation Furusaki and Matveev [16]. The section is structured in a similar way as Sec. (3.3). The mathematical mapping will be discussed in a first subsection while a second short subsection will be devoted to the discussion of an application.

3.4.1 Mapping

As a starting point we use the form Eq. (3.14) of the original backscattering Hamiltonian which we rewrite as

$$H_{bs} = \frac{J_0}{2\pi a}\left(r\mathrm{e}^{i\sqrt{2\pi}\phi_s(0)} + r^*\mathrm{e}^{-i\sqrt{2\pi}\phi_s(0)}\right)\hat{S}_x. \tag{3.38}$$

Here $r = (|r_1|\mathrm{e}^{i\pi N} + |r_2|\mathrm{e}^{-i\pi N})/2$ is a complex parameter and $J_0 = 4\sqrt{a\gamma E_C v_F}$. Exactly as in the previous section we have introduced an auxiliary impurity spin $\hat{S}_x$. The spin $\hat{S}_x$ is a good quantum number since it commutes with the total Hamiltonian (here $\hat{S}_x = 1/2$). It is important to note that therefore Eq. (3.38) is exactly equivalent to the original expression Eq. (3.14). Reformionizing as described in the last section gives

$$H_{bs} = \frac{iJ_0}{\sqrt{4\pi a}}\left(r\psi(0) + r^*\psi^\dagger(0)\right)b \tag{3.39}$$

where we again use the Majorana representation for the impurity spin. The Hamiltonian Eq. (3.39) is very similar to the resonant level model that occurs in the solution of the two-channel isotropic Kondo model at the Emery-Kivelson line (compare Eq. (3.26) with $J_y = 0$). The impurity correction to the ground state energy can again be obtained from the Green's function. The propagator for the impurity has exactly the form Eq. (3.29) with Γ_k replaced by

$$\Gamma = \frac{{J_0}^2|r|^2}{4\pi a v_F} = \Gamma_a + \Gamma_b. \tag{3.40}$$

The second equation can be verified by explicit calculation of the sum of the two resonance energies given in Eq. (3.30). The impurity correction can be found from Eq. (3.31) in the channel-symmetric limit. Furthermore the density of states of the impurity was defined in Eq. (3.32). Combining these expressions we find for the impurity energy

$$\delta\epsilon = -\frac{\Gamma}{2\pi}\ln\left(\frac{{E_C}^2 + \Gamma^2}{2\Gamma^2}\right) \approx -\frac{\Gamma}{\pi}\ln\left(\frac{E_C}{\Gamma}\right). \tag{3.41}$$

In the second equation we have used $\Gamma \ll E_C$. It is now clear that the use of the two-channel anisotropic model is justified whenever $\max\{\Gamma_a, \Gamma_b\} \approx \Gamma_a + \Gamma_b$. This condition is certainly met when N is very close either to an integer or to a half-integer value. Furthermore the range of N-values for which the equation is approximately true will be larger for stronger asymmetry between Γ_a and Γ_b i.e. for a weak asymmetry between the reflection amplitudes $|r_1|$ and $|r_2|$.

In the two cases of electrons with spin in zero magnetic field or with a weak magnetic field we have $\max(\Gamma_a) \ll \max(\Gamma_b)$ and the channel-anisotropic Kondo model is more convenient (See Fig. [3.2]): In particular, the asymmetry simply produces a new energy scale obviously affecting the properties of the system close to the degeneracy point $N = 1/2$. This also allows to make explicit links with the small transmission limit (See Sec. VII).

3.4.2 Applications

We will now discuss a case for which the isotropic model is particularly well suited. This is the case of strong asymmetry between the reflection amplitudes of the two transmitted channels. We assume that one of the two channels is very close to perfect transmission, e.g. $|r_1| \to 0$ and $|r_1| \ll |r_2| \ll 1$. Such a situation can be reached in a strong magnetic field where the electrons are essentially spin polarized. The number of open channels and their reflection amplitudes can then be adjusted changing the voltage applied to the gates used to define the QPC. The wave-functions for the electrons in the two channels are $\Psi_{\alpha=1} = \Psi^{n=1}_{\uparrow(\downarrow)}$ and $\Psi_{\alpha=2} = \Psi^{n=2}_{\uparrow(\downarrow)}$. In the limit of interest here, the energy $\delta\epsilon$ with the help of Eqs. (3.40) and (3.41) is found to be

$$\begin{aligned} \delta\epsilon &= \frac{\gamma E_C}{\pi^2}|r_2|^2\left(1+2\lambda\cos(2\pi N)\right) \\ &\times \ln\left((\gamma|r_2|^2/\pi)\left[1+2\lambda\cos(2\pi N)\right]\right) \end{aligned}$$

where $\lambda = |r_1|/|r_2|$ is a small parameter. To leading order in λ the correction to the capacitance is given by

$$\delta C = -8\gamma E_C \beta^2 |r_1||r_2| \ln\left(|r_2|^2\right)\cos(2\pi N).$$

First we observe that at perfect transmission $|r_1| = 0$ there is no signature of Coulomb blockade left as it is expected [10, 2, 13, 27]. Furthermore it is interesting to notice that with one channel very close to perfect transmission the Coulomb blockade oscillations are strongly reminiscent of the one-channel case, also discussed in Ref.[3].

3.5 Renormalization group formulation

We will now show that the energy scales Γ_a and Γ_b can also be found from a scaling argument. To do this we will use an approach similar to the one used in Ref.[13] which in turn is based on Ref.[28]. We will first discuss the channel symmetric case $|r_1| = |r_2|$ (electrons with spin and zero magnetic field). The backscattering Hamiltonian for this case is given by

$$H_{bs} = \frac{2|r_1|}{\pi a}\sqrt{a\gamma E_C v_F}\cos(\pi N)\cos(\sqrt{2\pi}\phi_s(0)). \tag{3.42}$$

The basic idea of the renormalization group treatment applied here is to calculate the partition function to second order in the small parameter $|r_1|$ and to choose $|r_1|$ as a function of the lattice step a in such a way that the partition function remains invariant under the transformation $a \to a' = a\exp(l)$. The correction to

the partition function due to the backscattering perturbation is

$$\begin{aligned}\delta Z &= -\int_0^\beta d\tau_1 d\tau_2 \langle H_{bs}(\tau_1) H_{bs}(\tau_2)\rangle \\ &= -\frac{{J_x}^2}{(2\pi a)^2}\int_0^\beta d\tau_1 d\tau_2 \frac{a}{v_F|\tau_1-\tau_2|}.\end{aligned}$$

Using the definition of J_x given in Eq. (3.16) it can be seen that the partition function δZ is independent of the lattice step a and thus $|r_1|$ is invariant under rescaling. We now introduce a *dimensionless* parameter $|\tilde{r}_1|$ via $|\tilde{r}_1| = J_x/v_F$. With the help of this parameter we can rewrite the backscattering Hamiltonian in the standard form

$$H_{bs} = \frac{v_F|\tilde{r}_1|}{2\pi a}\cos(\sqrt{2\pi}\phi_s(0)). \tag{3.43}$$

From this we can see that $|\tilde{r}_1| = 4|r_1|\sqrt{\gamma E_C a/v_F}\cos(\pi N)$ has the meaning of an effective reflection amplitude. Since $|\tilde{r}_1| \propto \sqrt{a}|r_1|$ it is clear that $|\tilde{r}_1|$ grows under the renormalization $a \to a' = a\exp(l)$. The renormalization flow equation for $|\tilde{r}_1|$ is given by

$$\frac{d}{dl}|\tilde{r}_1(l)| = \frac{1}{2}|\tilde{r}_1(l)|.$$

We can now integrate this equation from $l = 0$ ($a' = a$) to $l = l_c$ ($a' = a_c = a\exp(l_c)$), where a_c is the value of a' for which $J_x \propto |\tilde{r}_1|$ departs to strong coupling, that is $|\tilde{r}_1(a')| \sim 1$. Integrating we get $|\tilde{r}_1(a_c)|^2 = (a_c/a)|\tilde{r}_1(a)|^2 = 1$. The corresponding critical energy scale is defined through

$$E_{x,c} \approx v_F/a_c = v_F|\tilde{r}_1(a)|^2/a = {J_x}^2/(a v_F). \tag{3.44}$$

Comparing Eq. (3.44) to Eq. (3.30) we see that $E_{x,c}$ is equal to Γ_b up to a numerical factor. Further evaluation of Eq. (3.44) gives

$$E_{x,c} = 16|r_1|^2\gamma E_C a\cos^2(\pi N).$$

Similar considerations can be used in the more general case where $|r_1| \neq |r_2|$. Then we have to use e.g. the backscattering Hamiltonian Eq. (3.13) as a starting point. Expanding the partition function to the second order in this perturbation (the small parameters are $|R| = |r_1| + |r_2|$ and $|\delta r| = |r_2| - |r_1|$) we get

$$\delta Z = -\frac{{J_x}^2 + {J_y}^2}{(2\pi a)^2}\int_0^\beta d\tau_1 d\tau_2 \frac{a}{v_F|\tau_1-\tau_2|} \tag{3.45}$$

where the partition function is again independent of the lattice step a. Furthermore it is important to note that terms proportional to J_x and J_y do not mix in the expansion of the partition function up to second order.

For a small channel anisotropy, either the coupling J_x or J_y grows under renormalization which gives rise to two *independent* energy scales. The critical energy for which J_x (J_y) departs to strong coupling is $E_{x,c} = {J_x}^2/(v_F a) \propto$

$E_C|R|^2\cos^2(\pi N)$ ($E_{y,c} = {J_y}^2/(v_F a) \propto |\delta r|^2 E_C \sin^2(\pi N)$). Of course we have recovered here, up to a numerical factor the two energies $\Gamma_a(\propto E_{y,c})$ and $\Gamma_b(\propto E_{x,c})$ (see Eq. (3.30)). More generally, using Eq. (3.45) we find

$$\frac{d}{dl}\Big(|\tilde{R}(l)|^2 + |\tilde{\delta}r(l)|^2\Big) = \Big(|\tilde{R}(l)|^2 + |\tilde{\delta}r(l)|^2\Big)$$

where we defined $|\tilde{R}| = J_x/v_F$ and $|\tilde{\delta r}| = J_y/v_F$. In the case of a strong channel anisotropy, we deduce that the effective coupling ${J_x}^2 + {J_y}^2$ flows off to strong coupling at the critical energy $E_c = (E_{x,c} + E_{y,c})$. Again, we recover $E_c \propto \Gamma = \Gamma_b + \Gamma_a$. For a small anisotropy, of course this reduces to $E_c \propto \max\{\Gamma_a, \Gamma_b\}$.

3.6 Small transmission limit

Having so far concentrated on the limit where the quantum dot is strongly coupled to a reservoir through a highly transparent quantum point contact, we will in this section consider the limit of weak coupling. The similarity between the Coulomb blockade problem in this limit and a Kondo model was noticed by Glazman and Matveev [1]. An explicit mapping of the Coulomb blockade Hamiltonian on a Kondo model was used by Matveev to calculate the charge and the capacitance of the quantum dot in the weak transmission limit[2]. Recently a noncrossing approximation (NCA) has been generalized to this type of multichannel Kondo models [30].

We will here rederive Matveev's mapping and discuss the straight-forward extension of his model to the channel anisotropic case. Again our discussion will be restricted to the case of two transport channels through the point contact. The anisotropy between the transmission amplitudes for the two transport channels in the QPC will still give rise to a mapping on a channel-anisotropic Kondo model, but here, the system flows off to the usual *spin-isotropic* fixed point, i.e., $J_{\sigma,\perp} = J_{\sigma,z} \gg 0$. We will see below that the problem of calculating the average charge $\langle Q\rangle$ on the dot is now equivalent to the problem of finding the average of the z-component $\langle S_z\rangle$ of the impurity spin in the Kondo model. In addition the capacitance of the dot is the same as the magnetic susceptibility χ of the impurity. Once this equivalence is established, the problem is solved, since these quantities ($\langle S_z\rangle$, χ) can be found in the literature. The channel- and spin *isotropic* multichannel Kondo problem was solved exactly in this (weak coupling) limit in Refs. [31, 32], while the impurity-susceptibility for the *channel-anisotropic* (but spin-isotropic) two-channel Kondo problem can be simply extracted from Ref. [33]. Note in passing that the channel-anisotropic case was also solved (exactly) using the Bethe Ansatz in Ref. [34] .This model has also been investigated using conformal field theory and numerical renormalization-group calculations in Ref. [35].

We will now proceed to write down the model for our system in the small transmission limit. Instead of formulating it in momentum space as it was done

by Matveev we will here use a real space formulation which allows us to stress the analogy with the corresponding model in the strong transmission limit (see Sec. 3.2).

In the previous section we have treated the backscattering as a small perturbation to an otherwise perfectly transparent QPC. In this section the perturbation is a tunnelling Hamiltonian which couples two a priori independent systems (the 2DEG and the dot). A smooth transition can be made from the strongly to the weakly coupled limit by continuously increasing the auxiliary gate voltage to pinch off the QPC. In this transition a perfectly transmissive one-dimensional channel n will be cut into two weakly coupled halves. In the vicinity of the center of the QPC electron motion is still quasi one-dimensional. Electronic wave-functions to the left of the center of the QPC (in the reservoir) will be denoted $\Psi^n_{\sigma,0}$, wave-functions to the right of the center (in the QD) are $\Psi^n_{\sigma,1}$. Again σ is the spin index, n the channel index due to lateral confinement and here $\alpha = 0, 1$ indicates the location of the electron. Hopping between the two sides of the QPC constitutes a small perturbation. To model this perturbation we use the Hamiltonian

$$H_T = \sum_{\sigma=1,2} \left(|t_\sigma| \Psi^\dagger_{\sigma,1}(0) \Psi_{\sigma,0}(0) + h.c. \right). \tag{3.46}$$

Note that the kinetic energies $H^0_{kin}\left(\{\Psi^\dagger_{\sigma,0}, \Psi_{\sigma,0}\}\right)$ and $H^1_{kin}\left(\{\Psi^\dagger_{\sigma,1}, \Psi_{\sigma,1}\}\right)$ for electrons in the 2DEG and the dot have the form of Eq. (3.25). The boundaries for the integration along the x-axis are $-\infty, 0$ in H^0_{kin} and $0, \infty$ in H^1_{kin}. The Coulomb interaction can be modelled as in Sec. (3.2), Eq. (3.4). Here, however, it is more convenient to drop the constant (Q-independent) term ($E_C N^2$) from the total energy. This can be done since this operation does not change the charge dynamics. For the charge on the dot we use

$$Q = \int_0^\infty dx \left(\Psi^\dagger_{\sigma,1}(x) \Psi_{\sigma,1}(x) - \rho_0 \right).$$

The equilibrium charge density ρ_0 is chosen in such a way that the total charge Q on the dot is zero when no voltage is applied to the gate ($V_G = 0$).

We now want to concentrate on the point $N = 1/2$ where the states with $Q = 0$ and $Q = 1$ are energy degenerate (See Eq. (3.4)), and therefore charge fluctuations are large. We introduce the small parameter $U = e/(2C_{gd}) - V_G \propto N - 1/2$ to measure deviations of N from the degeneracy point. In terms of U the electrostatic energies of the two states $Q = 0$ and $Q = 1$ are $E_0 = 0$ and $E_1 = eU$ respectively.

If the two conditions $|U| \ll e/C_{gd}$ and $kT \ll E_C$ are met, only the two states with $Q = 0$ and $Q = 1$ are accessible and higher energy states can be removed from our theory introducing the projection operators P_0 and P_1. Here P_0 and P_1 are projecting on the states $Q = 0$ and $Q = 1$ respectively. The effective

Hamiltonian for this truncated system is

$$\begin{aligned} H_{eff} &= \left(H^0_{kin} + H^1_{kin}\right)(P_0 + P_1) + eUP_1 \\ &+ \sum_{\sigma=1,2} \left(|t_\sigma| \Psi^\dagger_{\sigma,1} \Psi_{\sigma,0} P_0 + |t_\sigma| \Psi^\dagger_{\sigma,0} \Psi_{\sigma,1} P_1 \right), \end{aligned} \tag{3.47}$$

where the operators in the tunnelling part are evaluated at $x = 0$ (see Eq. 3.46). From this equation we see that $\partial H/\partial U = eP_1$ and therefore $\langle Q \rangle = \partial E_0/\partial U$ where E_0 is the ground-state energy of the Hamiltonian Eq. (3.47). The first term in the tunneling Hamiltonian takes an electron from the 2DEG and transfers it to the QD. The projection operator P_0 makes sure that the charge on the dot is $Q = 0$ before the tunnelling takes place. The second term takes an electron from the dot to the lead. In our truncated system this process is allowed only when the charge on the dot is $Q = 1$. This restriction is implemented through the operator P_1. The main goal of the following manipulations will be to show the equivalence of the Hamiltonian Eq. (3.47) to a Kondo Hamiltonian.

To explicitly account for the charge on the dot we make the replacement $|\Phi\rangle \to |\Phi\rangle|Q\rangle$. Here $|\Phi\rangle$ is any state of our system with charge Q on the dot. The values of Q are limited to $Q = 0, 1$ and the states $|Q\rangle = |0\rangle$ and $|Q\rangle = |1\rangle$ can be considered as the basis of a two-dimensional vector space. However, the product $|\Phi\rangle|Q\rangle$ is no tensor product since the charge of the dot is of course not independent of the system's state. The state $|Q\rangle$ should rather be considered as an auxiliary label to $|\Phi\rangle$. In addition to introducing the label $|Q\rangle$ we make the replacement

$$\begin{aligned} \Psi^\dagger_{\sigma,1} \Psi_{\sigma,0} P_0 &\to \Psi^\dagger_{\sigma,1} \Psi_{\sigma,0} S^+, \\ \Psi^\dagger_{\sigma,0} \Psi_{\sigma,1} P_1 &\to \Psi^\dagger_{\sigma,0} \Psi_{\sigma,1} S^- \end{aligned}$$

in Eq. (3.47). Here S^+ and S^- are pseudo-spin ladder operators acting only on the charge part $|Q\rangle$.

Since $S^+|Q = 1\rangle = 0$ and $S^-|Q = 0\rangle = 0$ these operators ensure in the same way as the projection operators P_0 and P_1 that only transitions between states with $Q = 0$ and $Q = 1$ take place. In addition the charge Q on the dot is adjusted whenever a tunnelling process takes place since $S^+|0\rangle = |1\rangle$ and $S^-|1\rangle = |0\rangle$. We would like to emphasize again that only the combinations of pseudo-spin ladder operators and hopping operators introduced above are meaningful since $|Q\rangle$ and $|\Phi\rangle$ are not independent.

To get rid of the remaining projection operators in Eq. (3.47) we rewrite (eUP_1) as $[eU(P_0 + P_1)/2 + eU(P_1 - P_0)/2]$. We observe that

$$\begin{aligned} (P_1 \pm P_0)|0\rangle &= \pm|0\rangle, \\ (P_1 \pm P_0)|1\rangle &= +|1\rangle. \end{aligned}$$

This leads us to identify $(P_1 - P_0)$ with $2S_z$ and $(P_1 + P_0)$ with the identity operator on the space spanned by $|0\rangle$ and $|1\rangle$. Here we used that for the z-component S_z of the pseudo-spin we have $S_z|1\rangle = |1\rangle/2$ and $S_z|0\rangle = -|0\rangle/2$.

Gathering all terms we can rewrite the effective Hamiltonian Eq. (3.47) as

$$\begin{aligned} H_{eff} &= \left(H^0_{kin} + H^1_{kin}\right) + eU(2S_z+1)/2 \\ &+ \sum_{\sigma=1,2}\left(|t_\sigma|\Psi^\dagger_{\sigma,1}\Psi_{\sigma,0}S^+ + |t_\sigma|\Psi^\dagger_{\sigma,0}\Psi_{\sigma,1}S^-\right). \end{aligned} \tag{3.48}$$

We now introduce an additional pseudo-spin operator $s^\pm_\sigma(x)$ via

$$\begin{aligned} s^+_\sigma &= \Psi^\dagger_{\sigma,0}\Psi_{\sigma,1} \\ s^-_\sigma &= \Psi^\dagger_{\sigma,1}\Psi_{\sigma,0} \end{aligned} \tag{3.49}$$

where the matrices $\sigma^\pm = \sigma_x \pm i\sigma_y$ are standard combinations of Pauli matrices. It is important to note that these pseudo-spin operators again have nothing to do with the true spin of the electrons but are related to the location of an electron ($\alpha = 0$ for an electron in the 2DEG, $\alpha = 1$ for an electron in the QD). Introducing the definition of these pseudo-spins into Eq. (3.48) finally leads us to

$$\begin{aligned} H_K &= \sum_{\alpha=0,1} H^\alpha_{kin} + 2hS_z \\ &+ \frac{1}{2}\sum_{\sigma=1,2}\left(J_{\sigma,\perp}\left(s^+_\sigma(0)S^- + s^-_\sigma(0)S^+\right)\right) \end{aligned} \tag{3.50}$$

which has the form of a standard Kondo Hamiltonian. In Eq. (3.50) we have introduced the transversal Kondo coupling parameters $J_{\sigma,\perp} = 2|t_\sigma|$ and an effective external magnetic field $h = eU/2 \propto (N - 1/2)$ applied along the z axis. Note that Eq. (3.50) corresponds to the limit $J_{1,z} = J_{2,z} = 0$ of Eq. (3.2). We have dropped the constant $eU/2$ from the Hamiltonian in Eq. (3.50). Therefore the ground state energy $E_{K,0}$ of the Kondo Hamiltonian Eq. (3.50) is related to the ground state energy E_0 of the effective Hamiltonian Eq. (3.47) through $E_{K,0} + eU/2 = E_0$. Since $2\langle S_z\rangle = \partial E_{K,0}/\partial h$ and $\langle Q\rangle = \partial E_0/\partial U$ we are led to the obvious identification

$$\langle Q\rangle = e\left(\frac{1}{2} + \langle S_z\rangle\right).$$

Combining Eq. (3.6) with $U = e/(2C_{gd}) - V_G$ we find for the correction to the capacitance $C = -\partial\langle Q\rangle/\partial U \propto \chi = \partial\langle S_z\rangle/\partial h$, where χ is the impurity susceptibility (Since h only acts on S_z, χ is also equivalent to the local magnetic susceptibility χ_l).

Thus far, we have shown that a calculation of the capacitance of the quantum dot coupled to a 2DEG through a QPC with two transport channels with *different* transmission amplitudes is equivalent to a calculation of the impurity susceptibility in the channel-anisotropic two-channel Kondo model. It is known that both $J_{\sigma,z} = 0$ and $J_{\sigma,\perp} \ll 1$ grow under renormalization and that for small enough energies $J_{\sigma,z} = J_{\sigma,\perp} = J_\sigma \propto |t_\sigma|$ even if we start from a spin-anisotropic Kondo

model. The resulting spin-isotropic Kondo model was solved in Refs. [31, 32]. In the zero temperature limit the impurity susceptibilities for the one-channel case and the two-channel isotropic limit are

$$\chi \propto \begin{cases} cst. & J_2 = 0, \\ \log h & J_1 = J_2. \end{cases} \tag{3.51}$$

Note that the susceptibility for the two-channel case diverges in the zero magnetic field limit. The channel-anisotropic (but spin-isotropic) Kondo model was discussed by Coleman and Schofield[33] (and also by Andrei and Jerez[34] and by Affleck *et al.*[35]) who found for the susceptibility at zero magnetic field ($h = 0$)

$$\chi \propto 1 - \frac{\log(\nu)}{\nu - 1}, \tag{3.52}$$

where the anisotropy parameter $\nu \propto |\delta t|/\mathcal{T}$ with $|\delta t| \propto |J_1 - J_2|$ and $\mathcal{T} \propto (J_1 + J_2)$, is $\nu = 1$ in the one-channel limit ($J_2 = 0$) and $\nu = 0$ in the two-channel isotropic limit. Eq. (3.52) thus reproduces correctly the main characteristics of the result Eq. (3.51) in these two limiting situations. From the results for the susceptibility we immediately obtain the capacitance

$$\delta C \propto \begin{cases} cst. & J_2 = 0, \\ \log(N - 1/2) & J_1 = J_2, \\ \log|\delta t| & J_1 \neq J_2, N = 1/2. \end{cases} \tag{3.53}$$

The results for the one-channel and the two channel isotropic cases are due to Matveev[3]. The main observation we want to make here is that a small channel anisotropy cuts off the logarithmic divergence exactly in the same way as in the case discussed in the previous sections where the reflection amplitudes in the QPC could be treated as small parameters.

3.7 Conclusions

We have applied the channel- (and spin-) anisotropic two-channel Kondo model to study Coulomb blockade oscillations in the capacitance of a quantum dot. Our main interest has been to investigate the effect of an asymmetry between the reflection or transmission amplitudes of two different open channels in the QPC connecting the dot to a reservoir. Following Matveev[2, 3] we have studied the two exactly soluble limits of very weak ($|t_1|, |t_2| \ll 1$) and very strong coupling ($|r_1|, |r_2| \ll 1$). In both limits a mapping of the original problem onto a Kondo model is possible at low temperature. As temperature is increased, the Kondo physics eventually is wiped out by thermal fluctuations [3, 13, 21]. A summary of the results for the capacitance in different limits is given in Table 1.

For weak backscattering at the point contact ($|r_1|, |r_2| \ll 1$) the original problem can be mapped (see Sec. 3.3 and Ref. [14]) on a channel-anisotropic Kondo

model at the Emery-Kivelson[11] line ($J_{1,z} = J_{2,z} = 2\pi v_F$). For this particular value of the coupling constant the Kondo model is exactly solvable. The anisotropy of the reflection amplitudes for different channels is directly reflected in the channel-anisotropy of the Kondo model. In fact we found $J_{1,\perp} \propto |r_1|$ and $J_{2,\perp} \propto |r_2|$, where $J_{1,\perp}$ and $J_{2,\perp}$ are the coupling constants for the two channels in the Kondo model. The mapping allowed us to calculate the shift of the ground-state energy of our Hamiltonian due to the backscattering at the point contact and in turn to find the capacitance of the quantum dot. While the capacitance is logarithmically divergent for values of the gate voltage close to $N = n + 1/2$ (n is an integer) in the isotropic limit[3] ($|r_1| = |r_2|$), this divergence is cut off by a small anisotropy between the reflection amplitudes of different channels[14]. This can be interpreted as a manifestation of the restoration of the Fermi-liquid behavior close to the degeneracy points $N = n + 1/2$ due to the asymmetry between channels.

There are two intrinsic energy scales ($\Gamma_b \propto (|r_1|+|r_2|)^2$ and $\Gamma_a \propto (|r_1|-|r_2|)^2$) in the channel-anisotropic Kondo model. Each can be interpreted as the resonance energy related to coupling half an impurity to the conduction electrons. In the channel-isotropic case only half the impurity spin is screened by the conduction electrons. Coupling back the second half of the impurity to the conduction electrons leads to the emergence of a second energy scale Γ_a. It is this new energy scale that enters the expression for the capacitance and cuts off the divergence at $N = n + 1/2$. Unfortunately there is no direct correspondence between the magnetic susceptibility in the Kondo model and the capacitance of the quantum dot. Such an equivalence exists only in the limit of small transmission. It is true however that the behavior of the capacitance (found from the Kondo model at the Emery-Kivelson line) is reminiscent of the impurity susceptibility $\chi = \partial^2(\delta\epsilon)/\partial h^2$ away from the Emery-Kivelson line or of the local magnetic susceptibility $\chi_l = \partial\langle\hat{S}_z\rangle/\partial h$ at the Emery-Kivelson line.

Nbr of channels	barrier	δC at N=1/2	Ref.
1	$\|r_1\| \ll 1$, ($\|r_2\| \to 1$)	*const.*	[3]
2	$\|r_1\| = \|r_2\| \ll 1$	$-\ln\|N - 1/2\|$	[3]
2	$\|r_1\| \neq \|r_2\| \ll 1$	$-\ln(\|r_2\| - \|r_1\|)$	[14], Secs. 3.3-3.5
1	$\|t_1\| \ll 1$, ($\|t_2\| \to 0$)	*const.*	[2]
2	$\|t_1\| = \|t_2\| \ll 1$	$-\ln\|N - 1/2\|$	[2]
2	$\|t_1\| \neq \|t_2\| \ll 1$	$-\ln(\|t_1\| - \|t_2\|)$	Sec. 3.6

Table 1: We have here listed all the results for the capacitance of the quantum dot at $N \to 1/2$ and the respective references. The divergence occurring at $N \to 1/2$ in the channel-isotropic *two*-channel limit is cut off by a channel anisotropy for both weak and strong reflection at the QPC.

We have here extended previous work by Le Hur[14] deriving the mapping on the anisotropic Kondo model in a pedagogical way and carefully discussing its limits of validity. We have then given an alternative way for calculating the charge on

the quantum dot using a mapping[16] on a channel-isotropic two-channel Kondo model. In this approach the coupling constant is a complex parameter depending on both $|r_1|$ and $|r_2|$. While the latter approach has the advantage of being exact, it seems less intuitive since the anisotropy of the reflection coefficients is not directly reflected as an anisotropy between coupling parameters in the Kondo model. We have in addition used a simple scaling argument to recover the intrinsic energy scales Γ_a and Γ_b that occur in the expression of the capacitance.

From the experimental point of view, [4] it is interesting that the magnetic field dependent channel anisotropy gives rise to a controllable cut-off of the divergence of the capacitance at $N = n+1/2$. Of course, in an experiment a true divergence is never observed since it is already cut off by temperature, but by using the magnetic field as a controllable cut-off it may become possible to further test the theory of Ref. [3].

We relied on purely mathematical arguments to show the equivalence between the Coulomb blockade problem and the Kondo Hamiltonian in the strong tunnelling limit ($|r_1|, |r_2| \ll 1$). In the opposite limit $|t_1|, |t_2| \ll 1$ the similarity of these two problems can be understood using a comparably simple physical argument (see Ref.[3] and Sec. 3.6). The main observation is that at low enough temperatures $T \ll E_C$ and for voltages close to $N = n + 1/2$ only two charge states on the quantum dot are energetically accessible (e.g. $Q = 0$, $Q = 1$). The charge state of the dot is then interpreted as a pseudo-spin-1/2 degree of freedom which corresponds to the impurity spin in the Kondo model. The real spin of the conduction electrons in the Kondo model is replaced by an index α indicating the location of an electron (distinguishing between electrons to the left and to the right of the QPC) in the Coulomb blockade problem.

A first order process in the Kondo problem that flips the impurity spin from up to down and the spin of a conduction electron from down to up is then equivalent to a tunnelling process that takes an electron from the left to the right and changes the charge on the dot from $Q = 0$ to $Q = 1$. The Kondo coupling parameters simply are $J_{1(2),\perp} \propto |t_{1(2)}|$ and $J_{1(2),z} = 0$. As it is clear from the derivation of the mapping there exists an equivalence between the charge on the dot and the impurity spin, namely $\langle Q \rangle \propto \langle S_z \rangle$. It was furthermore shown that the capacitance is basically the same (up to some constant) as the impurity susceptibility. Since the model with $J_{1(2),\perp} \propto |t_{1(2)}|$ and $J_{1(2),z} = 0$ flows to the usual spin-isotropic fixed point we have been able to use the known result for the impurity susceptibility in the channel-anisotropic two-channel Kondo model with $J_{\sigma,\perp} = J_{\sigma,z} \gg 0$[33], to discuss the effect of channel-anisotropy on the capacitance. Exactly as in the limit of strong transmission the capacitance diverges in the channel-isotropic case[2], but the divergence is cut by the anisotropy. Note that no immediate connection can be made with the Kondo model at the Emery-Kivelson line ($J_{1(2),z} = 2\pi v_F$) which we obtained when treating the small reflection limit.

All the results on the behavior of the capacitance of the dot close to $N = 1/2$ are summarized in Table 1.

3.8 Bibliography

[1] L. I. Glazman and K. A. Matveev, Zh. Eksp. Teor. Fiz. **98**, 1834 (1990) [Sov. Phys. JETP **71**, 1031, (1990)].

[2] K. A. Matveev, Zh. Eksp. Teor. Fiz. **98**, 1598 (1990) [Sov. Phys. JETP **72**, 892, (1991)].

[3] K. A. Matveev, Phys. Rev. B **51**, 1743 (1995).

[4] D. Berman, N. B. Zhitenev, R. C. Ashoori, and M. Shayegan, Phys. Rev. Lett. **82**, 161 (1999).

[5] For a short review see L. Kouwenhoven and L. Glazman, Phys. World **14**, 33, (2001).

[6] D. Goldhaber-Gordon, H. Shtrikman, D. Mahalu, D. Abusch-Magder, U. Meirav, M. A. Kastner, Nature, **391**, 156, (1998); D. Goldhaber-Gordon, J. Göres, M. A. Kastner, H. Shtrikman, D. Mahalu, and U. Meirav, Phys. Rev. Lett. **81**, 5225 (1998).

[7] S. M. Cronenwett, T. H. Oosterkamp, and L. P. Kouwenhoven, Science, **281**, 540, (2001).

[8] For a review, see D. L. Cox and A. Zawadowski, Adv. Phys. **47**, 599 (1998).

[9] Ph. Nozières and A. Blandin, J. Physique **41**, 193, (1980).

[10] K. Flensberg, Phys. Rev. B **48**, 11 156 (1993).

[11] V. J. Emery and S. Kivelson, Phys. Rev. B **46**, 10 812 (1992); D. G. Clarke, T. Giamarchi, and B. I. Shraiman, *ibid.* **48**, 7070 (1993); A. M. Sengupta and A. Georges, *ibid.* **49**, 10 020 (1994).

[12] N. C. van der Vaart *et al.*, Phys. B **189**, 99 (1993).

[13] I. L. Aleiner, P. W. Brouwer, and L. I. Glazman, cond-mat/0103008.

[14] K. Le Hur, Phys. Rev. B **64**, 161302(R) (2001).

[15] M. Fabrizio, A. O. Gogolin, and Ph. Nozières, Phys. Rev. B **51**,16088 (1995).

[16] A. Furusaki and K. A. Matveev, Phys. Rev. B **52**, 16676 (1995).

[17] M. Büttiker, Phys. Rev. B **41**, R7906 (1990).

[18] L. I. Glazman, G. B. Lesovik, D. E. Khmel'nitskii, and R. I. Shekter, Pis'ma Zh. Eksp. Teor. Fiz. **48**, 218 (1988) [JETP Lett. **48**, 239 (1988)].

[19] F. D. M. Haldane, J. Phys. C **14**, 2585 (1981).

[20] M. P. A. Fisher and L. I. Glazman, in *Mesoscopic Electron Transport*, edited by L. Kouwenhoven, G. Schoen and L. Sohn, NATO ASI Series E, Kluwer Ac. Publ., Dordrecht; also cond-mat/9610037.

[21] I. L. Aleiner and L. I. Glazman, Phys. Rev. B **57**, 9608 (1998).

[22] M. Büttiker, H. Thomas, and A. Prêtre, Phys. Lett. A **180**, 364 (1993).

[23] V. A. Gopar, P. A. Mello, and M. Büttiker, Phys. Rev. Lett. **77**, 3005 (1996).

[24] A. O. Gogolin, A. A. Nersesyan, and A. M. Tsvelik, *Bosonization and Strongly Correlated Systems*, Cambridge University Press, (1998).

[25] For $\omega \ll \Gamma_k$, the impurity density of states become frequency-independent i.e. $n_k(\omega) = 1/\Gamma_k$: This explains why the frequencies smaller than $\omega_{min} = Max(\Gamma_b, \Gamma_a)$ donot contribute to the (main) logarithmic part of $\delta\epsilon$.

[26] Ph. Nozières, J. Low Temp. Phys. **17**, 31 (1974).

[27] Yu. V. Nazarov, Phys. Rev. Lett. **82**, 1245 (1999).

[28] C. L. Kane and M. P. A. Fisher, Phys. Rev. B **46**, 15 233 (1992).

[29] $N = 1/2$ is generally the condition for resonant tunneling through a double-barrier structure: A. Furusaki and N. Nagaosa, Phys. Rev. B **47**, 3827 (1993).

[30] E. Lebanon, A. Schiller, and V. Zevin, cond-mat/0110335.

[31] A. M. Tsvelik and P. B. Wiegmann, Z. Phys. B **54**, 201 (1984).

[32] N. Andrei and C. Destri, Phys. Rev. Lett. **52**, 364 (1984).

[33] P. Coleman and A. J. Schofield, Phys. Rev. Lett. **75**, 2184 (1995); For more details on the method, see: P. Coleman, L. B. Ioffe, and A. M. Tsvelik, Phys. Rev. B **52**, 6611 (1995).

[34] N. Andrei and A. Jerez, Phys. Rev. Lett. **74**, 4507 (1994).

[35] I. Affleck, A. W. W. Ludwig, H. B. Pang, and D. L. Cox, Phys. Rev. B **45**, 7918 (1992).

[36] L. I. Glazman, F. W. J. Hekking, and A. I. Larkin, Phys. Rev. Lett. **83**, 1830 (1999).

Part III

Electron-phonon interactions

CHAPTER 4

Electron-phonon scattering in quantum point contacts

4.1 Introduction

In this final chapter we leave the field of electron-electron interactions and turn to the investigation of electron-phonon interactions in a quantum point contact. We will show in the following that electron-phonon interactions lead to interesting deviations from the free electron model of transport through a QPC.

The quantization of conductance in units of $G_0 = 2e^2/h$ observed [1] in narrow one-dimensional constrictions—the quantum point contacts (QPC)—is well understood within a simple model of non-interacting electrons [2]. In this approach the electrons are backscattered by the effective one-dimensional potential created by the walls of the constriction, and the conductance follows the energy dependence of the transmission coefficient. In the last few years a number of experiments [3, 4, 5, 6, 7, 8] studied the deviations of the conductance from this picture that appear as a shoulder-like feature at a conductance near $0.7\,G_0$. Several experiments have demonstrated that when a strong in-plane magnetic field is applied, this 0.7 anomaly evolves into the spin-polarized conductance plateau at $0.5\,G_0$ [3, 4, 5]. This observation led to the proposal that the anomaly originated from a spin-dependent mechanism [3]. Subsequent theoretical attempts to understand the 0.7 anomaly mostly followed this conjecture [9, 10, 11, 12, 13, 14, 15, 16, 17].

Here we concentrate on another feature of the 0.7 anomaly, namely its strong temperature dependence. The experiments [3, 5, 6] showed that the anomalous shoulder is weak at the lowest available temperatures, but grows when the temperature is increased. A detailed study [6] revealed that the correction to the

conductance follows an Arrhenius law

$$\delta G \propto e^{-T_A/T} \tag{4.1}$$

with the activation temperature T_A of the order of one Kelvin. The activated temperature dependence implies that a certain backscattering mechanism turns on at temperature $T \approx T_A$ and leads to partial suppression of the conductance. The phenomenological proposals for this mechanism include scattering off a plasmon [18] or a spin wave [16] localized in the QPC, a low-lying spin-split subband [12], as well as spin-flip scattering by a Kondo impurity [5, 17].

In this paper we explore another backscattering mechanism, which results in the activated temperature dependence (4.1), namely the scattering of electrons by acoustic phonons. Electron-phonon scattering rates [19, 20] and phonon-scattering induced corrections to the conductance [21] were previously calculated for long, one-dimensional wires with several transport channels and at relatively high temperatures. Scattering of electrons from non-equilibrium phonons has also been investigated theoretically [22] and experimentally [23]. Finally, electron-phonon interactions in quantum point contacts were discussed in the case of scattering by surface acoustic waves [24, 25, 26].

4.2 Differential conductance

4.2.1 Low temperature limit

At low temperatures the effect of electron-phonon scattering on transport in quantum wires is strongly suppressed. Indeed, in order to backscatter an electron at the Fermi level the phonon must have a wavevector $q = 2k_F$ in the direction along the wire. Thus the minimum energy of such a phonon is

$$T_A = 2\hbar s k_F = \sqrt{E_s E_F} \tag{4.2}$$

where s is the speed of sound, E_F is the Fermi energy of electrons in the wire, $E_s = 8ms^2$, and m is the effective mass of electrons. At temperatures $T \ll T_A$ the occupation numbers of such phonons and their contribution to the conductance are exponentially suppressed, Eq. (4.1). For typical GaAs quantum wires one can estimate $E_s \approx 0.3$K and $E_F \sim 100$K, resulting in $T_A \sim 5$K. Thus the electron-phonon scattering is negligible in typical low-temperature experiments. On the other hand, the electron density in a QPC tuned into the vicinity of the first conductance step is very low. Estimating the Fermi energy at the center of a QPC to be about 2K, one obtains a value of $T_A \approx 0.8$K, in reasonable agreement with experiment [6].

To study transport in a QPC near a conductance step as a function of the gate voltage, one has to account for the effect of the confining potential. We follow the idea of Refs. [2, 27] and model the QPC by a one-dimensional electron gas

in an external potential approximated as $U(x) = -\frac{1}{2}m\Omega^2 x^2$. This approximation is valid in the vicinity of the conductance step, provided that the potential is sufficiently smooth. The transmission coefficient of such a barrier is well known [28],

$$T_0(E) = \frac{1}{1 + e^{-2\pi E/\hbar\Omega}}. \tag{4.3}$$

In this paper we concentrate on the case when the Fermi energy is well above the top of the barrier, $E_F \gg \hbar\Omega/2\pi$. In this regime the transmission coefficient (4.3) at the Fermi level equals unity up to an exponentially small correction, and even a weak backscattering by acoustic phonons gives a significant correction (4.1) to the quantized conductance G_0.

The amplitude of electron backscattering by a phonon with wavevector q_x is proportional to the matrix element

$$I(q_x) = \langle \psi_R | e^{iq_x x} | \psi_L \rangle, \tag{4.4}$$

where $\psi_{R,L}(x)$ are the wavefunctions of the right- and left-moving electrons. Due to the fact that the speed of sound is small, the typical phonon energy $\hbar sq$ is much smaller than $\hbar\Omega$. Therefore, in evaluating the matrix element (4.4), the right- and left-moving electrons can be assumed to have the same energy E_F. At $E_F \gg \hbar\Omega$ the calculation of the matrix element (4.4) can be further simplified by using semiclassical expressions for the wavefunctions:

$$\psi_{R,L}(x) = \sqrt{\frac{m}{2\pi\hbar p_F(x)}}\, \exp\left[\pm\frac{i}{\hbar}\int_0^x dx' p_F(x')\right]. \tag{4.5}$$

Here the quasiclassical Fermi momentum is defined as $p_F(x) = \sqrt{2m[E_F - U(x)]}$.

We begin by studying the regime of small temperature and bias, $T, eV \ll T_A$, when the dominant contribution to δG is due to long-wavelength phonons, $q_x \ll 2k_F$. (Here $k_F = \sqrt{2mE_F}/\hbar$ is the electron wavevector at the center of the QPC.) In this regime the integral (4.4) is easily evaluated by the saddle point method, and we find

$$\begin{aligned} I(q_x) &= \left(\frac{k_F^2}{2\pi\hbar\Omega E_F q_x \sqrt{4k_F^2 - q_x^2}}\right)^{1/2} e^{-F_1(q_x/2k_F)}, \\ F_1(u) &= \frac{2E_F}{\hbar\Omega}\left(\arccos u - u\sqrt{1-u^2}\right). \end{aligned} \tag{4.6}$$

Since E_F is assumed to be large compared to $\hbar\Omega$, this result is valid even when q_x approaches $2k_F$, as long as $F_1 \gg 1$.

At zero temperature only the processes of emission of phonons are allowed. The energy of the phonon cannot exceed applied voltage, and thus the maximum possible q_x in such a process is $eV/\hbar s$. Therefore, at $eV < T_A$ the correction to the differential conductance is exponentially small as $\delta G \propto \exp[-2F_1(eV/T_A)]$.

At non-zero temperature, both emission and absorption of phonons are possible. In the most interesting limit of zero bias, both processes are exponentially suppressed at $T \ll \hbar sq$. Thus the total backscattering rate is small as $\exp[-2F_1(q_x/2k_F) - \hbar s q_x/T]$. One can easily see that this rate assumes its maximum value at $q_x = 2k_F\sqrt{1-(\hbar\Omega T_A/8E_F T)^2}$. Thus, the temperature dependence of the correction to the quantized conductance has the following exponential behavior:

$$\delta G = -G^* \exp\left[-\frac{T_A}{2T}\left(\frac{\arcsin v}{v} + \sqrt{1-v^2}\right)\right], \tag{4.7}$$

where $v = \hbar\Omega T_A/8E_F T$. In a broad range of temperatures $\frac{\hbar\Omega}{E_F}T_A \ll T \ll T_A$ this correction shows activated behavior (4.1). The deviation from the Arrhenius law (4.1) at low T is due to the presence of the potential barrier $-\frac{1}{2}m\Omega^2 x^2$ for the one-dimensional electrons in the QPC.

4.2.2 General results

In order to find the preexponential factor G^* in Eq. (4.7) and to evaluate δG in the regime when either temperature or voltage exceed T_A, one has to perform a more formal calculation of the electron backscattering rate.

We start from the standard Hamiltonian for the interaction between electrons and acoustic phonons [29]

$$H_{ep} = \sum_{\mathbf{q},\lambda}\left(\frac{\hbar}{2\rho\omega_{\mathbf{q}\lambda}}\right)^{1/2} \bar{M}_\lambda(\mathbf{q})\hat{\rho}(q_x)\left(a_{\mathbf{q}\lambda} + a^\dagger_{-\mathbf{q}\lambda}\right).$$

Here λ labels the three possible polarizations of the acoustic phonons, $\omega_{\mathbf{q}\lambda} \propto q$ is the phonon frequency, ρ is the mass density of the material and $\hat{\rho}(q_x)$ is the Fourier transform of the density of the one-dimensional electrons. The operators $a_{\mathbf{q}\lambda}$ and $a^\dagger_{-\mathbf{q}\lambda}$ respectively annihilate a phonon with polarization λ and wavevector $\mathbf{q}$ and create a phonon with polarization λ and wavevector $-\mathbf{q}$. The coupling function

$$\bar{M}_\lambda(\mathbf{q}) = D|\mathbf{q}| + iM_\lambda(\mathbf{q})$$

is the sum of deformation potential $D|\mathbf{q}|$ and the piezoelectric coupling $iM_\lambda(\mathbf{q})$. At relatively high temperatures (see Refs. [30, 31] for experiments on a two-dimensional electron gas) the deformation potential coupling dominates, and $M_\lambda(\mathbf{q}) \propto q$. However, at low temperatures in GaAs the leading contribution is due to piezoelectric coupling, for which $M_\lambda(\mathbf{q})$ depends on the direction of $\mathbf{q}$, but not on its length q. Here we will thus concentrate exclusively on the piezoelectric coupling. We assume that the phonon modes in the GaAs/AlGaAs heterostructure are similar to those in a three-dimensional GaAs crystal. The main justification for this assumption is the reasonably good agreement between experiments [30, 31] and theory [32, 33, 34] (based on this assumption) for the electron-phonon scattering rates in a two-dimensional electron gas. For a crystal

with the zinc-blende structure the piezoelectric couplings $|M_l|^2$ for longitudinal and $|M_t|^2$ for transversal couplings, respectively, are

$$\begin{aligned} |M_l|^2 &= 36\eta_x^2\eta_y^2\eta_y^2, \\ 2|M_t|^2 + |M_l|^2 &= 4\left(\eta_x^2\eta_y^2 + \eta_y^2\eta_z^2 + \eta_z^2\eta_x^2\right). \end{aligned} \tag{4.8}$$

Here η_i is the direction cosine with regard to the three crystal axes $\mathbf{e}_i$ ($\mathbf{e}_x = (1,0,0)$ etc.).

Using the golden rule approach, one can find the following expression for the scattering rate of a right-moving electron of energy E to all the available left-moving states:

$$\begin{aligned} \tau_R^{-1}(E) &= 2\pi \sum_\lambda \int \frac{d\mathbf{q}}{(2\pi)^3} \frac{|M_\lambda(\mathbf{q})|^2}{2\rho\omega_{\mathbf{q}\lambda}} \int dE' |I(q_x)|^2 \\ &\quad \times [1 - f_L(E')]\{N(\omega_{\mathbf{q}\lambda})\delta(E - E' + \hbar\omega_{\mathbf{q}\lambda}) \\ &\quad + [N(\omega_{\mathbf{q}\lambda}) + 1]\delta(E - E' - \hbar\omega_{\mathbf{q}\lambda})\}, \end{aligned} \tag{4.9}$$

where $f_L(E')$ is the Fermi function of the left-moving electrons in the contact, $N(\omega_{\mathbf{q}\lambda})$ is the equilibrium occupation number of a phonon of wavevector $\mathbf{q}$ and polarization λ.

The backscattering of electrons by phonons reduces the total current carried by the right-moving electrons of energy E in the contact. One can therefore find the correction to the total current $I = G_0 V$ by integrating the backscattering rate (4.9) with the occupation numbers of the respective states:

$$\delta I = -2e \int_{-\infty}^{\infty} [\tau_R^{-1}(E) f_R(E) - \tau_L^{-1}(E) f_L(E)] dE. \tag{4.10}$$

Here the factor of 2 accounts for the electron spins; the expression for the scattering rate τ_L^{-1} of left-moving electrons is obtained from Eq. (4.9) by replacing the subscripts $R \leftrightarrow L$.

The correction δI depends on the voltage V across the contact through the difference of the chemical potentials $\mu_R - \mu_L = eV$ entering the Fermi functions $f_R(E)$ and $f_L(E)$. Thus, the correction to the conductance G_0 of the contact can be found as $\delta G = d\delta I/dV$. The resulting expression for δG is simplified greatly if one makes the following approximations. First, we again neglect the dependence of the matrix element (4.4) on the energies E and E', and assume $E = E' = E_F$. Second, following the standard procedure [35], we replace $|M_\lambda(\mathbf{q})|^2$ (cf. Eq. 4.8) and the sound velocities with their values $|M_\lambda|^2$ and s_λ averaged over the directions of $\mathbf{q}$.

Averaging the direction dependent couplings Eq. 4.8 over all three dimensions is in fact a rather crude approximation in the case of a quantum point contact. Instead, it would be better to average only over directions perpendicular

to the quantum point contact. Starting from Eq. 4.8 this can be easily done (see Refs. [32, 34] for a similar analysis for a 2DEG), but the resulting couplings are functions of both the momentum component q_x along the QPC, and the absolute value $|\mathbf{q}_\perp|$ of the momentum perpendicular to the direction of the QPC. This makes it very difficult to obtain any analytical results for the scattering rate. Still, it can be shown that the assumption of a constant coupling holds in the limit $eV, T \ll T_A$. In the opposite limit the assumption of constant coupling probably leads us to overestimate the prefactor in Eq. (4.7) (at least if the QPC is along one of the main crystal axes) but of course leaves intact everything we said about the activated behavior.

Within the approximation of constant coupling the integrals with respect to the energies E and E' as well as the transverse components of $\mathbf{q}$ can be done analytically, and we find

$$\delta G = -G_0 T \sum_\lambda \frac{|M_\lambda|^2}{2\rho s_\lambda^2} \int_{-\infty}^{\infty} dq_x |I(q_x)|^2 K_\lambda(q_x). \tag{4.11}$$

Here the function $K_\lambda(q_x)$ is given by

$$\begin{aligned} K_\lambda(q_x) &= 2\ln\frac{1}{1-e^{-\hbar s_\lambda|q_x|/T}} - \frac{\hbar s_\lambda|q_x|}{T} \\ &\quad + \frac{eV-\hbar s_\lambda|q_x|}{2T}\coth\frac{eV-\hbar s_\lambda|q_x|}{2T} \\ &\quad + \frac{eV+\hbar s_\lambda|q_x|}{2T}\coth\frac{eV+\hbar s_\lambda|q_x|}{2T}. \end{aligned}$$

Unlike our previous results, the expression (4.11) for the correction δG is not limited to the regime $T, eV \ll T_A$. In addition, when the temperature and voltage are small compared to T_A, Eq. (4.11) enables one to find the preexponential factors, such as G^* in Eq. (4.7).

To find G^*, we first notice that at $T \ll T_A$ the longitudinal phonon mode can be ignored. Indeed, the sound velocity s_t of the transverse modes is lower than that of the longitudinal mode, $s_t < s_l$. Accordingly, the activation temperature (4.2) is lower for the transverse modes, i.e., the longitudinal mode gives a negligible contribution to δG at low temperatures. We will therefore assume $s = s_t$ in the definition (4.2) of the activation temperature.

At zero bias and $T \ll \hbar s_t|q_x|$, we find $K(q_x) = (2\hbar s_t|q_x|/T)e^{-\hbar s_t|q_x|/T}$. The integral in Eq. (4.11) can then be evaluated by the saddle-point method. As a result we reproduce the exponential temperature dependence (4.7) with the prefactor

$$G^* = \gamma G_0 \sqrt{\frac{2T}{\pi T_A}} \frac{1}{\sqrt[4]{1-v^2}}, \quad \gamma = \frac{2|M_t|^2}{\rho s_t}\frac{m}{\hbar^2\Omega}. \tag{4.12}$$

The dimensionless parameter γ determines the magnitude of the phonon backscattering effect on conductance at $T = T_A$. The numerical value of γ can be estimated from the data available in the literature [35]. We write the coupling

parameter for the transverse phonons as $|M_t|^2 = \frac{8}{35}(ee_{14}/\epsilon)^2$, where for GaAs the permittivity $\epsilon = 13.2\,\epsilon_0$, and $e_{14} = 0.16$ C/m^2. Substituting $\rho = 5.36\,\mathrm{g/cm^3}$, $s = s_t = 3 \times 10^3\,\mathrm{m/s}$, and $m = 0.067\,m_e$, we find $\gamma = 0.0052\,\mathrm{meV}/\hbar\Omega$.

We now turn to the evaluation of the correction (4.11) to the conductance of the QPC in the regime when the temperature and/or bias are large compared to $T_A = 2\hbar s_t k_F$. In this case the typical wavevector q of the phonons emitted or absorbed by electrons is large, $q \gg k_F$. To find δG we notice that the matrix element $I(q_x)$ has a peak near $q_x = 2k_F \ll q$. Thus, the electron backscattering in this regime is dominated by phonons propagating in the direction normal to the channel. One can then substitute the asymptotic expression for K_λ at $q_x \to 0$ into Eq. (4.11) and find δG in the form

$$\delta G = -\tilde{\gamma} G_0 \left(\frac{T}{T_A} \ln \frac{T}{T_A} + \frac{eV}{2T_A} \coth \frac{eV}{2T} \right). \tag{4.13}$$

Here the dimensionless parameter $\tilde{\gamma}$ is defined as

$$\tilde{\gamma} = \sum_\lambda \frac{|M_\lambda|^2 s_t}{\rho s_\lambda^2} \frac{m}{\hbar^2 \Omega}. \tag{4.14}$$

Due to the contribution of the longitudinal phonon mode, $\tilde{\gamma} > \gamma$. To estimate $\tilde{\gamma}$ we write the average matrix element as $|M_l|^2 = \frac{12}{35}(ee_{14}/\epsilon)^2$, Ref. [35]. Then using the value $s_l = 5.12 \times 10^3$ m/s of the velocity of longitudinal sound in GaAs, we find $\tilde{\gamma} = 0.0065\,\mathrm{meV}/\hbar\Omega$.

It is interesting to note that the negative correction (4.13) to the quantized conductance G_0 grows not only with temperature, but also with bias. When V is increased, more left-going states become available for the right-moving electrons to scatter into, and the conductance decreases. Thus, the electron-phonon scattering gives rise to a zero bias anomaly similar to the one observed in experiments [5, 6]. The linear shape of the zero-bias peak at $eV \gg T$ is consistent with the one observed in Ref. [5]. The height of the peak is determined by the limits of applicability of Eq. (4.13) at high bias. The most important limitation of our derivation was the assumption that the electrons are purely one-dimensional. At sufficiently high bias the typical wavevector $q \sim eV/\hbar s$ of the phonons becomes comparable to the width w of the one-dimensional channel. Since the backscattering is mostly due to the phonons propagating in the transverse direction, their coupling to the electrons at $q > 1/w$ becomes weak, and the linear dependence $\delta G(V)$ given by Eq. (4.13) saturates. This saturation occurs at $eV \sim T_A\sqrt{\Delta/E_F}$, where $\Delta \sim \hbar^2/mw^2$ is the subband spacing in the QPC. Thus the height of the zero-bias peak in conductance is expected to be of the order $\tilde{\gamma} G_0 \sqrt{\Delta/E_F}$.

The zero-bias peak observed in experiment [5] had a height of about $0.15\,G_0$. To compare this result with our estimate $\tilde{\gamma} G_0 \sqrt{\Delta/E_F}$, we use the device parameters $\hbar\Omega \approx 0.3\,\mathrm{meV}$ and $\Delta \approx 0.9\,\mathrm{meV}$ reported for similar samples [36]. To estimate E_F we assume the transmission coefficient $T_0(E_F) \approx 0.9$ and from Eq. (4.3) find $E_F \approx \frac{1}{3}\hbar\Omega$. This results in the peak height $\tilde{\gamma} G_0 \sqrt{\Delta/E_F} \approx 0.07\,G_0$, which is reasonably close to the experimentally observed value $0.15\,G_0$.

Unlike the bias dependence of δG, the temperature dependence

$$\delta G = -\tilde{\gamma} G_0 (T/T_A) \ln(T/T_A)$$

obtained from Eq. (4.13) at $V = 0$ does not saturate at $T \sim T_A\sqrt{\Delta/E_F}$. The suppression of coupling to phonons with $q > 1/w$ does cut off the factor $\ln(T/T_A)$. However, the main linear in T dependence of δG originates from the phonon occupation numbers $N(\omega_q) = T/\hbar\omega_q$ at $T \gg \hbar\omega_q$, and remains even at $T \gg T_A\sqrt{\Delta/E_F}$ [1]. The experiment [5] does show a stronger suppression of conductance $\delta G \sim -0.3\, G_0$ at high temperature than $\delta G \sim -0.15\, G_0$ at high bias. It is also worth noting that a device with a higher value of $\hbar\Omega = 2.6\,\mathrm{meV}$ and, consequently, lower $\tilde{\gamma}$ shows a weaker temperature dependence of δG, Ref. [38].

4.3 Discussion

A quantitative comparison of the effect of electron-phonon backscattering with experiments should account for the Coulomb interactions between the electrons. In two- and three-dimensional systems the main effect of the interactions upon the electron-phonon scattering is due to the screening, which leads to suppression of coupling at low energies [35]. On the contrary, in quantum point contacts the electron-phonon scattering should be *enhanced* by the Coulomb interactions between electrons. Indeed, it is well known [37] that the backscattering probability for an electron in an interacting one-dimensional system is enhanced by a factor $(D/T)^{1-g_\rho/2}$. Here $D \sim E_F$ is the bandwidth, and g_ρ is the parameter describing the strength of the interactions in the Luttinger liquid. The one-dimensional electron gas at the center of a quantum point contact at gate voltage corresponding to the first quantized step of conductance is extremely dilute. Consequently, the Coulomb interactions of electrons are very strong, and $g_\rho \ll 1$. Thus, we expect the correction δG to be enhanced by a large factor of order E_F/T_A due to the Coulomb interactions.

The phonon-induced backscattering effect discussed in this paper is not limited to the first conductance step. Although most experiments observe the anomalous shoulder in the conductance at the first step, several observations of similar behavior at the second [4, 7, 38] and even higher steps [38] have been reported.

By applying an in-plane magnetic field B one can polarize the electron spins and observe a conductance step of height $0.5G_0$. The phonon-induced backscattering should then result in a negative correction to conductance similar to the 0.7 anomaly at $B = 0$. However, the experiments [3, 4, 5, 39] do not show an anomalous plateau at $0.7 \times (0.5G_0)$. The likely reason for the apparent absence of the phonon backscattering effects is that at temperatures $T \gtrsim T_A$ the electrons in the channel are no longer completely spin-polarized. Indeed, in the experiment [39] the spin-split conductance plateau at $G = 0.5G_0$ *rises* to values about

[1] The correction (4.13) will eventually saturate at $|\delta G| \sim G_0$ due to the higher-order terms in the electron-phonon coupling constant.

$0.6G_0$ when the temperature is increased from 80mK to 1.3K, indicating that the second spin-split subband contributes to the conductance. This conclusion is supported by the estimate of the spin-splitting $g\mu_B B \approx 3\,\mathrm{K}$ in a typical field $B = 10\mathrm{T}$. Thus, at temperature of order $T_A \sim 1K$ the second spin-split subband gives a significant positive contribution to the conductance that compensates for the decrease in conductance due to the phonons. To observe the phonon-induced backscattering features in conductance, magnetic fields significantly higher than 10T are required.

To test the validity of the mechanism we have proposed for the 0.7-anomaly it would be interesting to perform conductance measurements on QPCs in materials other than GaAs. Particularly interesting candidates from the point of view of electron phonon scattering are III-IV nitride alloys (e.g. $\mathrm{Ga}_{1-x}\mathrm{In}_x\mathrm{N}$) in which the piezoelectric coupling is strong (see [40] and references therein). Unfortunately, current technology allows to make sufficiently pure samples only in GaAs.

A second possible test would rely on the direction dependence of the piezoelectric coupling Eq. 4.8: a very rough estimate based on Eq. 4.8 shows that the parameter $\tilde{\gamma}$ (see Eq. 4.14) that determines the overall size of the correction to the conductance in the limit $T, eV \gg T_A$ is about twenty percent larger for a QPC along the $(1,1,0)$ direction than it is for a QPC along the $(1,0,0)$ or $(0,1,0)$ direction. The difference is probably even larger in the low energy limit, but there the correction is exponentially small and more difficult to measure.

In conclusion, we have studied the effect of backscattering of electrons in quantum point contacts by acoustic phonons. We found a significant negative correction to the quantized conductance. The correction grows exponentially as a function of temperature or voltage at $T, eV \ll T_A$. Above the activation temperature T_A, the correction grows roughly linearly with T and V, Eq. (4.13). Our results are consistent with the experimentally observed features of the conductance near $0.7(2e^2/h)$.

4.4 Bibliography

[1] B. J. van Wees, H. van Houten, C. W. J. Beenakker, J. G. Williamson, L. P. Kouwenhoven, D. van der Marel, and C. T. Foxon, Phys. Rev. Lett. **60**, 848 (1988); D. A. Wharam, T. J. Thornton, R. Newbury, M. Pepper, H. Ahmed, J. E. F. Frost, D. G. Hasko, D. C. Peacock, D. A. Ritchie, and G. A. C. Jones, J. Phys. C **21**, L209 (1988).

[2] L. I. Glazman, G. B. Lesovik, D. E. Khmel'nitskii, and R. I. Shekhter, Pis'ma Zh. Eksp. Teor. Fiz. **48**, 218 (1988) [JETP Lett. **48**, 238 (1988)].

[3] K. J. Thomas, J. T. Nicholls, M. Y. Simmons, M. Pepper, D. R. Mace and D. A. Ritchie, Phys. Rev. Lett. **77**, 135 (1996).

[4] K. J. Thomas, J. T. Nicholls, N. J. Appleyard, M. Y. Simmons, M. Pepper, D. R. Mace, W. R. Tribe, and D. A. Ritchie, Phys. Rev. B **58**, 4846 (1998).

[5] S. M. Cronenwett, H. J. Lynch, D. Goldhaber-Gordon, L. P. Kouwenhoven, C. M. Marcus, K. Hirose, N. S. Wingreen, and V. Umansky, Phys. Rev. Lett. **88**, 226805 (2002).

[6] A. Kristensen, H. Bruus, A. E. Hansen, J. B. Jensen, P. E. Lindelof, C. J. Marckmann, J. Nygard, C. B. Sørensen, F.Beuscher, A. Forchel, and M. Michel, Phys. Rev. B **62**, 10950 (2000).

[7] D. J. Reilly, G. R. Facer, A. S. Dzurak, B. E. Kane, R. G. Clark, P. J. Stiles, A. R. Hamilton, J. L. O'Brian, N. E. Lumpkin, L. N. Pfeiffer, and K. W. West, Phys. Rev. B **63**, 121311(R) (2001).

[8] K. J. Thomas, J. T. Nicholls, M. Pepper, W. R. Tribe, M. Y. Simmons, and D. A. Ritchie, Phys. Rev. B **61**, R13 365 (2000).

[9] C.-K. Wang and K.-F. Berggren, Phys. Rev. B **57**, 4552 (1998).

[10] S. M. Reimann, M. Koskinen, and M. Manninen, Phys. Rev. B **59**, 1613 (1999).

[11] B. Spivak and F. Zhou, Phys. Rev. B **61**, 16730, (2000).

[12] H. Bruus, V. V. Cheianov, and K. Flensberg, Physica E **10**, 97 (2001).

[13] V. V. Flambaum and M. Yu. Kuchiev, Phys. Rev. B **61**, R7869 (2000).

[14] T. Rejec, A. Ramšak, and J. H. Jefferson, Phys. Rev. B **62**, 12985 (2000).

[15] K. Hirose, S. S. Li, and N. S. Wingreen, Phys. Rev. B **63**, 033315 (2001).

[16] Y. Tokura and A. Khaetskii, Physica E, **12**, 711 (2002).

[17] Y. Meir, K. Hirose, and N. S. Wingreen, Phys. Rev. Lett. **89**, 196802 (2002).

[18] H. Bruus and K. Flensberg, Semicond. Sci. Technol. **13**, A30 (1998).

[19] U. Bockelmann and G. Bastard, Phys. Rev. B **42**, 8947, (1990).

[20] R. Mickevicius and V. Mitin, Phys. Rev. B **48**, 17 194, (1993).

[21] V. L. Gurevich, V. B. Pevzner, and K. Hess, Phys. Rev. B**51**, 5219 (1995); V. L. Gurevich, V. B. Pevzner, and E. W. Fenton, Phys. Rev. B**51**, 9465 (1995).

[22] M. Blencowe and A. Shik, Phys. Rev. B **54**, 13 899, (1996).

[23] A. J. Kent, A. J. Naylor, P. Hawker, and M. Henini, Phys. Rev. B **61**, R16 311, (2000).

[24] H. Totland, Ø. L. Bø., and Y. M. Galperin, Phys. Rev. B 56, 15299 (1997); F. A. Maaø, Y. Galperin, Phys. Rev. B 56, 4028-4036 (1997).

[25] J. M. Shilton, V. I. Talyanskii, M. Pepper, D. A. Ritchie, J. E. F. Frost, C. J. B. Ford, C. G. Smith, and G. A. C. Jones, J. Phys. C **8**, L531, (1996).

[26] J. Cunningham, V. I. Talyanskii, J. M. Shilton, M. Pepper, A. Kristensen, and P. A. Lindlof, Phys. Rev. B **62**, 1564, (2000).

[27] M. Büttiker, Phys. Rev. B, **41**, 7906 (1990).

[28] E. C. Kemble, Phys. Rev. **48**, 549 (1935).

[29] G. D. Mahan, *Many-Particle Physics* (Kluwer Academic / Plenum Publishers, New York, Third Edition, 2000).

[30] Y. Ma, R. Fletcher, E.Zaremba, M. D'Iorio, C. T. Foxon, and J. J. Harris, Phys. Rev. B **43**, 9033.

[31] A. Mittal, R. G. Wheeler, M. W. Keller, D. E. Prober, and R. N. Sacks, Surf. Sci. **361/362**, 537, (1996).

[32] P. J. Price, Ann. Phys. (NY), **133**, 217 (1981); P. J. Price, J. Vac. Sci. Technol. **19**, 599, (1981).

[33] P. J. Price, J. Appl. Phys. **53**, 6863, (1982).

[34] V. Karpus, Sov. Phys. Semicond. **22**, 268, (1988).

[35] B. K. Ridley, *Quantum processes in semiconductors* (Oxford University Press, Oxford, 1982).

[36] R. Taboryski, A Kristensen, C.B. Sørensen, and P.E. Lindelof, Phys. Rev. B **51**, 2282 (1995).

[37] C.L. Kane and M.P.A. Fisher, Phys. Rev. B **46**, 15233 (1992).

[38] A. Kristensen, J. Bo Jensen, M. Zaffalon, C. B. Sørensen, P. E. Lindelof, M. Michel, and A. Forchel, J. Appl. Phys. **83**, 607 (1998).

[39] S. M. Cronenwett, Ph.D. Thesis (2001).

[40] A. Al-Yacoub, L. Bellaiche, and S.-H. Wei, Phys. Rev. Lett. **89** 057601, (2002).

Remerciements

J'ai eu la chance de pouvoir faire une thèse sous la direction du professeur M. Büttiker. Pendant ce travail j'ai énormément profité de sa compréhension profonde de la physique mésoscopique, de ses idées et de son intuition remarquable. Je voudrais également le remercier pour m'avoir laissé une grande autonomie.

Je suis très reconnaissant aux professeurs Yaroslav Blanter, Thierry Giamarchi et Poul-Erik Lindelöf d'avoir accepté le rôle de juré de thèse.

C'est grâce à Karyn le Hur que j'ai compris le modèle Kondo. C'était un grand plaisir de collaborer avec elle et je lui suis infiniment reconnaissant de son soutien.

J'ai passé deux mois très intéressants aux Laboratoires Bell à Murray Hill (NJ) où j'ai eu l'occasion de travailler avec Konstantin Matveev. Il m'a beaucoup impressionné par son adresse mathématique et son éducation étendue en physique.

Sebastian Pilgram a contribué d'une manière importante à mon travail sur la décohérence et je l'en remercie beaucoup. J'ai collaboré avec lui en particulier sur le chapitre 1.5 de la thèse.

Un grand merci à Christophe Texier pour sa correction soigneuse de l'introduction en Français de cette thèse.

Finalement je tiens à remercier mes collègues et collaborateurs Pascal Cedraschi, Christophe Texier, Yaroslav Blanter, Tooru Taniguchi, Andrew Martin, Kirill Nagaev, Karyn Le Hur, Eric Lutz, Sebastian Pilgram, Michael Moskalets, Peter Samuelsson, Rosa Lopez, David Sanchez, Andrew Jordan, Eugene Sukhorukhov et Valentin Rytchkov du groupe de la physique mésoscopique pour les discussions amusantes, variées et instructives dont j'ai profitées pendant ces trois années passées à Genève.

Georg Seelig